PARAMETRIC STUDIES ON THE TEMPERATURE DEPENDENT BEHAVIOUR OF STEEL STRUCTURES WITHIN A FIRE CONTEXT

Stanton Wesley Govender

In fulfilment of the academic requirements for the degree, *Master of Science in Mechanical Engineering*, College of Agriculture, Engineering and Science, University of KwaZulu-Natal.

December 2012

Supervisor: Professor Sarp Adali

DECLARATION 1 - PLAGIARISM

As the candidate's Supervisor I agree/do not agree to the submission of this thesis.

Signed: …… Date: ……..

Professor Sarp Adali

I, Stanton Wesley Govender, declare that

i. The research reported in this dissertation, except where otherwise indicated, is my original research.
ii. This dissertation has not been submitted for any degree or examination at any other university.
iii. This dissertation does not contain other persons' data, pictures, graphs or other information, unless specifically acknowledged as being sourced from other persons.
iv. This dissertation does not contain other persons' writing, unless specifically acknowledged as being sourced from other researchers. Where other written sources have been quoted, then:
    (a) Their words have been re-written but the general information attributed to them has been referenced.
    (b) Where their exact words have been used, then their writing has been placed in italics and inside quotation marks, and referenced.
v. This dissertation does not contain text, graphics or tables copied and pasted from the Internet, unless specifically acknowledged, and the source being detailed in the dissertation and in the References sections.

Signed: …… Date: ……..

DECLARATION 2 – PUBLICATIONS

Details of contribution to publications in preparation that form part and/or include research presented in this thesis:

Publication 1

S.W. Govender and S. Adali, Experimental and computational study of reusability of steel structures after exposure to elevated temperatures, in preparation for submission to Fire and Materials

Signed: …… Date: ……..

ACKNOWLEDGEMENTS

Firstly I would like to thank my Supervisor Professor Sarp Adali for his guidance and direction throughout the duration of this study. His vast experience and keen input has been a motivational support for me.

I would like to thank the technical staff at the University of KwaZulu-Natal Mechanical Engineering Workshop and my colleagues at ArcelorMittal South Africa for availing their expertise and resources to ensure the completion of this project.

I would also like to thank my family and friends for their understanding during the long periods of my absence as I worked long and hard to bring this study to its completion.

Finally to God be all the Praise, Honour and Glory.

To my parents, Desmond and Irene, whose endless love and support encompassed with selfless sacrifices throughout my life, have enabled me to achieve success in all my endeavours...

ABSTRACT

The mechanical and material properties of structural steel at elevated temperatures play an important role in structural fire design. The South African 350W and S355 structural steels are common in building structures with S355 slowly replacing the older 350W. The cost and feasibility of full scale fire tests are some of the causes for the lack of experimental data on the behaviour of steel structures when exposed to fire. Therefore excessively conservative design codes based on isolated laboratory experiments are used in practice which leads to increased material costs. Another area of concern with respect to building safety is the reusability of structural steels post fire exposure, which is not effectively addressed within these codes.

This study aims to establish greater insight into structural fire design and simulation on which further research can be built. Experimental programs on the temperature dependent behaviour of these steel members loaded axially are conducted and compared with theory and the Eurocode 3 standard [1]. The reusability of steel exposed to fire and after being cooled down is investigated and compared to the findings by Outinen [2]. Further testing on material to determine the relationship between remaining life and hardness degradation after cooling down was conducted.

Experimental data from various external studies are used to develop novel computer models using the finite element analysis software, SimXpert [3]. These are verified against the original data and compared to existing design codes. A parametric approach is used with these models to demonstrate the advantages of computer simulations in structural fire design. Different cross sections and slenderness ratios are evaluated for their susceptibility to buckling at elevated temperatures.

The results of this study show that as temperature and exposure time increase the integrity of steel members decrease. The current design codes accurately predict the behaviour of isolated specimens but lack data on real situations where the specimen is part of a complex structure. It was found that steel members can be reused if their exposure temperature does not exceed 700°C, after which their strength can reduce to 90%. This temperature dependant behaviour was successfully modelled using basic computer simulations and then demonstrated the ease in which they can be used in place of experimental regimes. The parametric advantages of these simulations were demonstrated by predicting the effects of slenderness ratios and geometry cross sections on the buckling behaviour.

TABLE OF CONTENTS

LIST OF TABLES

LIST OF FIGURES

NOMENCLATURE

Symbols

A	Cross Sectional Area	[m^2]
b	Width	[mm]
E	Young's Modulus	[Pa]
E_T	Elastic Modulus at Elevated Temperatures	[K]
F	Load Vector	[-]
F_1, F_2	Node Load	[N]
f_y	Yield Strength	[Pa]
f_{Yt}	Yield Strength at Elevated Temperature	[Pa]
G	Shear Modulus	[Pa]
I	Second Moment of Inertia	[m^4]
J	Polar moment of Inertia	[m^4]
K	Stiffness Matrix	[-]
k	Thermal Conductivity	[$W.m^{-1}.C^{-1}$]
L	Length	[m]
L_e	Effective Length	[m]
LMP	Larson-Miller parameter	[-]
M	Bending Moment	[Nm]
n	Bending Mode	[-]
P	Applied Load	[N]
P_{cr}	Critical Load	[N]
R_T	Thermal Shock Parameter	[-]

r	Radius of Gyration	[m]
T	Torque	[Nm]
T	Temperature	[K]
T_0	Initial Temperature	[K]
T_S	Temperature of Steel	[K]
t	Thickness	[mm]
t	Time	[min], [hrs]
U	Displacement vector	[-]
U_1, U_2	Node Displacements	[m]
v	Lateral Deflection	[m]
v	Poison's Ratio	[-]
π	Pi	[rad]
σ_{cr}	Critical Stress	[Pa]
σ_T	Maximum Tensile Stress	[Pa]
ϵ	Strain	[-]
λ_s	Thermal Conductivity	[$W.m^{-1}.C^{-1}$]
α, α_S	Thermal Expansion Coefficient	[$m.m^{-1}.C^{-1}$]
c_s	Specific Heat	[$J.kg^{-1}.C^{-1}$]
τ_{max}	Maximum Shear Stress	[Pa]
Φ	Yield Angle	[rad]

1. INTRODUCTION

With the continuing advances in computer technology, computational analysis has become much more feasible and convenient. It has the advantage of allowing the modelling of situations which are difficult or impossible to observe experimentally. It also facilitates the use of parametric studies which do not require repetitive test setups. This reduces the need for large amounts of material and expensive experimental equipment. By eliminating the cost factor, the range of tests and investigations possible are greatly extended. Finite element analysis can be applied in numerous ways to solve engineering problems. It is useful in analysing full scale tests which are difficult to replicate in a laboratory such as structural members in fire. This specific application is important as it governs the design of buildings whose structural integrity has a significant impact on safety.

1.1. BACKGROUND TO STUDY

Steel and its alloys are widely used in building structures due to its high strength, ductility and ease of fabrication as stated by Ding, Li and Sakumoto [4]. However, the design of these structures must include the possibility of fire exposure. Especially in the case of public safety where buildings are situated in highly populated areas, the steel members must preserve its load bearing capabilities. According to Li and Lou [5], steel structures without fire protection may collapse prematurely when exposed to high temperatures which would be fatal to fire fighters and evacuation operations. Due to its metallic nature steel is more susceptible to fire than concrete and timber as noted by Ng and Gardner [6]. This is due to its high thermal conductivity which results in a rapid temperature development. Fire-Resistant steels have been introduced which increase the fire-resistant capabilities of steel structures. However, the need to reduce costs and lead time calls for more efficient design codes to be developed which will minimize the dependence on fire-resistant coating. According to comparisons done by Ng and Gardner [6] to numerical models, design codes generally show a very conservative approach. This can be attributed to the lack of experimental data available in literature with regards to the behaviour of steels structures in fire. This is particularly true for high strength steels as well as stainless steels as stated by Outinen [2].

1.2. PROBLEM STATEMENT AND OBJECTIVES

In South Africa a commonly used structural steel is 350W. This steel grade was introduced to replace 300W structural steel as the standard structural steel [7]. Internationally the S355 material specification is used for structural purposes and is becoming the choice of material in South Africa. In building structures, design against buckling is very important due to the high loads that are supported. The design of steel columns under buckling must in addition, include exposure to fire. This is especially important when the steel is unprotected. In many situations where a fire hazard has occurred immediate damage may not be recognizable. Therefore research into the critical temperatures and residual strength of steel structures after cooling down need to be carried out. A set of guidelines need to be established as to indicate at what critical temperature a steel member is reusable or not.

The objectives of this investigation are, therefore:

- To evaluate the reusability of structural steel and its residual stresses after fire exposure for design safety.

- To use finite element analysis to model the behaviour of structural steel under various loads at elevated temperatures.

- To use a parametric approach to observe the buckling susceptibility of structural steel and investigate this phenomena for different cross sections and slenderness ratios.

1.3. RESEARCH METHODOLOGY AND THESIS OUTLINE

The research methodology used in this study consisted of four phases. The first phase starting off in chapter 1, introduces the reader to the background of the topic and the motivation for this research. The aims and objectives are clearly stated as well as the outline of how the research will be presented. Chapter 2 reviews relevant literature pertaining to the topic at hand and delves into the theoretical concepts of structural fire design.

Chapter 3 sets the foundation for the second phase which deals with the specifications, methods and setups of the experiments conducted. Chapter 4 presents the results of these

experiments and compares them with literature and theory where possible. Chapter 5 scrutinizes these results and provides explanations to some of the deviations and highlights the important findings.

The third phase involves the simulation aspect of this study. Chapter 6 presents the development of the simulation model and validates the accuracy and scope for application. Chapter 7 demonstrates the possible applications for the simulation model by using a parametric approach to investigate the effects of slenderness ratio and cross section geometry on steel member load bearing capacities. These results are discussed at length in Chapter 8 and where applicable, limitations and assumptions are stated.

The final phase of this research is brought to a close in Chapter 9. The outcomes and findings of this research with their implications are summarized as well as the shortcomings and gaps that could not be addressed. Recommendations for future work to be done which can be built upon this research are mentioned.

2. LITERATURE REVIEW

This chapter provides a literary review on the current investigation in order to develop an understanding of the topic at hand. Literature relevant to this study will be examined and put in perspective. The scope of this chapter includes material behaviour, mechanical properties, modelling and simulation techniques, fire safety design practice and Column buckling theory. Specifically 350W and S355 structural steel will be the material of concern and relevant existing design codes will be discussed.

The material behaviour of various steel alloys used in building construction will be presented and similarities will be drawn between various design codes. This will further be extended to behaviour of steels at elevated temperatures and an investigation into the experimental procedures of different institutions and how the raw data is obtained and processed. Different failure modes of steel members with respect to high temperatures are investigated. Finite element theory is presented with a concentration on the software package used in this research namely, MSC SimXpert 2010 [3]. Fundamental theory on buckling of steel columns is briefly looked at with a focus on design and geometry.

Numerous experimental and numerical studies are overviewed with their respective results and recommendations which are relevant to the South African industry. The Eurocode design code [1, 8] is compared with these studies and this allows for a clear understanding of what is lacking in this current field of research.

2.1. MATERIAL BEHAVIOUR

When conducting mechanical tests it is important to be familiar with the various properties possessed by materials and the various terms used to describe these properties. The most fundamental concepts in the mechanics of materials are the stress and strain. By definition, the stress is equal to the average uni-axial tensile force acting on the specimen divided by the original cross-sectional area of the specimen. Strain is the ratio of the change in length of a metal sample in the direction of the force divided by the original length of the sample considered [9]. Strain is commonly represented as a percentage. The stress and strain values are obtained by conducting standardized tension and compression tests on the specimens. From these quantities a stress-strain diagram can be drawn which is characteristic of the material being tested. This diagram presents

information on the mechanical properties and behaviour of a particular material [10]. Figure 2-1 below shows a typical stress strain diagram of a ductile material such as steel.

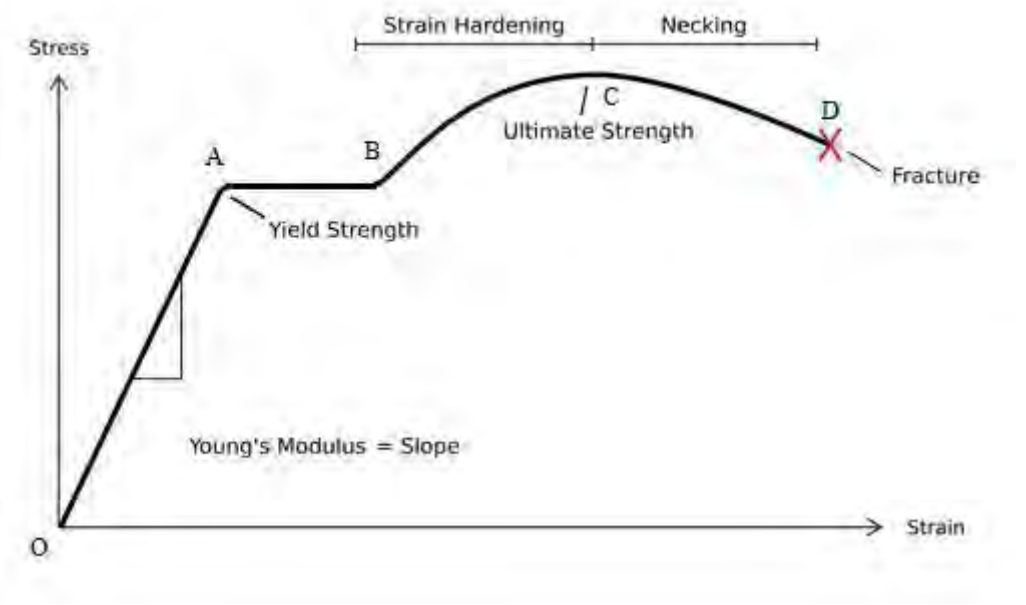

Figure 2-1: Typical stress strain diagram developed by Gere [10]

Ductility is defined as the ability of a material to withstand plastic deformation without rupture. When a material is tensile tested, initially it is exposed to an elastic deformation which is not permanent. This can be seen from the linear section OA of the diagram. During this phase the stress is proportional to the strain. The slope of OA is known as Young's Modulus of elasticity. After point A the material reaches its proportional limit. This occurs just before the materials yield point after which plastic deformation begins. From point A to B the material yields and becomes completely plastic. The material will elongate dramatically with no increase in load needed. At point B the material begins to strain harden due to the crystalline changes which are induced by the movement of dislocations [10]. This phenomenon resists deformation and thus an increase in tensile load is required to continue the elongation. The load reaches a maximum at point C which is known as the ultimate strength. Further loading of the material will result in a reduction in the cross-section which is known as necking and will eventually lead to fracture at point D.

2.2. MATERIAL PROPERTIES

Structural steel is a low carbon steel with about 0.2% carbon content. It is an alloy of iron. With an increase in carbon content steels become less ductile but stronger. Temperature effects also have a significant impact on the behaviour of materials which will be discussed in the following sections of this chapter. In South Africa the standard structural steel used is SANS 1431 350W [11]. It is readily weldable and has a yield strength of 350MPa. Another structural steel S355 has similar properties to 350W and is slowly replacing it. S355 falls under the EN 10025:2004 standard [12]. When dealing with steels across different standards, even those accepted as equivalent steels do not have the exact chemical composition and properties [13]. Tables 2-1 and 2-2 below show the chemical composition and mechanical properties of 350W and S355 structural steel.

Table 2-1: Chemical composition of 350W and S355 [14]

Grade	Maximum Chemical Composition												
	C	Mn	Si	P	S	Nb	V	Nb+V	Al	Cu	Ni	Cr	Mo
350WA	0.22	1.60	0.50	0.040	0.040	0.10	0.10	0.10	0.10	0.35	0.30	0.30	0.10
S355 JR+AR	0.24	1.60	0.55	0.035	0.035	0.10	0.10	0.10	0.10	0.55	0.30	0.30	0.10

Table 2-2: Mechanical properties of 350W and S355 [14, 15]

Grade	Ultimate tensile strength (MPa)	Min Yield stress (MPa) for thickness t (mm)				
		t≤16	16<t≤25	25<t≤40	40<t≤63	63<t≤100
350WA	480/650	350	345	345	340	325
S355 JR+AR	490/630	355	345	345	335	325

In industry, common materials used for construction are steels, aluminium and concrete. In most cases the steel is reinforced with concrete. However, when structural steel is exposed it is vulnerable to fire. To overcome this problem a fire-protection coating was sprayed onto the steel. Spray-on fire protection can efficiently slow down the heat transfer to the steel when exposed to fire. This results in a lower rate of temperature increase in the steel [16]. However, the disadvantages of spray-on fire protection are that it is very fragile and can thus be easily damaged by mechanical action. This reduction in fire resistance can lead to local structural failure if exposed to fire and result in progressive collapse of structures as was seen in the World Trade Centre. A study by Li, Wang and Chen [16] on the modelling of the fire resistance of steel columns with locally damaged fire protection concluded that an increase in the length of the damaged fire protection reduces the load bearing capacities of the steel column at a given temperature. In Japan, building regulations do not allow the temperature of steel members to exceed 350°C [17]. Therefore building costs are extremely high due to the amount of fire protection and insulation needed. This prompted the development of fire-resistant (FR) steels. The advantages of FR steel are that it has significantly higher strength characteristics at elevated temperatures than that of conventional steel and eliminates the need for insulation or any post fabrication. This saves time, space and money. Parametric studies were conducted by Ding, Li and Sakumoto [4] on the fire-resistance of FR steel members. Mechanical properties of FR steel at elevated temperatures where modelled based on test data from Nippon Steel Corporation. See Appendix A for mathematical models. It is noted that at 350°C the yield strength of conventional steel reduces to $\frac{2}{3}$ of its specified value at room temperature, whereas FR steel displays the same behaviour at 600°C. Ding Li and Sakumoto [4] concluded that conventional structural steel has 55% of the fire duration time of FR steel under the same conditions. Figures 2-2 and 2-3 below developed by Bailey [17] compare the mechanical properties of various FR steels developed by Kawasaki Steel and Nippon Steel.

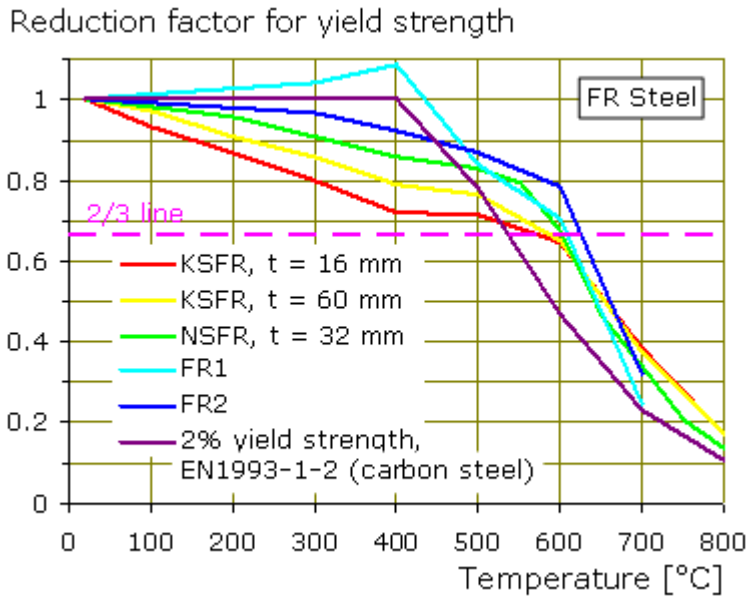

Figure 2-2: Reduction Factors for Yield Strength of FR Steel Vs Temperature [17]

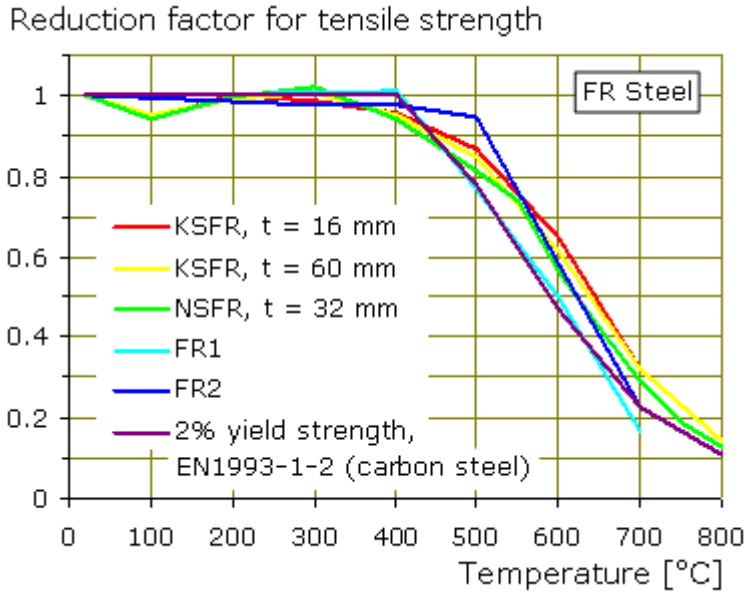

Figure 2-3: Reduction Factors for UTS of FR Steels Vs Temperature [17]

Even though the various FR steels do not behave similarly, the yield stress reduces to approximately $\frac{2}{3}$ at 600°C in all cases. The discrepancies between the results may be due to different test setups and procedures carried out in tests done outside of Japan [17].

2.3. HIGH TEMPERATURE FAILURE MECHANISMS

At elevated temperatures steel structures may be at risk to failure. Even though the steel members are not brought to melting point, the high temperatures have a significant effect on the microstructure of the material. A steel structure can suffer from various high temperature failure mechanisms. These include creep, thermal shock, thermal fatigue and high temperature corrosion.

2.3.1. Creep

The most common and important high temperature failure mechanism in steel structures is creep. It is defined as the progressive plastic deformation of a material under stress. It occurs when a material is exposed to high levels of stress that are below its yield strength over a period of time. This strain is time and temperature dependant. Creep becomes more severe with an increase in temperature. Therefore it is important to incorporate creep in the design process when working with high temperatures. The creep rate is dependent on exposure time, temperature and applied load. Therefore it is the limiting factor in most designs. The effects of creep become noticeable at about 30% of a metals melting temperature. Creep occurs in three distinct stages, primary, secondary and tertiary. Below in Figure 2-4 is a diagram of a typical creep curve for a metal.

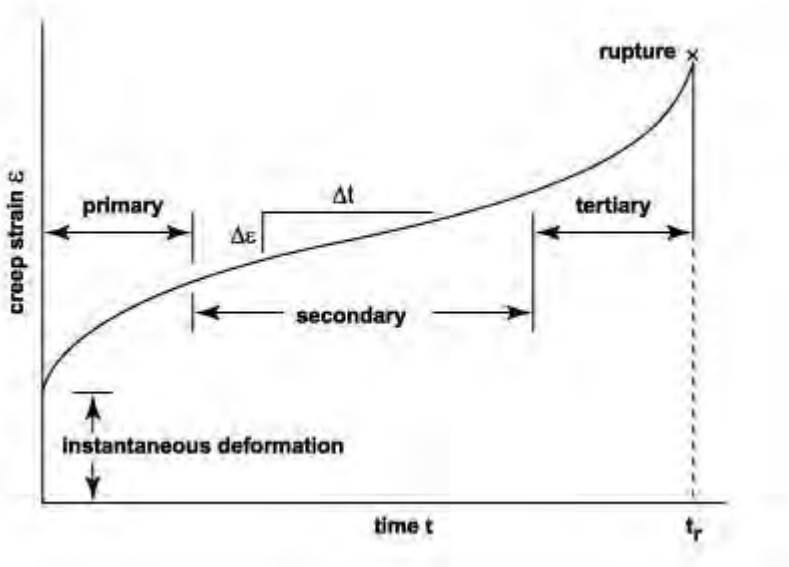

Figure 2-4: Typical creep curve for a metal [10]

The creep curve represents the time versus creep strain behaviour of a metal under constant stress at a constant temperature. The shape of this curve depends on the type of material, applied load and temperature. Initially there is a rapid instantaneous elongation of the material due to high strains. Thereafter in the primary stage the strain rate decreases due to strain hardening until it eventually reaches its minimum. In the secondary stage the creep rate is constant and is known as steady-state creep. This occurs due to the balancing of the stain hardening and annealing processes. This stage is of most interest since extensive creep occurs in this stage and the constant slope of the curve is characterized as the creep rate of the material. In the tertiary stage the creep rate and strain increase exponentially due to necking and will eventually lead to fracture.

A study done by Li and Zhang [18], investigated the buckling behaviour of axially restrained steel columns when considering creep. It was found that the buckling temperatures were significantly different from results where creep was not considered.

2.3.2. Thermal shock

When a material experiences a rapid change in temperature, the damage caused is known as thermal shock. The high temperature gradients present in the material may cause uneven heat transfer and parts of the material will expand at different rates. This is very severe in materials with a low thermal conductivity and a high coefficient of thermal expansion. This sudden expansion causes stresses in the material. When these stresses become large enough cracks will form in the material. The robustness of a material to thermal shock is characterized with the thermal shock parameter [19]. See Appendix B.

2.3.3. Thermal fatigue

When a material is exposed to cyclic thermal stresses, thermal fatigue can occur. The continuing heating of the material causing residual stresses can lead to fatigue cracking. Creep fatigue can also contribute to this failure mechanism at high temperatures and large exposure time. This failure mechanism is crucial in structural design if structures are reused after high temperature exposure. Kadlec et al. [20] concluded that thermal cycling has the same effect as cyclic mechanical loading.

2.3.4. High temperature corrosion

This type of corrosion is non-galvanic. It is caused by carburization. When a metal is exposed to high temperatures in a carbon rich environment, carburization takes place i.e. Carbon forms on the metal surface which forms cracks in the metal. This makes the metal more brittle and reduces its strength. Similarly in a sulphide rich environment at high temperatures, sulphide forms on the grain boundaries of the material. Oxidation starts to occur on these boundaries, which then reduces strength and ductility. High temperature corrosion reactions occur at excessively high rates in unprotected materials at elevated temperatures such as steel [21].

2.4. FIRE DESIGN AND BEHAVIOUR

2.4.1. Fire Curves

When modelling the behaviour of fire there are many aspects to consider. In order to develop a way of comparing the fire resistance capabilities of different structural elements, a standard heating pattern must be used in laboratory tests. There exist many different fire curves for particular scenarios. The most common is the standard temperature-time curve shown below, which is widely used in controlled tests. It is also known as the ISO 834 curve [22] shown in Figure 2-5 below. This is categorized as a nominal curve. It is very simple and is independent of the environment conditions. According to Tan et al. [23] the standard temperature-time curve does not represent real fire behaviour. Heating rate and duration of exposure differs from real fires as the ventilation and surrounding material is not taken into consideration. The decay phase of a fire is not catered for as well. However, it is suitable for conducting simplified experiments and simulations to compare component behaviour under fire.

The standard temperature-time curve is defined by the Eq. (2.4.1) [22]:

$$T = T_0 + 345 \log_{10}(8t + 1) \qquad (2.4.1)$$

Where, t is time (min)

T is the furnace temperature (°C)at time

T_o is the initial furnace temperature (°C)

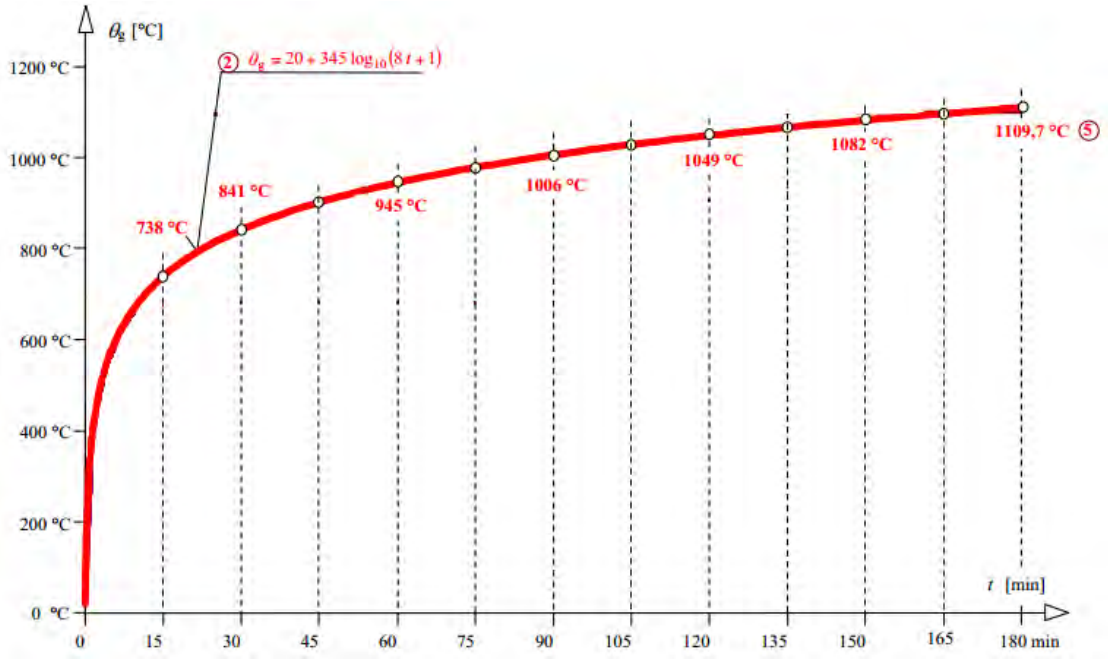

Figure 2-5: Standard Temperature-Time Fire Curve [24]

The alternative category of curves is the natural fire curves. These curves are more complex as they take into account the environment and the type of combustible materials in the affected area. Figure 2-6 below illustrates the 3 phases of a typical natural fire. The first phase is the growth period where temperature increases with time. The second phase is known as full development where the fire will reach its maximum temperature if Flashover occurs. Flashover normally occurs when the gas in the enclosure reaches 600°C and all the combustible material in the vicinity burst into flames.

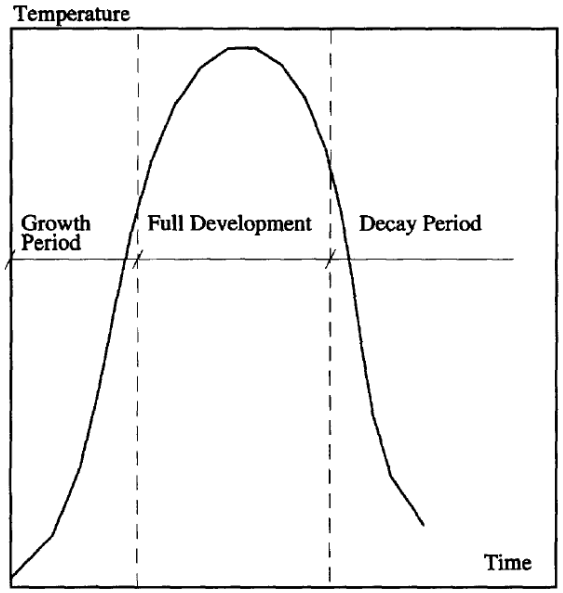

Figure 2-6: Typical Natural Fire Curve [25]

For the sake of thoroughness one must mention the third type of fire curves available which are parametric fire curves. These are much more accurate than the standard fire curves. Here a specific curve can be formulated for a specific compartment fire. This will depend on the ventilation, size of the compartment, the type of combustible materials and fuel as well as the thermal properties of the compartment. Rein et al. [26] investigated the differences between fully distributed fires and travelling fires within building structures and found that the effects of each were significantly different. Fully distributed fires are typical of small compartments were it can be assumed that the temperature throughout the compartment rises uniformly. Travelling fires are more localized and therefore result in uneven thermal loading on the structures which is constantly changing.

2.4.2. Residual stress due to fire

When predicting the behaviour of materials exposed to fire, greater emphasis is usually placed on the heating phase as opposed to the cooling process. This is due to the fact that the full development phase of a fire is the greatest threat to structural failure. However, when investigating the reusability of steel members, the decay phase must also be considered to determine the residual stresses within the material.

Typical data seen in literature presents the high temperature behaviour of materials by means of stress strain curves for each specific temperature. When cooling down occurs,

strain reversal is observed which is not accounted for in these curves. This is especially true when the material has been loaded past its yield limit and permanent deformations are present. El-Rimawi et al. [25] acknowledged this deviation from typical stress strain curves and presented simple models to account for strain reversal.

When temperature unloading occurs within building structures it is assumed that the load remains unchanged. The methodology used by Wang et al. [27] to account for these residual stresses is explained in the Figure 2-7 below. Typical load deformation curves are represented, an ambient temperature curve and a significantly higher temperature curve common with fire exposure. The load P is large enough to cause yielding at the high temperature which is represented by point A. If strain reversal is ignored, once ambient temperature is reached assuming a constant load, point B will represent the load deformation characteristics. However, this is incorrect as was shown by El-Rimawi et al. [25] who stated that the steel member will unload elastically and not follow the original curve. This is true only if the elastic limit was exceeded during heating otherwise the unloading and loading path will be the same. In order to determine the correct load deformation characteristic after cooling down it must be assumed that the specimen is completely unloaded at the high temperature and then reloaded at ambient temperature. In Figure 2-7 the unloading and loading paths are parallel to the elastic portion of the specific curve for that temperature. Point C would therefore be the new equilibrium position if load remained constant and the effect of strain reversal was accounted for.

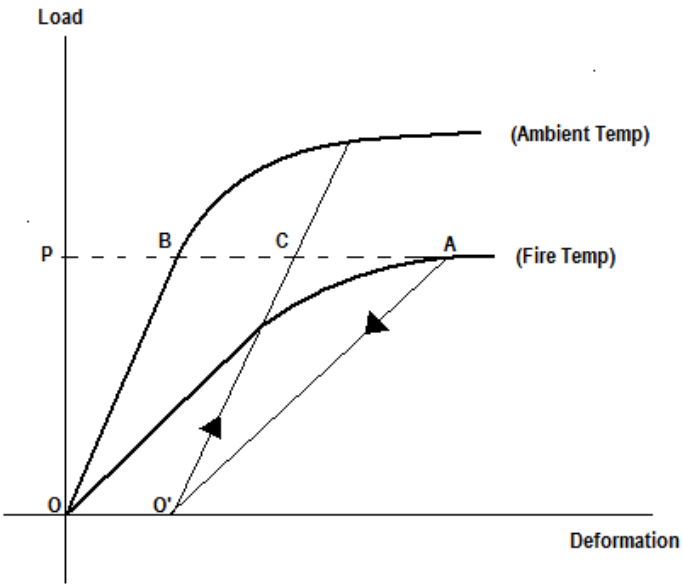

Figure 2-7: Method For strain reversal consideration

2.4.3. Hardness Due To Heat Treatment

In the context of this study, hardness is the property of a metal to resist plastic deformation when a load is applied [9]. Therefore it is directly linked to the strength of material. One must keep in mind that hardness may also result in more brittle material and thus not allow elastic deflections which can be detrimental within building structures. When changing these properties of steel, the type of heat treatment is crucial. By looking at a few heat treatment processes, the effects of fire on steel can be approximated. The Iron – Carbon phase diagram is shown in Figure 2-8 to help explain the behaviour of steels with approximately 0.22% carbon content during and after fire exposure.

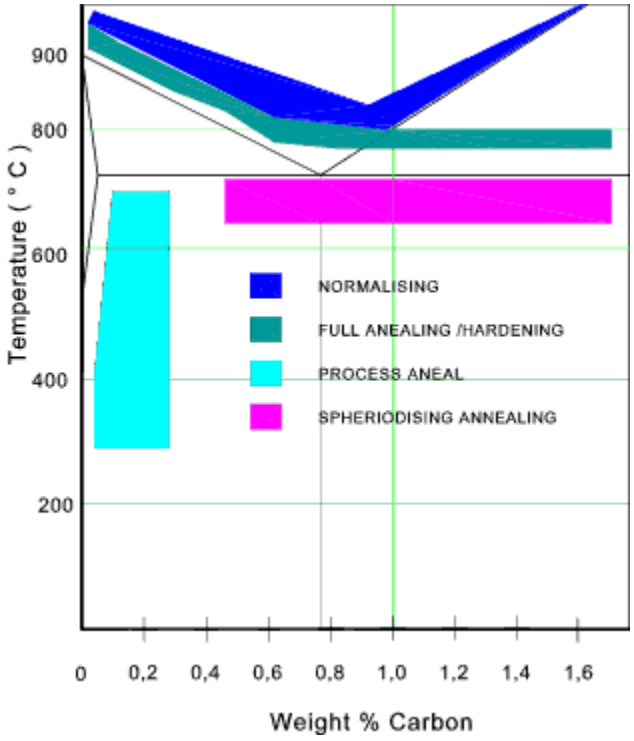

Figure 2-8: The Fe-C phase diagram [28]

There are two types of annealing treatments. With process annealing, the steel is heated to between 550°C and 650°C and held there for a considerable length of time. It is then cooled in a controlled manner usually within a furnace. Full annealing follows the same procedure except that the steel is heated above the transformation temperature of 727°C [29] as shown in the Figure 2-8. This relieves the stresses within the material causing softening. If a building is well ventilated then a fire cannot be likened to an annealing process as the cooling rates would be much higher.

Normalizing is conducted by heating the steel above the transformation temperature and then letting the material air cool. This refines the grain structure. This type of heat treatment is very close to the behaviour of natural fires.

Tempering is conducted by heating the steel to below the transformation temperature and holding it until it softens. The hardness reduces with an increase in temperature [30]. This will usually be the case if high temperatures were not reached in a fire and rapid cooling did not take place.

Precipitation strengthening occurs in steel alloys by forming precipitated particles which obstruct the movement of dislocations in the material and thus strengthen it [31]. The steel is heated until a solid solution structure is formed and then quenched to room temperature. There after the supersaturated solid solution structure is allowed to age to enable the formation of the precipitates. This is possible in fires where fire fighting services have extinguished the fire rapidly and in doing so cause a quenching effect.

When all the above types of heat treatments are considered, it is clear that the change in hardness of a material exposed to fire is not dependant on temperature alone. Cooling rates and holding times make a significant contribution to the end result. Mukhopadhyay et al. [32] investigated the remaining life assessment model based on hardness. The change in hardness was correlated to the Larson-Miller parameter (LMP). This parameter combined the effects of temperature and service time as shown in Eq. (2.4.2) below:

$$LMP = T[20 + \log t] \times (10^3) \qquad (2.4.2)$$

Where, T is service temperature in °K,

And, t is service time in hours.

This value is then plotted against the change in hardness as shown in Figure 2-9 [32]. The resulting curve indicates that hardness shows negligible changes for LMP factors of 19 and less. However, for LMP factors greater than this, the hardness degradation increases exponentially. In addition the applied stresses alter the curve in the exponential region.

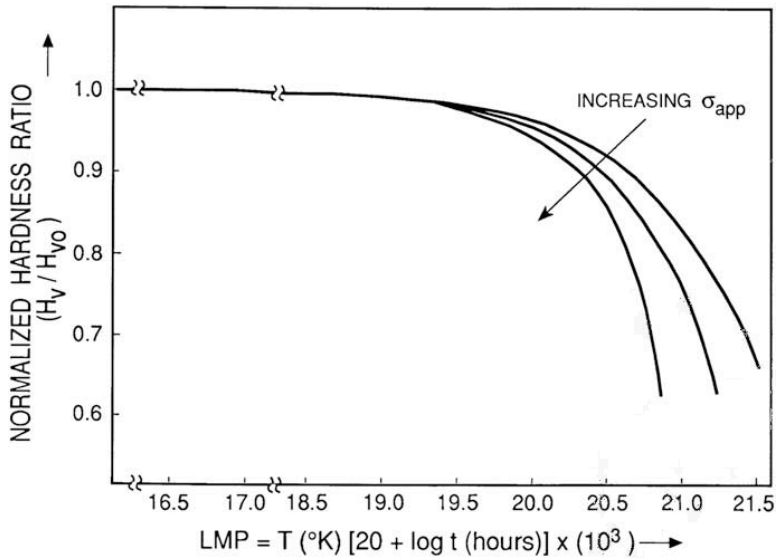

Figure 2-9: Variation of hardness with LMP as a factor of applied stress [32]

2.5. BUCKLING THEORY

Failure due to buckling is a very critical subject when dealing with structures. Columns commonly fail by buckling rather than direct compression. Columns are long slender members that carry axial loads in compression and are thus very susceptible to buckling. The relation between the stiffness and strength of a material has an effect on the buckling behaviour. The main concern of interest is the critical loads. This is the value of a specific axial force applied to a column for which there is a transition between the stable and unstable conditions.

2.5.1. End Conditions

The end conditions of the column have a significant effect on critical loads which the column can support. Quimby [33] indicated that the end conditions influence the compressive strength of the column. Huang et al. [34] investigated numerous studies and concluded that the behaviour of steel columns under fire is predominately affected by the restraints of the adjoining structure. Typically expansion and rotation is suppressed causing additional axial forces and bending moments. The ends of the columns can either be pinned or fixed in theory. However, in actual structures they can be a mixture of these two conditions. Moreover, depending on which axis the column bends about, the end conditions can vary. In the case of loads applied uniformly over the columns cross section,

the actual axis about which bending occurs is certain. The critical loads are determined by using the Euler equation which is developed below.

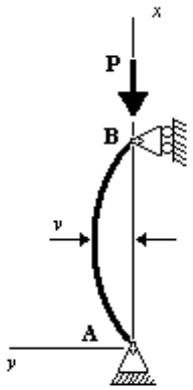

Figure 2-11: Pin –ended column with buckled shape

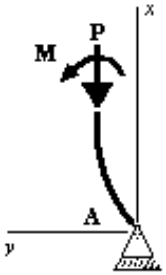

Figure 2-10: Axial force and bending moment acting on a cross section

Using the bending moment Eq. (2.5.1):

$$EIv'' = M \qquad (2.5.1)$$

Where, M is the bending moment at any cross section, v is the lateral deflection and EI is the flexural rigidity of the material.

The differential equation of deflection for the pin ended column in Figure 2-11 becomes:

$$EIv'' + Pv = 0 \qquad (2.5.2)$$

Where, P is the applied load.

Using,

$$K^2 = \frac{P}{EI} \qquad (2.5.3)$$

And solving,

$$v'' + k^2 v = 0 \qquad (2.5.4)$$

The critical loads are

$$P_{cr} = \frac{n^2 \pi^2 EI}{L^2} \qquad (2.5.5)$$

Where,

n=1, 2, 3….

Using the similar procedure as for pin-ended columns, the critical loads for fixed-ended columns are given by,

$$P_{cr} = \frac{4\pi^2 EI}{L^2} \qquad (2.5.6)$$

Or by using the effective length formula,

$$P_{cr} = \frac{\pi^2 EI}{L_e^2} \qquad (2.5.7)$$

Where, L_e is the effective length with comparison to a pin-ended column in Figure 2-12. From Figure 2-12, due to the symmetric nature of the curve, there exist inflection points at a distance of L/4 from the ends. Thus the effective length of a fixed-end column is L/2.

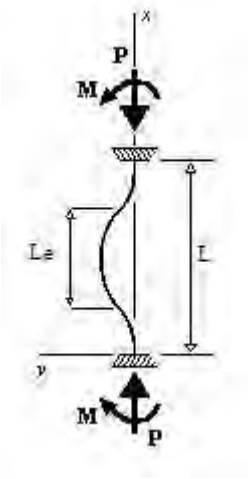

Figure 2-12: Buckled shape of fixed-ended column in first mode

The type of buckling discussed here is Euler Buckling. More specifically it deals with general buckling as opposed to localized buckling. With general buckling a distorted longitudinal axis of the column is evident. Distortion of the longitudinal axis is not characteristic of localized buckling which will be discussed later. Euler buckling can only be applied to problems with small deflections and the assumption of ideal columns. This means that the column has no imperfections and is linearly elastic. In addition, the load

must be applied precisely. Seputro [35] found that pin ended columns survive longer than fix ended columns when exposed to fire. However, it was also noted that the pin ended columns showed excessive deformations. Within building structures these deformations are not acceptable. From these studies it can be seen that the end conditions cannot be overlooked. A study conducted by Heidarpour and Bradford [36] found that the stiffness of the end connections of a steel beam exposed to fire directly effects the yielding and catenary actions of the beam. Furthermore, it must be noted that the thermal expansion within a member will cause stiffness in the beam if the ends are axially restrained.

2.5.2. Slenderness and the Euler Curve

From the critical loads the corresponding critical stresses can be obtained by dividing the load by the cross sectional area in Eq. (2.5.8):

$$\sigma_{cr} = \frac{P_{cr}}{A} = \frac{\pi^2 EI}{AL^2} \qquad (2.5.8)$$

If,

$$r = \sqrt{\frac{I}{A}} \qquad (2.5.9)$$

Then,

$$\sigma_{cr} = \frac{\pi^2 E}{\left(L/r\right)^2} \qquad (2.5.10)$$

Where L/r is the slenderness ratio.

This ratio depends on the dimensions of the column only. A higher slenderness ratio will result in a lower critical stress and vice versa. According to Ng and Gardner [6] critical temperature reduces with increasing load ratio which is defined as applied load divided by the compression resistance at room temperature. More importantly the variation of critical temperature with load ratio is slenderness dependant. Therefore this parameter is very important for use in the design of columns. By graphing the equation of critical stress the Euler curve is produced below in Figure 2-13.

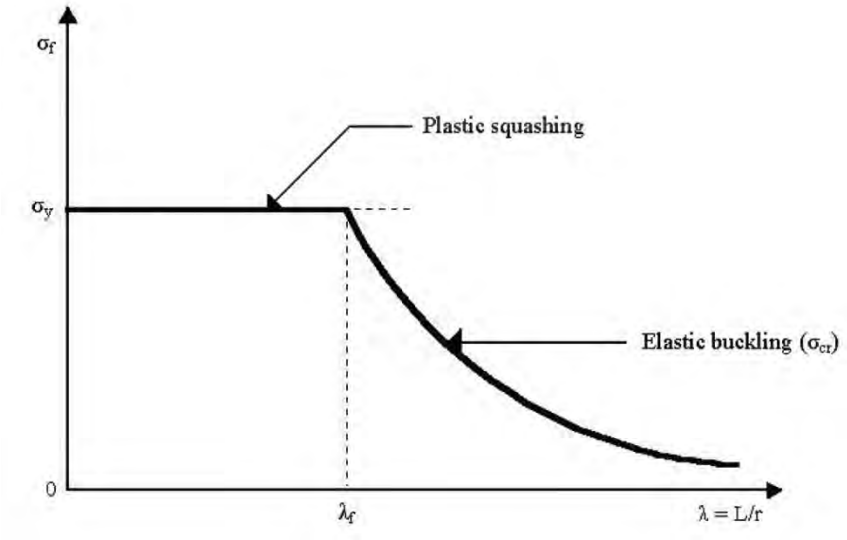

Figure 2-13: Euler Curve [37]

One can observe from the Euler curve that high slenderness ratios result in very low critical stresses. This part of the curve demonstrates the elastic behaviour of columns categorized as slender. As the slenderness ratio reduces the predicted critical stress can exceed the yield strength of the material. Therefore the material strength becomes the limiting factor as the column experiences plastic squashing as opposed to bending. Experimentally the data points fall below this curve in practice and the transition from elastic to plastic behaviour takes place gradually.

2.5.3. Localized Buckling

Column cross sections can be viewed as an assembly of plate elements. When these plate elements are slender in geometry, localized buckling will occur under high compressive stresses. Here the buckling of individual plate members occurs before the full strength of the column is reached as shown in Figure 2-14. This therefore has a significant impact on the critical stress of the column.

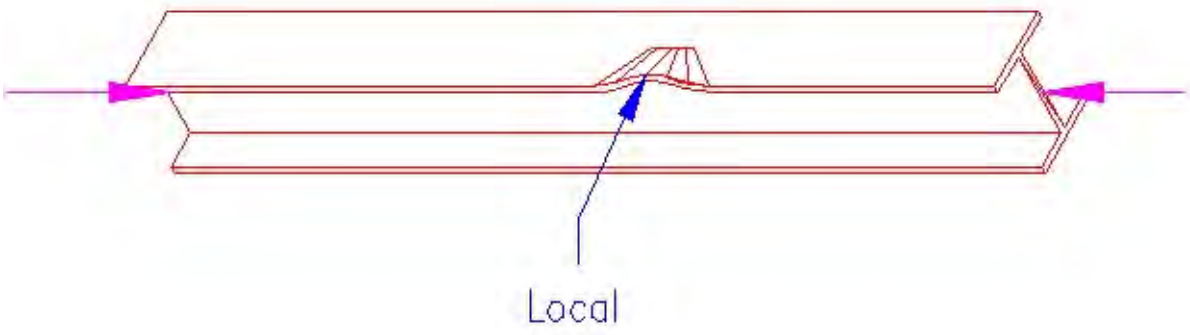

Figure 2-14: Localized Buckling [33]

The slenderness of these plate elements is determined by their width to thickness ratio as indicated in Figure 2-15 below. The higher this ratio the more susceptible these elements are to localized buckling. This ratio can be used in a similar fashion as with the slenderness ratio on the Euler curve. The plate elements are classified as compact and slender if the ratio falls within the plastic or elastic region respectively. One way to overcome this type of failure mechanism is to stiffen the plate elements. This can be done by restraining the edges of the elements. Typically an "L" shaped cross section is not stiffened as the both elements are only restrained on one edge. However, the web of a channel section can be classified as stiffened since both edges are restrained.

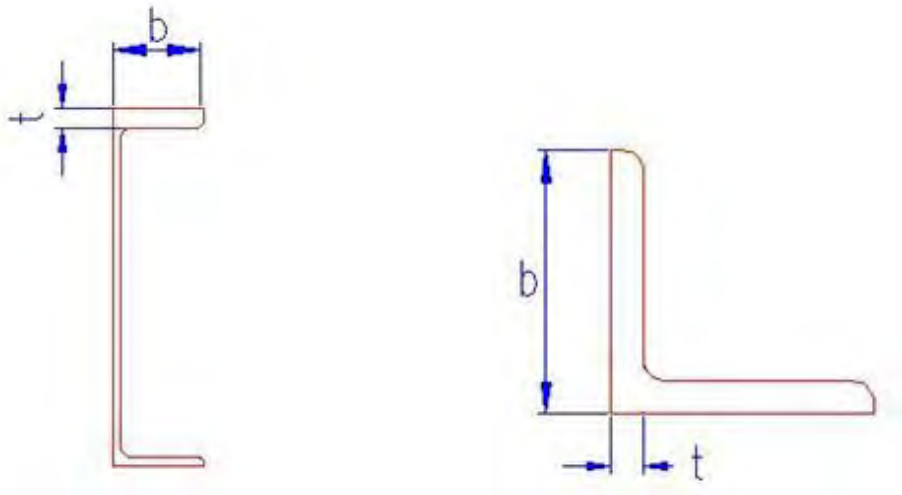

Figure 2-15: Plate Element Slenderness

The cross section geometry also plays an important role when predicting localized buckling. A study done by Guo and Fukumoto [38] indicated that the rounding of the cross

section corners delays the local buckling mechanism. These tests were conducted on stub columns and showed that an increase in the rounding radius inhibits localized buckling to an extent. Shown below is Figure 2-16 developed by Guo and Fukumoto [38].

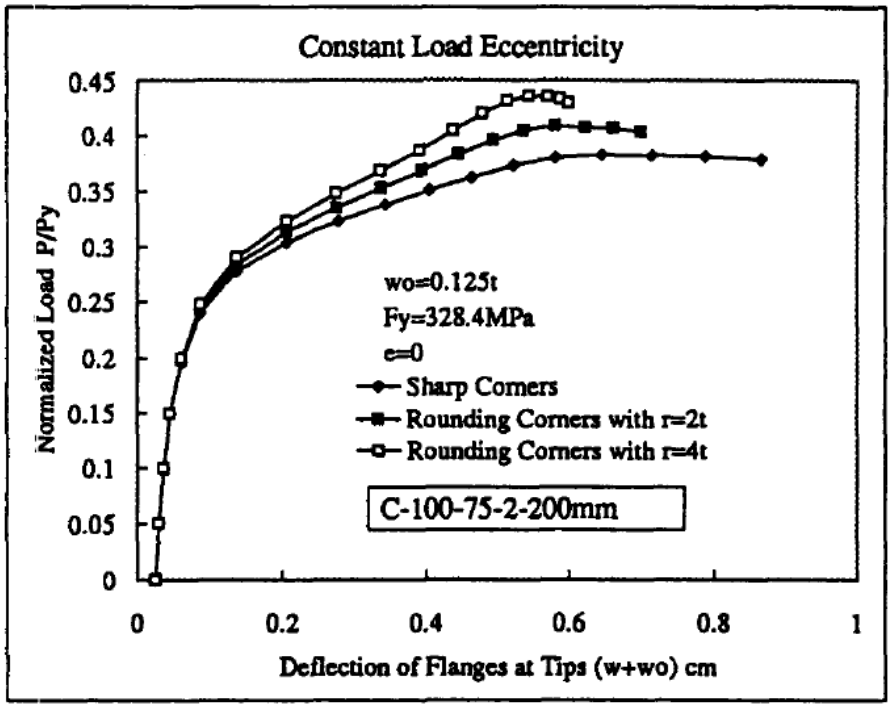

Figure 2-16: Graph of Load Vs Deflection for different rounding radii [38]

2.6. EXPERIMENTAL STUDIES

In order to understand the behaviour of steels in fire, the change in the mechanical properties of the steels at elevated temperatures need to be studied. Accurate material data is needed for finite element analysis in order to obtain reliable results. There are many simplified material models used to estimate the fire resistance of steels. Material data should be obtained from mechanical testing. Some of the widely known studies dealing with fire testing are outlined below. It must be noted that reference to the Eurocode 3 standard [1] is relevant within a South African context, as the SANS 10162 standard [39] was determined by Wellmanns [40] using a study by Mahachi [41] that these standards were ±10% within range of each other.

2.6.1. Helsinki University of Technology Transient State Tensile Tests

In the Laboratory of Steel Structures at Helsinki University of Technology (HUT), high temperature mechanical testing was carried out using the transient state tensile test method. Thereafter the results were compared to the European design standard, EN1993-1-2, [1]. The aim of this research was to provide results which would aid in the improvement of structural fire design and safety of steel structures. Material models based on these tests are suggested and existing material models are presented. Steel grades S355, S420M, S460M, S350GD+Z, S355J2H and EN 1.4301 were used in ambient and high temperature testing. In addition, the residual strength of materials at ambient temperature was investigated after fire exposure.

The tensile testing equipment used at Helsinki University of Technology has been verified in accordance with the standard EN 10 002-2:1992 [42]. The maximum load that can be applied using this equipment is 250kN. The heating action was accomplished by using an oven fitted with 3 resistor elements. The maximum temperature that the oven can reach is 1200°C. The maximum length of any specimen tested was approximately 220mm. Three separate temperature detecting devices where used to measure the temperature of the air with an accuracy of ±3°C. A high temperature strain gauge which was situated outside the oven, measured the strain on the specimen. Microsoft Excel was used to record and analyse the data and results from the tests. The tensile test specimens were in accordance with the European standard EN 10 002-5:1992 [43].

Transient-state and steady-state test methods were both used to carry out the high temperature tests. In transient-state tests the applied load is kept constant while the temperature is increased at a constant rate. A temperature strain curve is obtained from the recorded data which is then converted into a stress strain curve which allows for the calculation of the material's mechanical properties. Thermal elongation is accounted for in this process. The transient-state tests were carried out at different stress levels as well as different heating rates i.e. 10°C min^{-1}, 20°C min^{-1} and 30°C min^{-1}. It was noted that the creep effect gets bigger when the heating rate gets slower. The transient-state test method produces more accurate and reliable results than does the steady-state test method. In the steady-state tests the specimen is heated to a specific temperature and there after a load is applied to it. These tests can be strain or load controlled, where the strain rate or the load rate is kept constant respectively. It is noted that the strain rate has a significant effect on the results as indicated by Outinen [2].

The residual strength of steel after cooling down is dependent on the properties of the steel and the heating process. At high temperatures the strength of structural steel decreases but recovers quite well after cooling down. There is very limited experimental data available concerning the residual strength of steel after fire exposure according to Outinen [2].Furthermore, Outinen notes that prior research suggests a rough limit of 600°C, after which permanent loss of strength occurs. At lower temperatures, provided the steel structures are not distorted, the strength should still be adequate. Tests on S355 steel grade were done before and after high temperature testing. When the results were compared it was noted that the material strength is quite well preserved since the residual strength is found to be over its nominal value. These specimens were exposed to a maximum temperature of 710°C and were tested till collapse. It was concluded that if the distortions of the steel structure are within the tolerance limits then the material strength is still adequate. A more conservative approach is to use 90 % of the nominal yield strength.

2.6.2. Cardington Fire Tests

A study conducted by the University of Edinburgh titled, "Behaviour of steel framed structures under fire conditions" [44], found that steel beams in standard fire tests runaway well below temperatures achieved in real fires. The Cardington fire tests showed that runaway failure did not occur in real frame structures when subjected to realistic compartment fires. The study aims to understand this behaviour using computational models of the Cardington fire tests. The mechanics responsible for the robust behaviour of composite frames in fire is explained in detail. The main objective was to exploit the results of the large scale fire tests at Cardington in order to develop rational design guidance for steel frameworks at the fire limit state.

The fire resistance of structures based on single element behaviour in standard fire tests is a gross simplification of what actually happens when these elements act as part of a structural framework. Single element behaviour can be associated to determinate structures. A determinate structure has only one load path and its internal forces and stresses can be solved for by equilibrium conditions alone. Under collapse conditions, determinate structures fail when the most highly stressed region reaches capacity. This can be seen as runaway failures in the standard fire tests. Indeterminate structures on the other hand have multiple load paths and its internal forces and stresses cannot be solved

by equilibrium conditions alone. In contrast to determinate structures, when the load capacity is reached in a single section, the redundant structure can find different load paths and load carrying mechanisms in order to support additional load. Therefore in framed structures extensive redistribution of the load occurs during fire and this creates reserve capacity which reduces structural damage. This behaviour calls for the structural elements to be considered as a whole unit when evaluating its fire resistance.

Robust finite element models were developed using commercial software, thereafter being validated using results of the Cardington fire tests. Different models were developed to test the model sensitivities and assumptions. Methods of post-processing of results were developed to facilitate easier understanding. Parametric studies were conducted with simplified models to determine changes in structural behaviour. Results were compared to fundamental concepts and used to develop appropriate theory.

The key findings of [44] were that a composite steel framed building exhibits inherently stable behaviour under fire conditions due to the redundant nature of its' structural form. This behaviour can be characterized by thermo-mechanical phenomena which are dependent on the structural layout and thermal regime of the scenario. These phenomena include, buckling due to restrained thermal expansion, thermal bowing due to both temperature gradients and differences, high axial forces and large deflections due to large thermal straining, as well as material degradation and alternative load carrying mechanisms.

2.7. FINITE ELEMENT METHOD

Finite element analysis (FEA) is a numerical technique used to find approximate solutions of partial differential equations (PDE). It can also be used on integral equations. Both steady state and transient problems can be solved. In the latter a system of approximating ordinary differential equations (ODE) replaces the PDE and these are integrated using techniques such as Euler's method and Runge-Kutta. These techniques have been optimized in many ways as to reduce errors accumulated during intermediate calculations which affect the final solution. Various methods are applied to choose numerically stable ODE's which satisfy the original equation.

With advances in computer technology it has become very convenient and feasible to develop programs to solve these complex equation sets. FEA is very useful for problems in structural mechanics due to its ability to solve complex problems with elasticity. This is

due to mesh discretization, where a continuous domain is broken up into a set of smaller discrete sub-domains. These smaller sub-domains are called elements. Each element approximates the load displacement characteristics of a geometrically simple region. This is ideal for problems where the domain changes or the solution is not smooth. When modelling a system a set of finite elements are used. These elements are interconnected by nodes. Nodes are used to define a region in space where an element exists. Any motion of a node will cause the shape of an element attached to it to change. A node can have up to 6 degrees of freedom (DOF). Translation can occur in three directions and rotation about three axes. The number of nodes an element has depends on its type. The type of element used is dictated by the problem application. The strain in an element is determined from the motion of the nodes to which it connects.

2.7.1. Types of Elements

1 Dimensional (Beam)

2 Dimensional (Shell)

3 Dimensional (Solid)

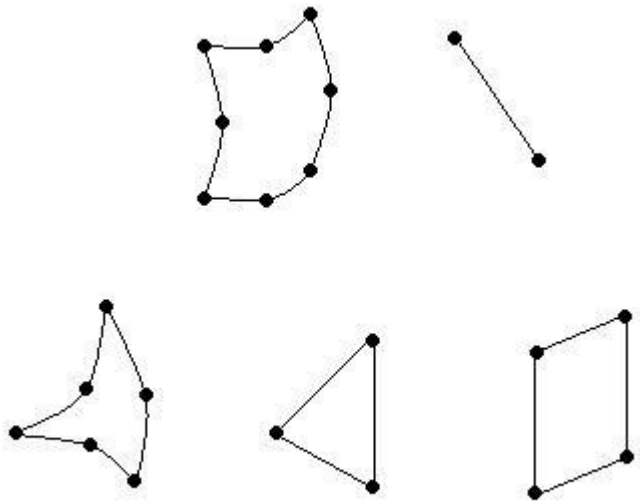

Figure 2-17: Various element shapes

FEA has a wide range of element shapes which can be used as shown in Figure 2-17. 1D elements or line elements are used when the members are long, slender and have a constant cross section. 2D elements or plate elements are used when the structure has a very small thickness in comparison to the larger dimensions. 3D elements are used when the dimensions are similar in all directions and the thickness is larger than what is acceptable for using a plate element. These classes of elements can be further categorised

according to shape and order. First order elements have a node at each corner which can model linear deformation of an edge. However, second order elements have a node at each corner as well as a node in the middle of the edge. This allows second order elements to model parabolic deformation of an edge. Even though second order elements are much more accurate than first order elements, the latter reduces solving time, is more robust in terms of distortion and works well with multi-type element meshes.

2.7.2. System Solution

In very simplified terms, the finite element method can be summarized in terms of the Eq. (2.7.1) below:

$$[F] = [K][U] \tag{2.7.1}$$

In most cases $[U]$ is the unknown parameter which is being solved for. $[U]$ is the displacement vector which represents the motion of the nodes. $[K]$ is the stiffness matrix which defines how loads are transferred between nodes. This is usually calculated using computer software. $[F]$ is the applied load vector which generally is defined from the outset and includes any constraints placed on the system as well as reaction forces.

Sample problem – Elongation of a thin rod

Due to the simplicity of this problem in Figure 2-18, the system can be modelled as a 1-Dimensional element with nodes 1 and 2 at either end. U_1 and U_2 represent the displacement of nodes 1 and 2 respectively. Node 1 has a fixed constraint as compared to node 2 which is constrained to move in the *x* direction only. Therefore F_1 is a reaction force opposite to the direction of the applied force F_2.

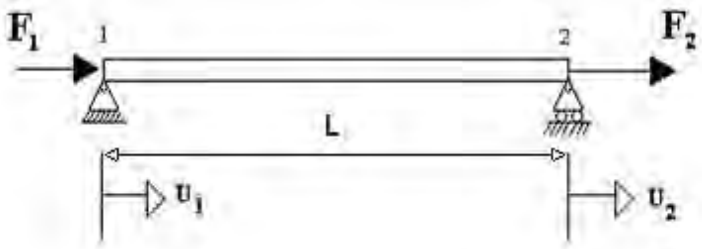

Figure 2-18: Simply supported thin rod

Strain:

$$\varepsilon = \frac{\Delta L}{L} = \frac{U_2 - U_1}{L} \tag{2.7.2}$$

Where, *L* is the original length of the rod.

Stress is given by:

$$\sigma = E\varepsilon = E\frac{(U_2 - U_1)}{L} \tag{2.7.3}$$

Where, *E* is Young's Modulus.

$$F_2 = \sigma A = \frac{EA}{L}(U_2 - U_1) \tag{2.7.4}$$

$$F_1 = \frac{EA}{L}(U_1 - U_2) \tag{2.7.5}$$

In matrix form:

$$\begin{bmatrix} F_1 \\ F_2 \end{bmatrix} = \frac{EA}{L}\begin{bmatrix} 1 & -1 \\ -1 & 1 \end{bmatrix}\begin{matrix} U_1 \\ U_2 \end{matrix} \tag{2.7.6}$$

To solve for $[U]$:

$$[U] = [K]^{-1}[F] \tag{2.7.7}$$

2.7.3. Software Package

The software package used in this research is SimXpert 2010 [3]. It is a fully integrated multi-discipline simulation environment. It uses an MSC solver, MD Nastran, to carry out the various computations. SimXpert has many features which make the modelling and simulation process as efficient as possible. These include native CAD access with bi-directional interoperability, pre-processing, solving, post-processing and automation capabilities [45].

2.8. CHAPTER SUMMARY

This chapter has put the current research in perspective with regards to current literature and developed theory. It has covered various material properties and mechanical behaviour of structural steels including fire resistant steels and their coatings. High temperature failure mechanisms were briefly mentioned along with their importance to the topic at hand. The behaviour of fire and how it affects the stability of structures were looked at, giving a basic introduction to fire modelling. Post fire effects were discussed with respect to residual stresses and the degradation of hardness due to heat treatment. An overview on the fundamentals of buckling theory, specifically on end conditions and modes of failure were presented in order to grasp a firmer understanding of the problem. An independent experimental study on high temperature behaviour of steel was reviewed to gain insight into methods and procedures used by other leaders in this field of research. Within in this the reusability of steel after fire exposure was touched on. In addition, a report on the benchmark for full scale fire tests conducted at Cardington was discussed which highlighted the major differences between isolated experimental methods and full scale fire tests. Finally this literature review is brought to a close by introducing the concept of finite element analysis and outlining the fundamentals for a novel understanding.

3. EXPERIMENTAL FRAMEWORK

This chapter contains the crucial information on the type of experiments conducted in the laboratory, any assumptions made and the procedure of obtaining the experimental data which is the basis for this research. The Steady state tests with tensile and combined loading for 350W were carried out as an undergraduate project at the University of KwaZulu-Natal to aid in this research and provide data for comparison between computer simulations. A high temperature test rig which allowed for various cross sections to be subjected to combined loading at various temperatures was designed and built. Reusability tests were conducted at the ArcelorMittal South Africa Quality Management Material Laboratory on S355. The reusability tests were carried out by heat treating metals and recording stress, strains and hardness numbers after cooling down. Equipment used in these tests will be presented as well as the testing methods and preparation of the test pieces.

3.1. STEADY STATE TENSILE AND COMBINED LOADING TESTS

The tensile and combined loading tests were carried out using the steady state method presented below due to its ease and convenience. Transient tests were not possible with the current equipment even though these are more accurate as experienced by Outinen [2]. The stress strain curves, as well as the yield and ultimate tensile strength were captured at various temperatures.

3.1.1. Testing Equipment

An Instron 5500R Universal testing machine was used in addition to heating elements, insulation and temperature measuring devices. Together these components allowed for tensile testing of Dog-bone shaped test pieces at elevated temperatures. This machine accurately recorded the results and automatically generated computer graphs of load versus extension. In order to obtain high temperatures the test pieces were inserted through a 30mm diameter aluminium cylinder which was wound with 3m of heating tape. Brass wool was used to fill the gaps between the test piece and cylinder in order to increase the conduction rate of heat to the test piece and to improve the heat distribution. U-Thermo Mat 3 which is a glass fibre wool insulator was used to increase the efficiency of

the heating tape. Figures 3-1 and 3-2 below illustrate the setup of the Instron 5500R with the heating mechanism.

Figure 3-1: Inston5500R Setup for Steady State Tensile Temperature Tests

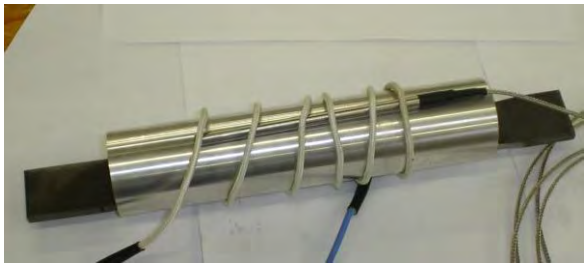

Figure 3-2: Trace Heating Setup

The heating system used a constant wattage heating tape which provided even heat distribution at 50 watts per meter. A digital temperature controller was connected to the tape to regulate the power supplied to it. The controller accuracy is within 3 to 5 degrees of the desired value. Two J-Type thermocouples were used to measure the temperature of the cylinder surface as well as the surface of the test piece.

3.1.2. Combined Loading Test Rig

In order to conduct tests on a larger scale, a rig was built using a hydraulic actuator to create linear stresses and a lever arm to create torsion (Figure 3-3). By varying the weight applied on the lever arm the required torsional stresses were induced in the specimens. This device has a modular design to incorporate specimens of various cross sections. The gripping devices can therefore be replaced to accommodate the particular test piece. This study uses the angle iron gripping device seen in Figure 3-4. The heating system is similar to that used on the Instron but on a larger scale. The length of heating tape is increased to 6m and the aluminium cylinder has an increased diameter of 100mm. U-Thermo Mat 3 was also used as an insulator.

Figure 3-3: Combined Loading Test Rig with Heating Mechanism

Figure 3-4: Angle Iron Gripping Device

3.1.3. Test Pieces

For the combined loading tests, 1 meter lengths of 50x50x4 350W angle iron were used as shown in Figure 3-5. According to best practices if smaller scale tests are to be carried out, these test pieces must be cut from the original large scale specimen. Therefore the steady state tensile test specimens were cut from the 1 metre long angle iron beam sections of dimensions 50 by 50 by 4mm using a CNC milling machine. Each specimen was 300mm long and fashioned in a Dog bone shape seen in Figure 3-6 below. The ends of the specimen are wider to allow for a larger gripping area and to ensure compatibility with the gripping device used. The mid-section was reduced in order to decrease the cross sectional area and therefore ensure failure in that region. This also allowed for a more controlled gauge length. The preparation was guided by SABS and ASTM [46] standards where possible, specifically SANS 6892:1998 [47] and SANS 7500-1:2009 [48]. See Appendix C for detail drawings.

Figure 3-5: 50x50x4 350W Angle Iron Test Piece

Figure 3-6: Dog-bone Test piece cut from 50x50x4 350W Angle Iron

On the large scale combined loading tests the angle iron had to be drilled on either end to allow for it to be secured to the grips of the machine. This naturally will be the weakest point of the specimen where failure will occur. Since this is not acceptable to maintain the accuracy of the results, these ends were reinforced with an extra metal piece which was

welded on (Figure 3-7). To ensure that the point of failure occurred within the middle region of the specimen where the heating mechanism is applied, a notched area was created as shown in Figure 3-8. As stated in SANS 6892 [47], this reduction in area will not affect the test results as long as there is a transition curve between the different dimensions.

Figure 3-7: Reinforced Ends

Figure 3-8: Notched Area

3.1.4. Testing Procedure

In both the steady state tests the heating procedure remained the same. The temperatures at which the specimens were evaluated included; 25°C (room temperature), 100°C, 200°C, 300°C and 350°C. The test pieces were secured in the respective machines with the heating apparatus setup as mentioned above. The test pieces were heated to the required temperature at an approximate heating rate of 6°C/min. This low heating rate increased accuracy by ensuring a more even heat distribution on the specimen. Thereafter the test pieces were held at the final temperature for approximately 30 minutes. The respective loading scenarios were then applied at the elevated temperature till fracture occurred. The strain rate was controlled at 5mm/min. In the combined loading tests, once the test piece was held at the final temperature the specimen was yielded using a torsional load calculated using the data from the tensile tests on the Dog-bone shaped specimens. See Appendix E for yield angle calculations. Thereafter a tensile load was applied to fracture the material.

3.2. REUSABILITY TESTS

For the determination of the reusability of 350W and S355 Structural Steel, tensile tests were carried out using tensile testing machines as in the steady state tensile tests. However, no heating elements were incorporated as all tensile tests were done at room temperature. Dog-bone shaped test pieces with the same dimensions as stated before and cut from the same 50x50x4 350W angle iron were used. S355 specimens were cut from hot rolled steel coils with identical dimensions. The results were again generated electronically using tensile testing machines. Rockwell Hardness testing was also carried out to predict strength properties. The 350W tests were carried out at the University of KwaZulu-Natal, Discipline of Mechanical Engineering. The S355 tests were carried out at ArcelorMittal South Africa Material Laboratory.

3.2.1. Testing Equipment

In order to preserve some consistency in the tests done at both institutions, similar equipment specifications were used. A heating oven was used to treat the Dog-bone shaped specimens as well as smaller rectangular specimens of the same material. The rectangular specimens had dimensions of 60mmx20mmx4mm. The dimensions of the oven were 40cm x 30cm x 25cm. The oven was well insulated and allowed a maximum temperature of 800°C. The accuracy of the temperature readings were ± 5°C. A thermocouple with a probe was used to measure the oven temperature.

A hardness testing machine was used to test the hardness of materials before and after heat treatment. Preliminary tests revealed that the Rockwell C Hardness test did not cover the hardness range of the material. Therefore the Rockwell B Hardness test which caters for softer materials was used. All hardness testing machines used were calibrated before use and testing was in line with SANS 6508-1:2009 [49].

3.2.2. Testing Procedure

The testing procedure for the 350W and S355 specimens differ only in the heating patterns. In both cases the oven was preheated to 150°C. This was done to ensure that the oven was evenly heated and that all test pieces experience the same initial thermal shock and heat distribution. Regardless of the heating pattern used, once complete, all specimens were allowed to air cool overnight.

There after Tensile tests were than conducted on the tensile testing machine using the specimens which were heated and cooled down. A specimen which was not exposed to any heating and cooling was also tested for each material to form a baseline for comparison of the results. The loading rate was kept at 5mm/min.

Hardness tests were carried out on the rectangular specimens once they were cooled. A steel brush was used to scrape of as much scale as possible on the specimens to reduce errors. There after the specimens were soaked in a HCL solution. The beaker containing the specimens with the solution was placed in a bowl with boiled water to increase the pickling speed. Again the above specimens which were not subjected to heating and cooling were also tested. Each specimen was tested 10 times each at different areas of the specimen on both sides. In this way an average value for the hardness was arrived at.

The heating patterns for the two materials were as follows:

- **350W**

A Dog-bone shaped test piece as well as a rectangular specimen initially at room temperature was placed in the heated oven. The test pieces were heated to the required temperature at an average rate of 8°C/min. Irrespective of the final temperature each set of specimens were held in the oven for a duration of 4 hours including the heating phase. This process was repeated three times with different specimens at holding temperatures of 400°C, 650°C and 767°C. The specimens were allowed to be air cooled overnight back to room temperature. For a graph of the heating pattern see Appendix D.

- **S355**

All Dog-bone and rectangular shaped specimens were placed in the heated oven at the same time. The test pieces were initially at room temperature. An average heating rate of 8°C/min was used to get the specimens to the required holding temperatures. The holding temperatures in order were 400°C, 600°C and 800°C. At each holding temperature the specimens were held for 20 minutes after which one pair of Dog-bone and rectangular shaped specimens were removed and air cooled. For graph of heating pattern see Appendix D.

4. EXPERIMENTAL RESULTS

This chapter presents the results and outcomes of the experimental work performed in the laboratory. These include the steady state tensile tests, the combined loading tests as well as the reusability and hardness testing. Any calculations used in the recording and analysis of the results are elaborated on. Comparisons to other literary results in this field are evaluated as well as the conformance to fundamental theory.

4.1. STEADY STATE TENSILE TESTING

The results of the tensile tests were captured as load versus extension graphs. From these computer outputs the stress versus strain graphs were calculated. Using the 0.002 strain offset method the yield strength was obtained. Figure 4-1 below illustrates the stress strain graph at room temperature.

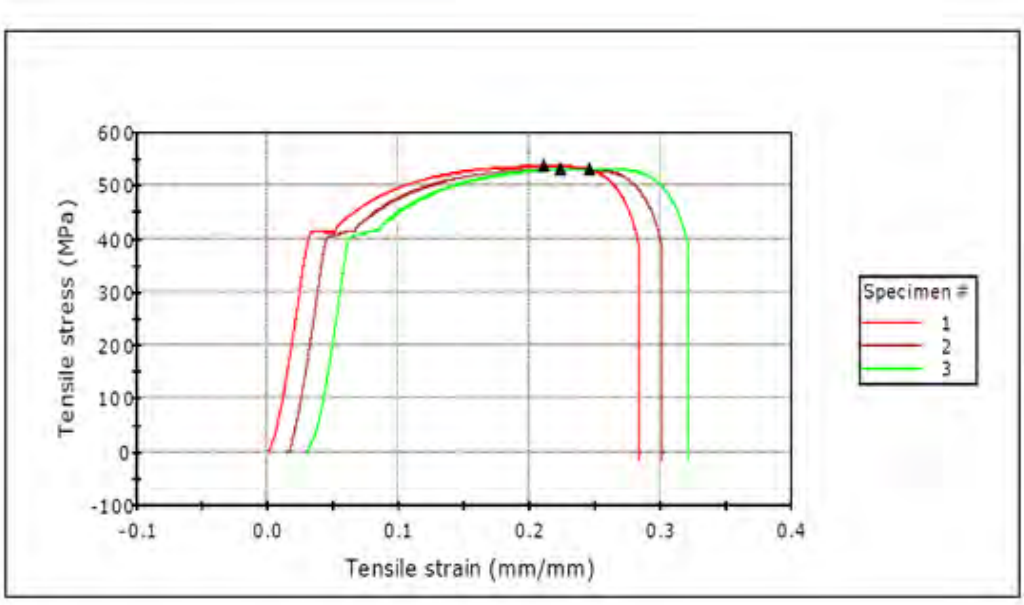

Figure 4-1: Stress Vs Strain graph at room temperature

The torque and yield angle were also calculated to aid in the setup of the combined loading tests. See Appendix E for calculations. To better understand the results obtained, yield strength reduction factors were calculated at the various temperatures and plotted. The results of the steady state tensile tests are summarized in Table 4-1 below.

Table 4-1: Data and Results of steady state tensile tests

Temperature (°C)	Yield Strength (MPa)	Yield Angle (°)	UTS (MPa)	Torque (Nm)	Yield Strength Reduction Factor
25	355	70	533	182	-
100	330	65	526	169	0.93
200	299	59	520	153	0.85
300	278	55	516	142	0.78
350	271	53	513	137	0.76

The results showed an inversely proportional relationship between temperature and yield strength as well as temperature and ultimate tensile strength. This is supported by Chen et al. [50] in the study of the behaviour of high strength steels at elevated temperatures. Chen et al. [50] used higher strength steels with yield strengths in excess of 600MPa at room temperature. This can be a cause for the higher reduction factors as compared to that of 350W structural steel. At a temperature of 350°C the reduction factors differ by 0.1 which is acceptable due to the fact that the material and test programs differ substantially. Figure 4-2 below illustrates the common trend between the two studies.

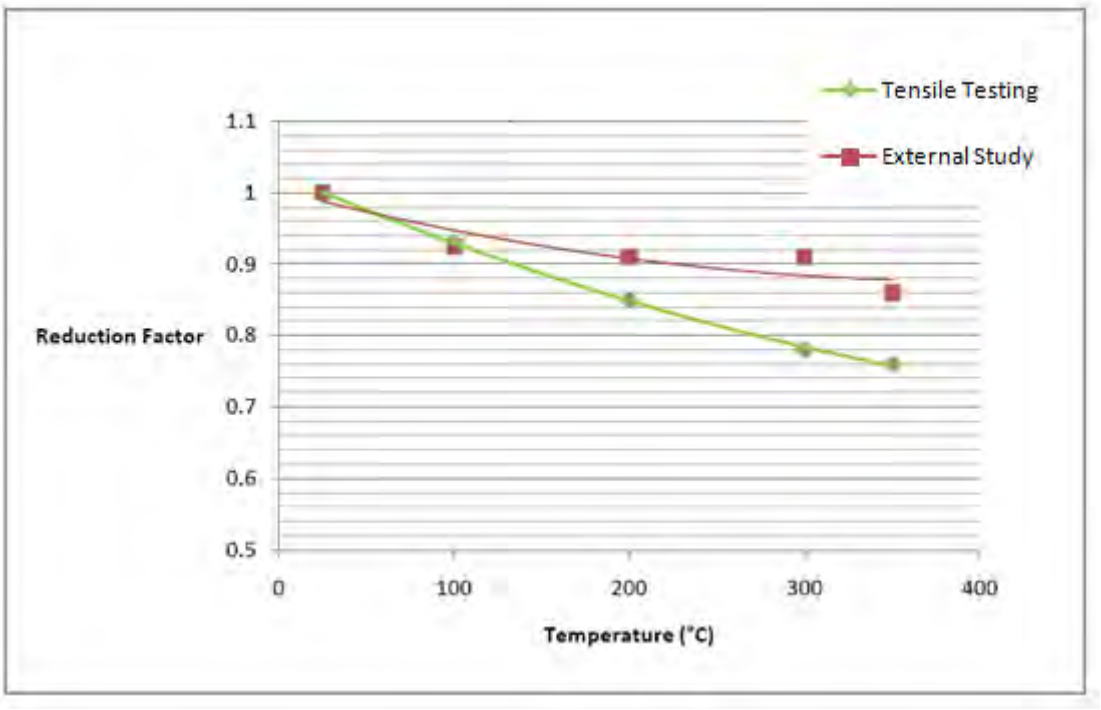

Figure 4-2: Comparison of yield strength reduction factors

The experimental studies done at the Helsinki University of Technology by Outinen et al. [51] compared their test results to those of various design codes. It can be seen from the Figure 4-3 below which has been developed by Outinen et al. [51], that the Eurocode 3 model is very close to the behaviour of the transient state tests conducted by [51]. The results of this study were superimposed on the Helsinki data in Figure 4-3 and indicated a close trend to the French design recommendations. The metallurgical composition of the material tested at Helsinki was S355 as compared to 350W used in this study which can explain the slight discrepancies. The overall trend between the S355 and 350W materials is very similar, in that the only difference is the initial yield strength at room temperature which shifts the trend vertically. Chen et al. [50] found that yield strength reduction factors to be similar to the Eurocode 3 standard, but falling on the un-conservative side.

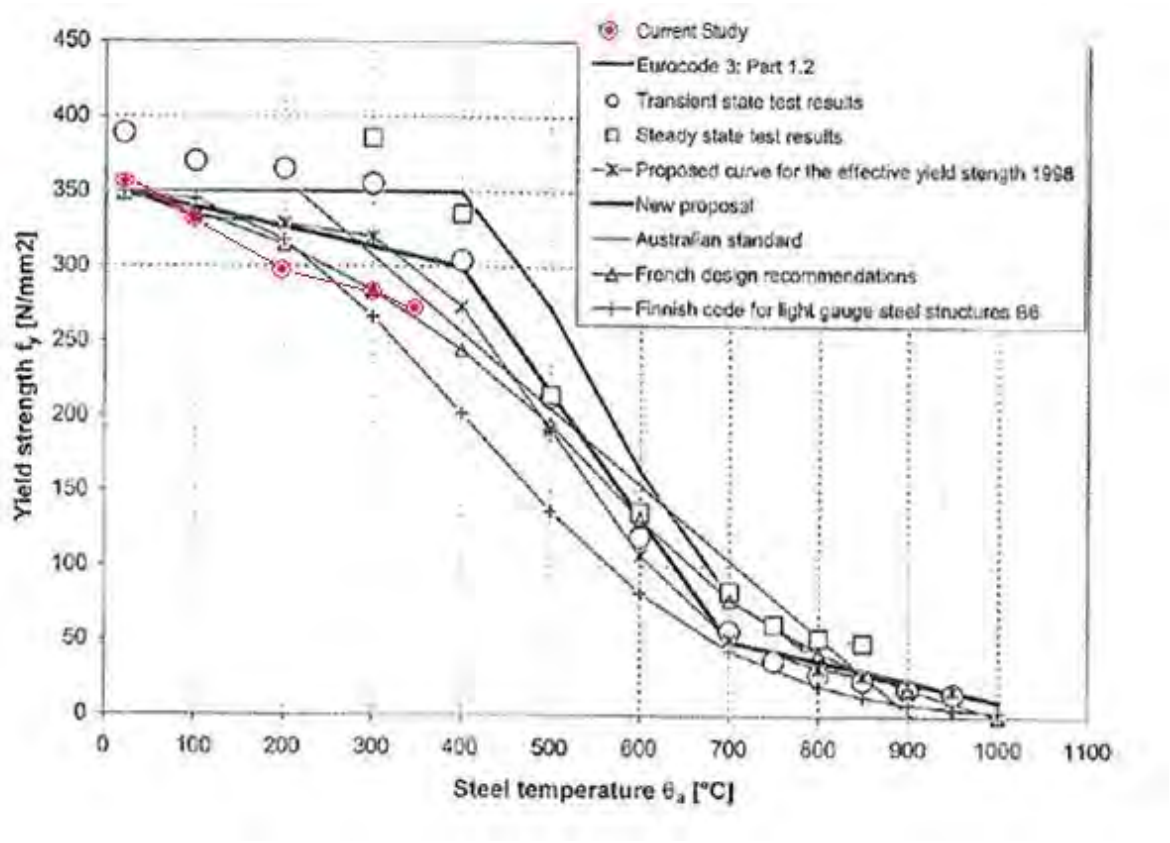

Figure 4-3: Comparison of yield strength Vs temperature with Helsinki Study

4.2. COMBINED LOADING TESTS

These tests were done in a steady state fashion where the specimen was heated to the desired temperature and torsionally yielded by using the yield angle data from the steady state tensile tests and then loaded in tension till fracture. An inversely proportional relationship between temperature and ultimate tensile strength was observed. The results of these tests are presented in Table 4-2 below.

Table 4-2: Results of Combined loading tests

Temperature (°C)	Critical Loads (KN)	UTS (MPa)	UTS Reduction Factor
25	137	634	-
215	124	574	0.91
280	118	546	0.86
380	104	482	0.76

Figure 4-4 below compares the ultimate tensile strength reduction factors for both the tensile tested and combined loading specimens. It can be seen that the combined loading specimens have an exponential reduction in ultimate tensile strength as temperature increases as compared to the approximate straight line trend of the steady state tensile tests. Therefore combined loading has a significant impact on the strength of a specimen at higher temperatures.

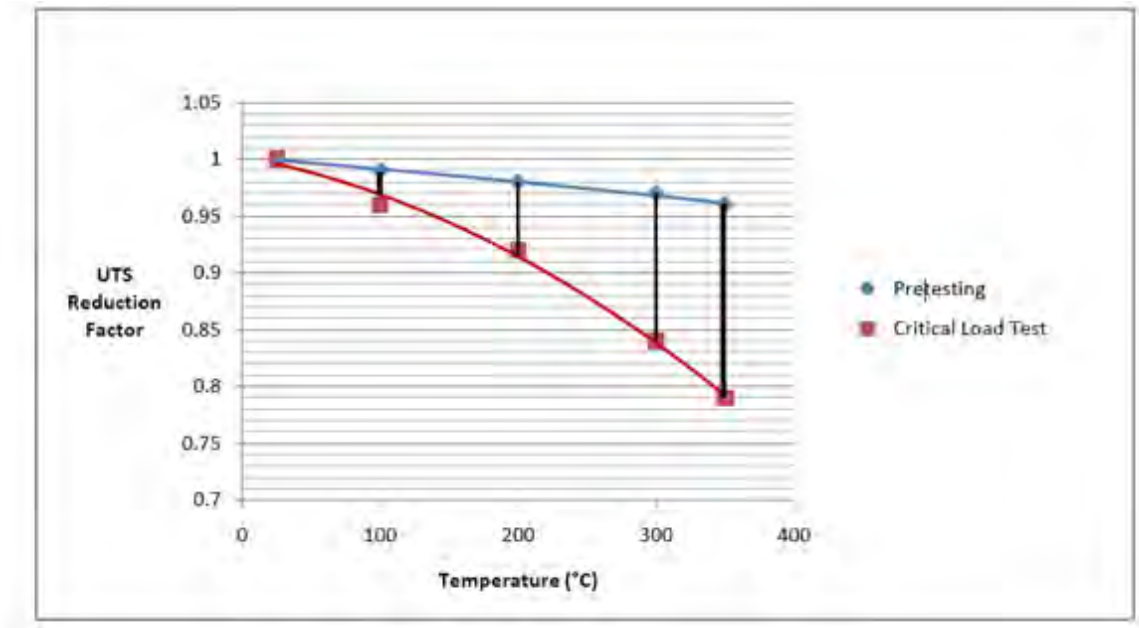

Figure 4-4: Comparison of tensile and critical load tests' UTS Reduction factors

4.3. REUSABILITY TESTS

Dog-bone shaped specimens and rectangular specimens were heated to various temperatures as laid out in Chapter 3. After being air cooled to room temperature the dog bone pieces were tensile tested. Hardness testing was then carried out on the rectangular test pieces. Tables 4-3 and 4-4 below present the average hardness on each rectangular specimen as well as the ultimate tensile and yield strength from the tensile tests for both material grades.

Table 4-3: Reusability test results for 350W

Specimen	Maximum Temperature (°C)	Hardness - Rectangle (HRB)	Ultimate Tensile Strength (MPa)	Yield Strength (MPa)
1	25	73	438	306
2	400	71	435	291
3	650	69	398	278
4	750	67	411	271

Table 4-4: Reusability test results for S355

Specimen	Maximum Temperature (°C)	Hardness – Rectangle (HRB)	Ultimate Tensile Strength (MPa)	Yield Strength (MPa)
1	25	87	533	461
2	400	85	553	492
3	600	83	553	497
4	800	75	448	371

From the test data for the 350W experiments, an important trend is seen with respect to the yield strength of the material. As the maximum exposure temperature is increased the yield strength after cooling down decreases. This is important as the yield strength of the material is the typical value considered for design purposes. However, this is still a minor change of approximately 10% with heating temperature at 767°C. Figure 4-5 below illustrates this trend. The graphs are staggered along the x-axis to make the difference more clear.

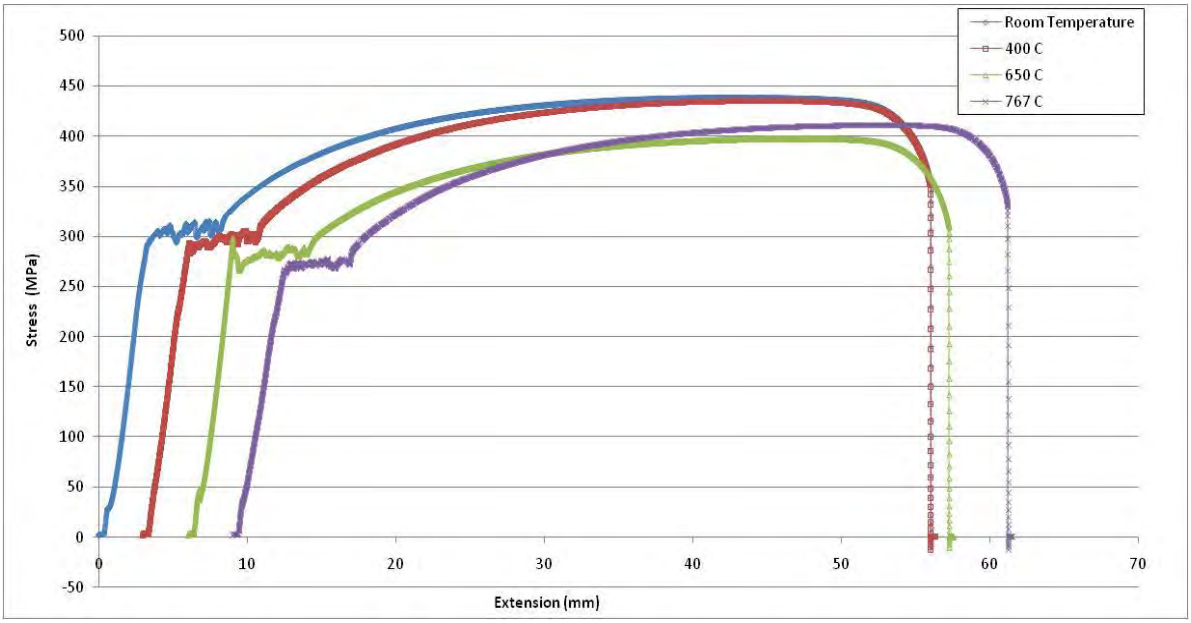

Figure 4-5: Stress Vs Extension graph of heated and cooled 350W specimens

When looking at the results from the tests done on the S355 specimens, a slightly different trend is seen. In Figure 4-6, for the maximum exposure temperatures of 400°C and 600°C, the yield strength showed minor increases from the room temperature value. However, the specimen exposed to 800°C showed significantly lower yield strength than that of the unheated specimen. This is due to the actual changes within the microstructure of the material and will be discussed in more detail in Chapter 5.

If the behaviour of the ultimate tensile strength for both materials is observed, it can be approximated to follow the same trend as that of its respective yield strength as shown in Figure 4-7. However, the average hardness values for each material both follow a similar decreasing trend as the exposure temperature increases. It must be noted that these values are all obtained at room temperature to alleviate any confusion. It can also be seen that the hardness of both materials decrease more rapidly as the 700°C temperature is reached and beyond.

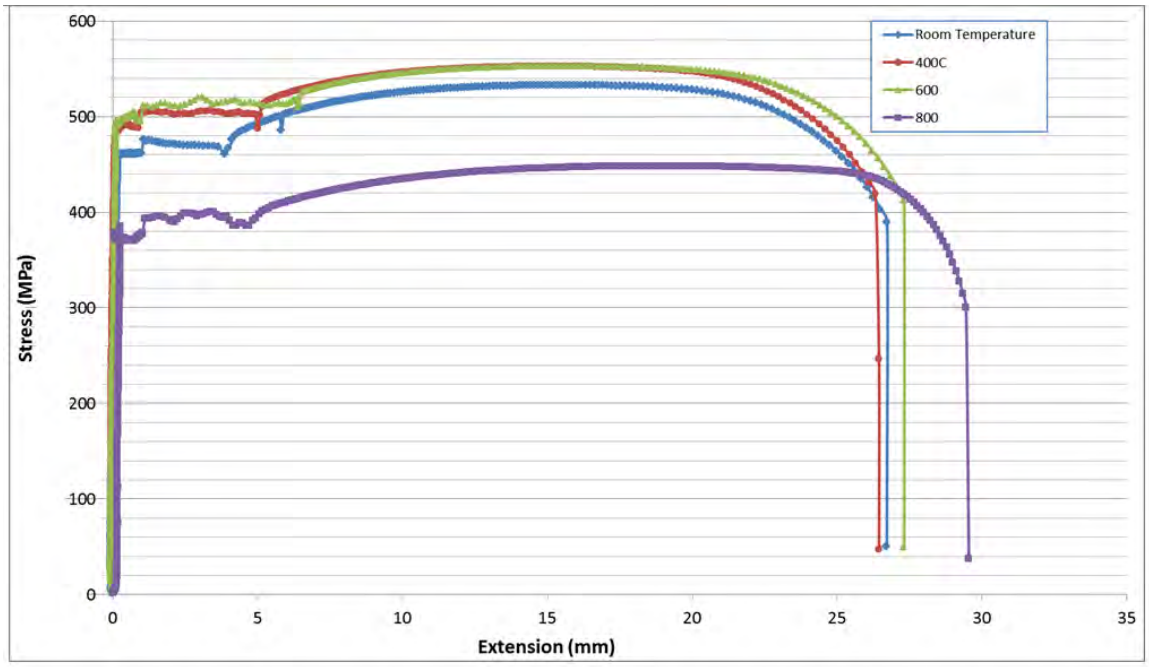

Figure 4-6: Stress Vs Extension graph of heated and cooled S355 specimens

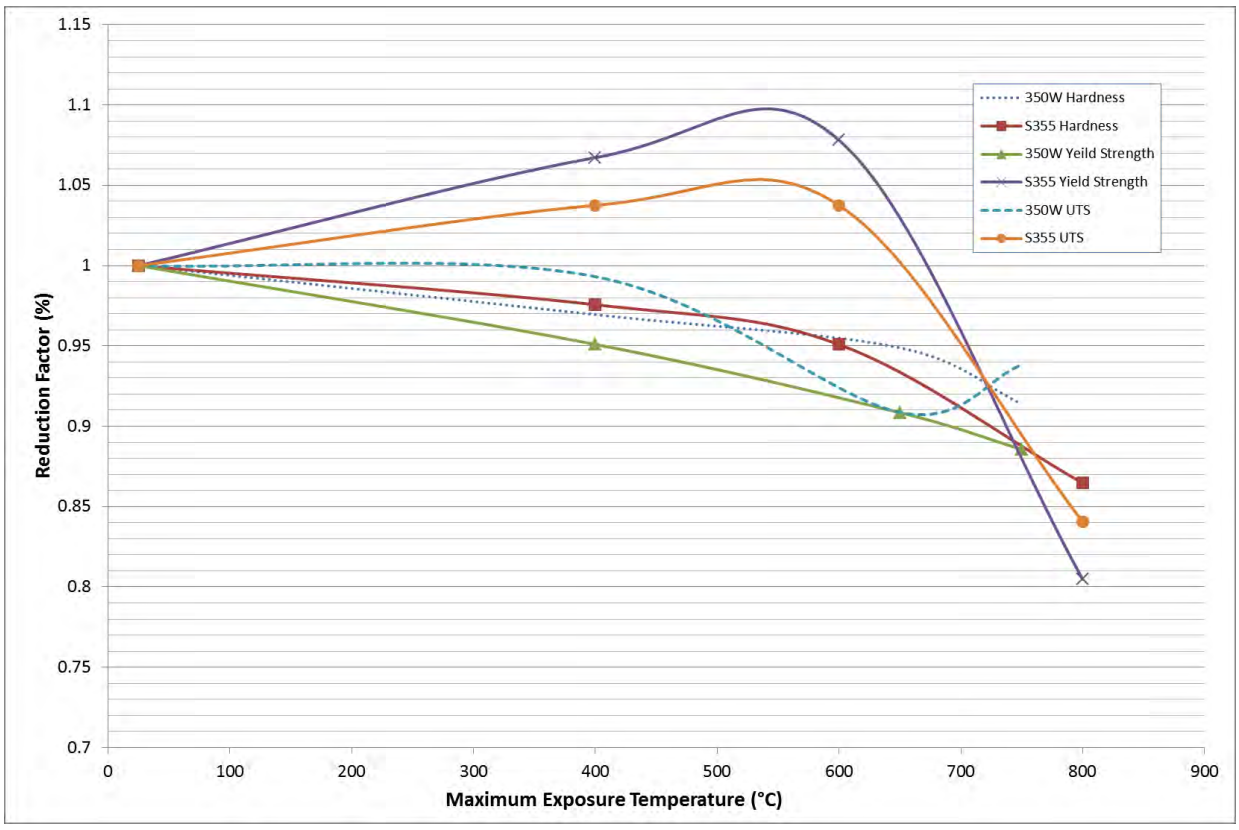

Figure 4-7: Reduction factors of UTS and Hardness Vs Temperature

5. DISCUSSION OF EXPERIMENTAL RESULTS

5.1. STEADY STATE TENSILE TESTS

As was expected the initial tensile tests conducted at the University of KwaZulu-Natal illustrated the inverse relationship between yield strength and temperature. Even though the less accurate steady state method was used as opposed to the transient state method, the results agree with the study by Chen et al. [50] on the behaviour of high strength steels at elevated temperatures. The maximum temperature reached of 350°C showed a reduction in yield strength of 0.76. This was compared to a 0.86 reduction seen by Chun et al at the same temperature. It can be seen that even materials with yield strengths in excess of 600MPa, there is still a close correlation between yield strength and temperature. A difference of 0.1 in the reduction factors can be attributed to the differences in yield strengths. Softening of the material is a direct cause for these reductions.

When compared to the design codes and experimental data of the study conducted at the Helsinki University of Technology [51], these results are on the lower end of the spectrum. However, they do fall within 20% of the design code recommendations. Although the design codes are drawn up for S355 the results follow the French design recommendations quiet closely. Again this cannot be assumed the same for temperatures greater than 400°C as the temperature range in these tests were limited. If reduction factors are used, then the results of this study correlate well with the transient state results of [51]. This indicates that the Eurocode 3 standard can be applied with confidence when working with 350W at temperatures below 400°C. For temperatures above 400°C it is highly possible that the Eurocode 3 standard can model the behaviour of 350W, however, more experimental data must be gathered.

With respect to a building fire these tests are very basic. As with a building fire the load is applied from room temperature and is not uniformly distributed. In a building, members are not isolated but form part of complex structure, which creates various temperature and load distributions. Typically the load is more likely to be a compression load rather than a tensile load. Here tensile loads were only applied once the specimen had reached the test temperature as opposed to a constant load. One point of concern is that in a fire, temperatures are closer to approximately 800°C and this test has not come close to those values. This would be a more critical temperature range as the trend predicts greater and more significant yield strength reduction.

5.2. COMBINED LOADING TESTS

The combined loading tests were developed to simulate a much closer building fire scenario than that of a tensile test. Here the larger specimens had a common cross section found in buildings. However, the limits of the test rig did not allow for axial compression. Therefore the specimens were torsionally yielded to represent torsional buckling and a tensile load applied at the same time. This resulted in a much more significant reduction in ultimate tensile strength than for the steady state tensile tests. A reduction factor value of 0.78 compared to 0.96 at 350°C shows that combined loading in this way produces more significant decrease in strength than axial forces alone. This demonstrates that various design standards must be used with caution as there are many other factors affecting the integrity of a steel member in real situations. These tests were carried out at specific temperatures while the load was gradually increased until fracture occurred. In a real building fire this load is not gradual and is present throughout the entire heating process.

5.3. REUSABILITY TESTS

The reusability tests were done to determine what effect on strength if any does high temperatures cause after the steel structures have cooled down. In real world situations this is a very complex process and difficult to replicate within a laboratory. Two sets of specimens were used, each set exposed to a distinct heating pattern. Basic tensile tests were carried out on Dog-bone shaped specimens for both heating patterns after they were cooled down. With 350W specimens a clear trend between Yield strength and temperature was seen. The higher temperature the specimen was previously exposed to, the lower the yield strength at room temperature. However, the changes were not very significant as a reduction to only 90% of the yield strength was seen at 767°C. These findings are in line with those determined by Qiang et al. [52] who observed that members exposed to fires below 600°C where not effected and could be reused. It must be noted that the heating pattern used on the 350W material in this study, ensured the specimens were heated for duration of 4 hours. This is enough time to allow for some softening of the material. Looking at the S355 specimens which were held at elevated temperatures for a considerably shorter period of time, an increase in yield strength is seen with increased exposure temperature. However, for the specimen exposed to 800°C, a decrease in yield strength is seen. This slight increase in strength at the lower temperatures is due to partial re-crystallization which occurs in the microstructure when the transformation temperature has not been reached and a high cooling rate is present. Even though air cooling was conducted, the size of the specimens allow for induced quenching. The 800°C

specimen reached well over the transformation temperature and had a temperature exposure duration which was longer than the rest. Therefore softening was able to take place as was seen with the 350W specimens.

With regards to the ultimate tensile strength a similar trend was seen as with the yield strength for both 350W and S355. Some minor irregularities were seen but this could be due to uneven cooling or material defects. Overall the ultimate tensile strength followed the behaviour of the yields strength. The yield strength was more sensitive to the temperature and showed greater differences from room temperature values. Therefore the ultimate tensile strengths were treated as a secondary effect. It can be said that a test piece is reusable until 700°C after which its strength will be reduced to less than 90 % of its original yield strength. This is supported by Outinen [2] in the study of the mechanical properties of structural steels at high temperatures and after cooling down.

The Hardness tests that were conducted also showed very minor changes. At the temperature range tested no direct correlation could be found between hardness and the yield or ultimate tensile strengths. Other studies [53-55] have correlated hardness to ultimate tensile strength but this change in hardness was brought about by cold forming and not heat alone. Hardness does show a decreasing trend with increase in exposure temperature, however, at temperatures below 600°C this change is negligible for both materials irrespective of the heating pattern. At temperatures higher than this the Hardness decreases more rapidly. Hardness as a result of temperature is also dependant on the duration of the exposure as investigated by Mukhopadhyay et al. [32]. Therefore a more accurate behaviour of hardness with respect to temperature can be done by keeping the exposure time constant.

It is important to note that in real life situations the heating and cooling process are all conducted with the presence of a constant load. This causes residual stresses as explained in the literature review. In addition, it is assumed that there are no distortions in the structure due to explosions or “Flashover” which is common in building fires. In these tests the specimens were allowed to cool down in ambient air. Often structures on fire may experience some sort of quenching from the efforts of a fire department etc. Uniform cooling is not always possible. In many cases the heat on the surface of the structure is much higher than the actual temperature within the cross section of the structural member.

6. SIMULATION FRAMEWORK

This chapter contains an overview of the type of computer simulations carried out in this study, the development of these models and all assumptions and parameters used. These simulations will be verified with the theory and experimental work. The significance of these simulations will be highlighted and the scope it presents as a solution to further problems. This study aims at presenting a basic application of the FEA software to demonstrate the fundamental advantages of computer simulations. From the experimental work done in this study it can be assumed that the S355 and 350W materials show negligible differences in their composition and behaviour and can therefore be modelled using the same data. In retrospect, it must be noted that much more complex setups are possible, but for clarity sake are not included in this study.

6.1. LINEAR ANALYSIS

With a linear analysis the behaviour of the material within the proportional range is of concern. In this study the yield strength was assumed to be the ultimate stress limit where an acceptable amount of linear behaviour is observed accurately. The solver used is the SOL101 [45], which is suited for a linear static analysis. The load is applied statically without a ramp and can be associated with a step function. Young's Modulus and Poison's Ratio determines the behaviour of the geometry. No stress-strain data is required. At elevated temperatures Young's Modulus changes for that specific temperature load and the thermal coefficient of expansion makes a significant contribution to the end result.

6.2. NON-LINEAR ANALYSIS

With a non-linear approach, results are more accurate and the entire range of the specimen's behaviour can be simulated. This is limited to the fracture point which requires a more complex analysis. In order to accommodate non-linear data input the SOL400 [45] solver is used. Again a static analysis will be conducted for simplicity sake. Effectively this resembles the steady state tests but with a step load applied. Stress Strain curves for different temperatures are inputted into the model along with the thermal coefficients of expansion. Again Poisson's ratio is also required.

6.3. S355 EUROCODE MODEL

6.3.1. Geometry

All geometry was drawn using CAD software. These objects were then imported into the SimXpert structures workspace as parasolids. The test piece specifications were in accordance with EN 10 002-5(1992) [43] as used in the study by Outinen [2]. This was a cylindrical Dog-bone shaped specimen as shown in the Figure 6-1 below. See Appendix F for dimensions.

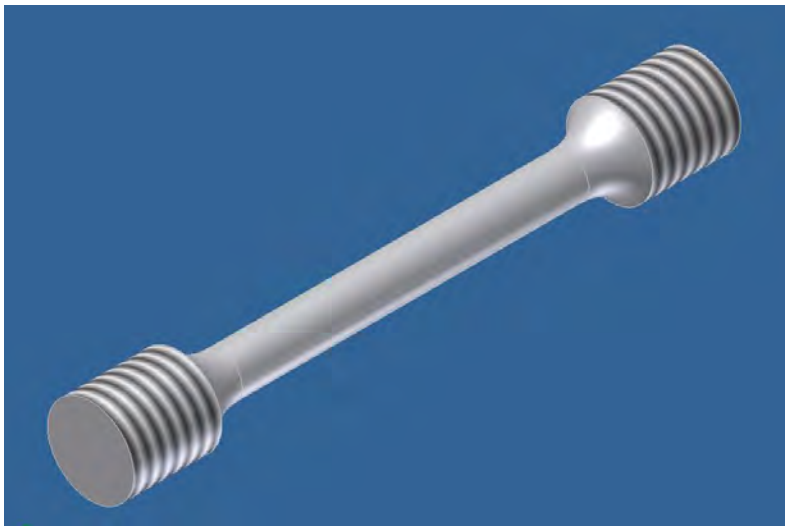

Figure 6-1: Type 3 Test Piece Used in Helsinki Study

6.3.2. Material Definition

An isotropic material was created and defined by Young's modulus at various temperatures and the temperature dependant thermal coefficient of expansion. Poisons ratio was set at a constant value of 0.3. This was sufficient for linear static analysis. For nonlinear behaviour past the proportional limit, temperature dependant stress-strain data must be inputted. This was done by adding a constitutive elasto-plastic model to the material and defining the stress-strain curves. The geometry was defined as a solid having properties of the defined isotropic material. Please see Figures 6-2, 6-3 and 6-4 below representing the data input to the model within SimXpert [3]. Table of values is presented in Appendix G.

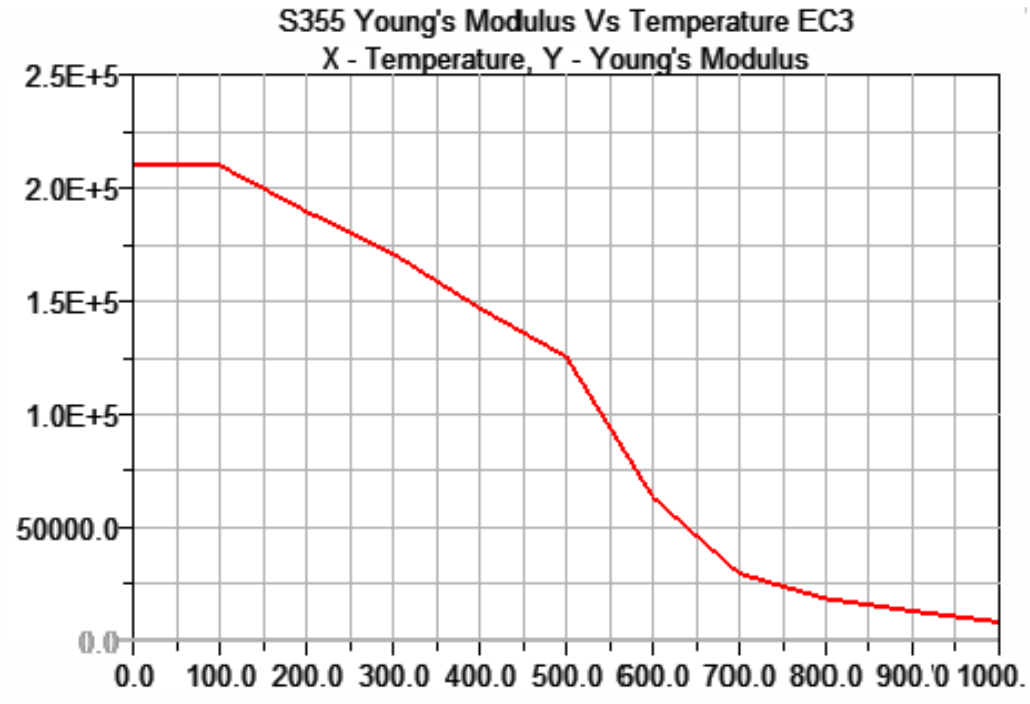

Figure 6-2: Model Input for Young's Modulus Vs Temperature

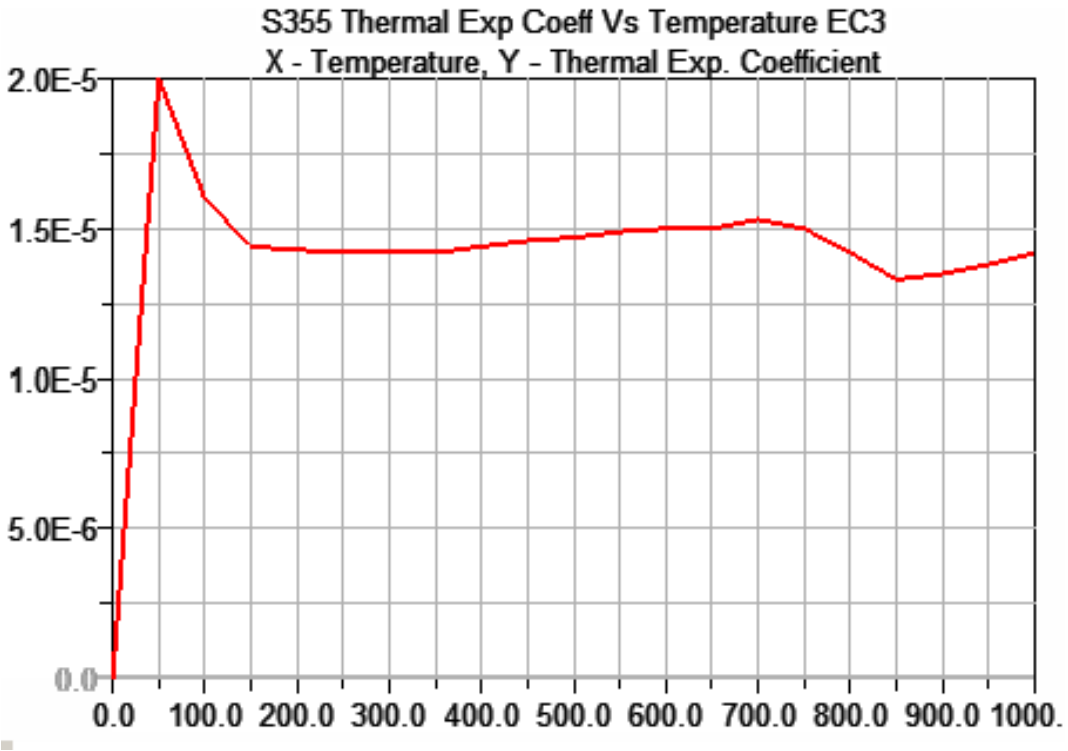

Figure 6-3: Model Input for Thermal Coefficient of Expansion Vs Temperature

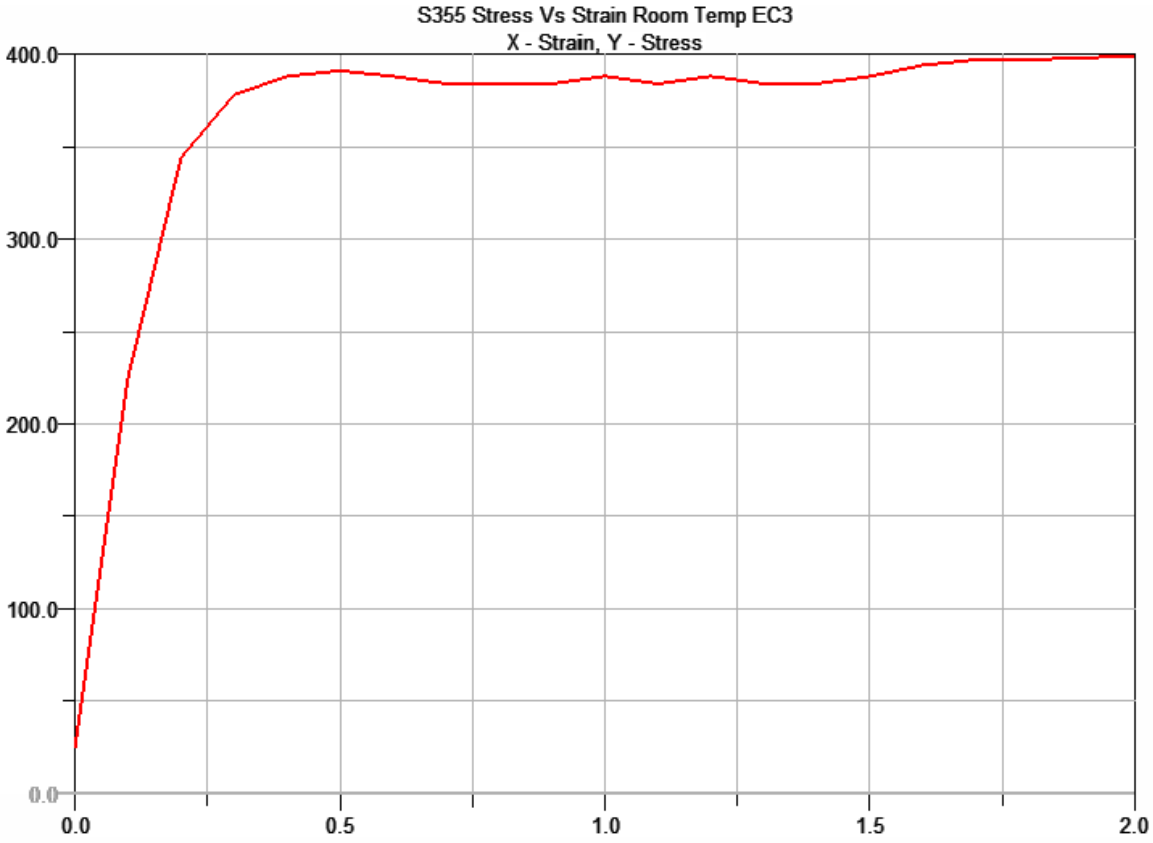

Figure 6-4: Model Input for Stress Strain Data at Room Temperature

6.3.3. Mesh

The meshing was done using the Auto-mesh function which simplifies the meshing process. A solid mesh was chosen which incorporated quadratic elements. Relative element size was set at a value of 2 to produce a finer mesh pattern. The chordal deviation, minimum length and maximum length ratios were set at values of 0.1, 0.2 and 2 respectively. Figure 6-5 below shows the final mesh wire frame superimposed on the transparent geometry.

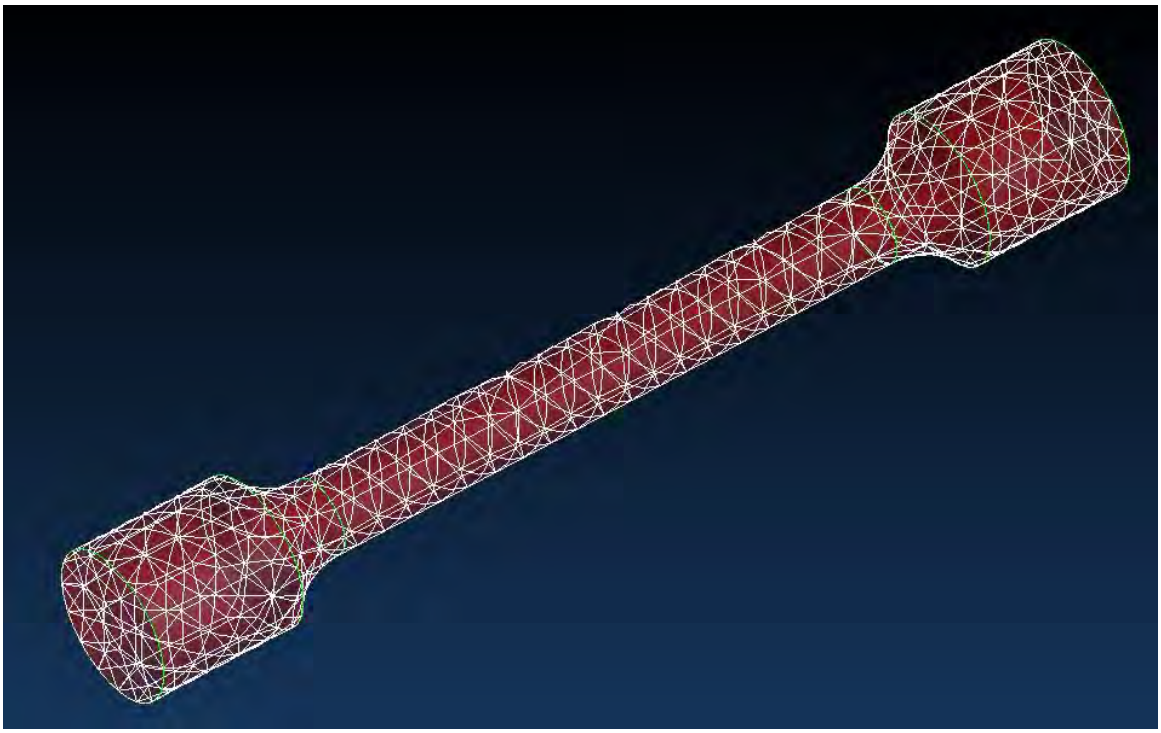

Figure 6-5: Finite Element Wire Mesh

The tet meshing method was used and internal coarsening was applied to the mesh. The area of concern is near the surface of the geometry as this is where maximum stresses will occur. The mesh elements below the surface can progressively increase in size as their accuracy is not crucial. This allows for a finer mesh at the surface without significantly increasing the number of nodes and thus the computing power needed. The quality of the mesh developed is of great importance as this directly affects the accuracy of the model. A quality analysis was done on the mesh which gave an overall rating of 80%. In Figure 6-6 below one can see that the mesh quality in the radius of the specimen was low. However, the main area of concern is the reduced area of the specimen which was at an acceptable standard for the purposes of this study.

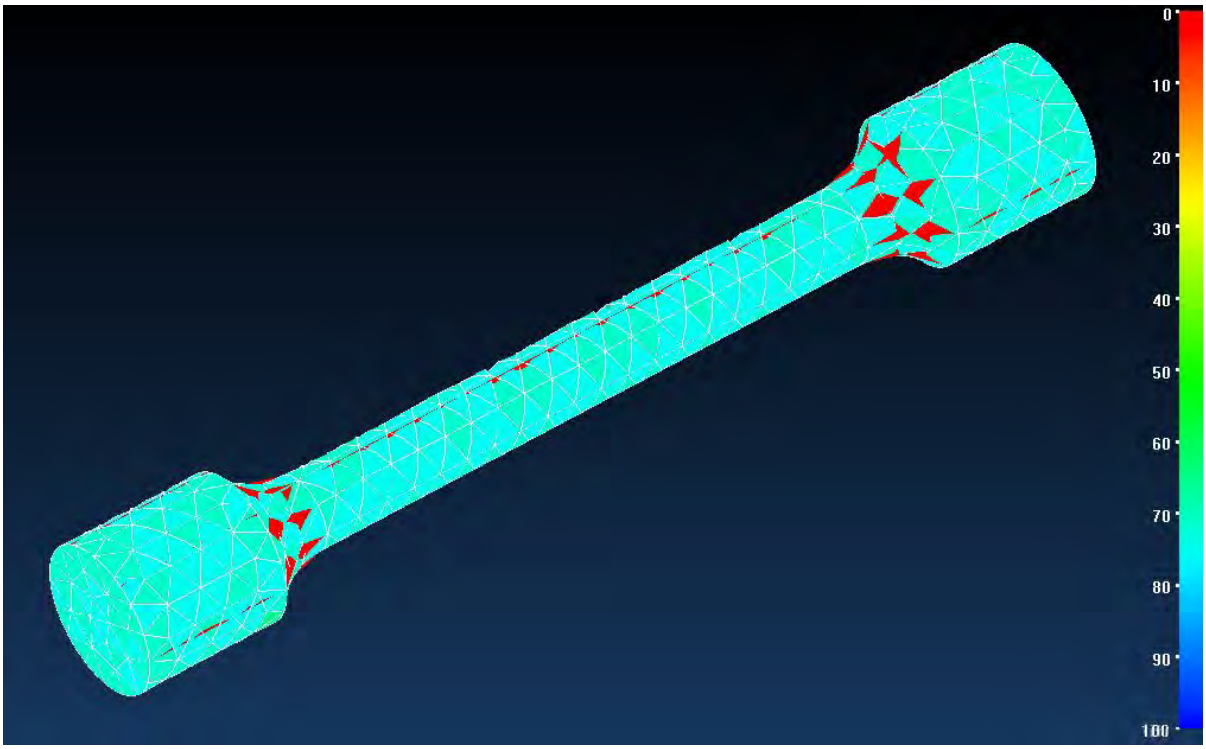

Figure 6-6: Mesh Quality Fringe Plot

6.3.4. Loads and Constraints

As far as is reasonably possible the exact end conditions and loading behaviour must be replicated in the model. In the experimental procedure this test piece would have been held in a tensile testing machine. Therefore it is assumed that the one end is fixed in its entirety within the machine grip. To achieve this, a fully fixed constraint was applied to all the nodes in that grip section of the test piece. Therefore only the nodes within the radius of the test piece and through its reduced section including the opposite grip end were able to move. A total load force was applied to the 2 surfaces bounding the opposite grip end of the test piece. This ensured that the grip ends would not participate in the actual analysis. The loads and constraints are visualized in Figure 6-7 below.

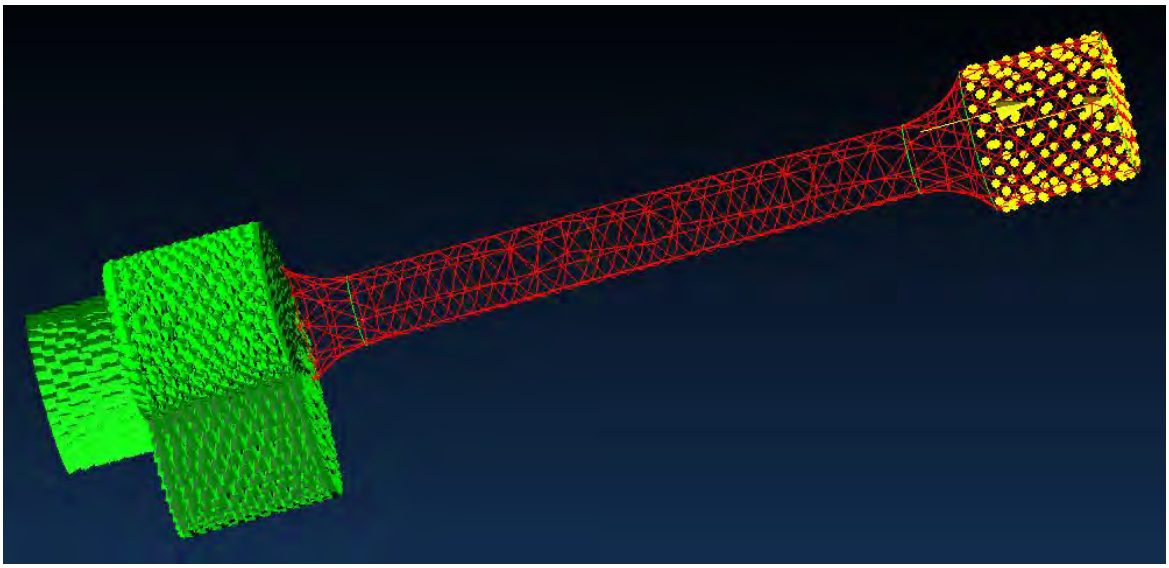

Figure 6-7: Loading Conditions and Constraints

6.3.5. Assumptions and limitations

It is assumed that the material of concern is completely isotropic and homogeneous. The material does not include any defects or inclusions within its self. Furthermore, the load is not gradually applied as occurs in practice but acts as a static force. The transient heating of the test piece is not taken into account but rather specified as a constant uniform temperature throughout including the surroundings. Room temperature was assumed to be 25°C unless otherwise stated.

For a linear solution this model can only be applied in situations below the proportional limit of the material. This is also determined by the temperature load being specified. As the temperature increases, the proportional limit decreases and hence lower stresses can only be modelled.

In non-linear solutions this model cannot predict failure explicitly and therefore can only be used to model behaviour below the ultimate tensile strength at any given temperature load.

6.3.6. Baseline Verification

In order to build confidence in this model each aspect must be verified with existing data from various papers and expected outcomes derived from theory. Firstly a linear static analysis was conducted at room temperature. Working within the upper end of the proportional range, an applied load of 5890N was calculated to result from a stress of 300MPa on the test piece. Looking at the fringe plot of the von Mises stress tensor component, an approximate stress of 306MPa was observed in the reduced section of the test piece for the same applied force. The corresponding von Mises strain component within the reduced section of the test piece had a value of 0.13%. These results can be seen in the Figures 6-8 and 6-9 below.

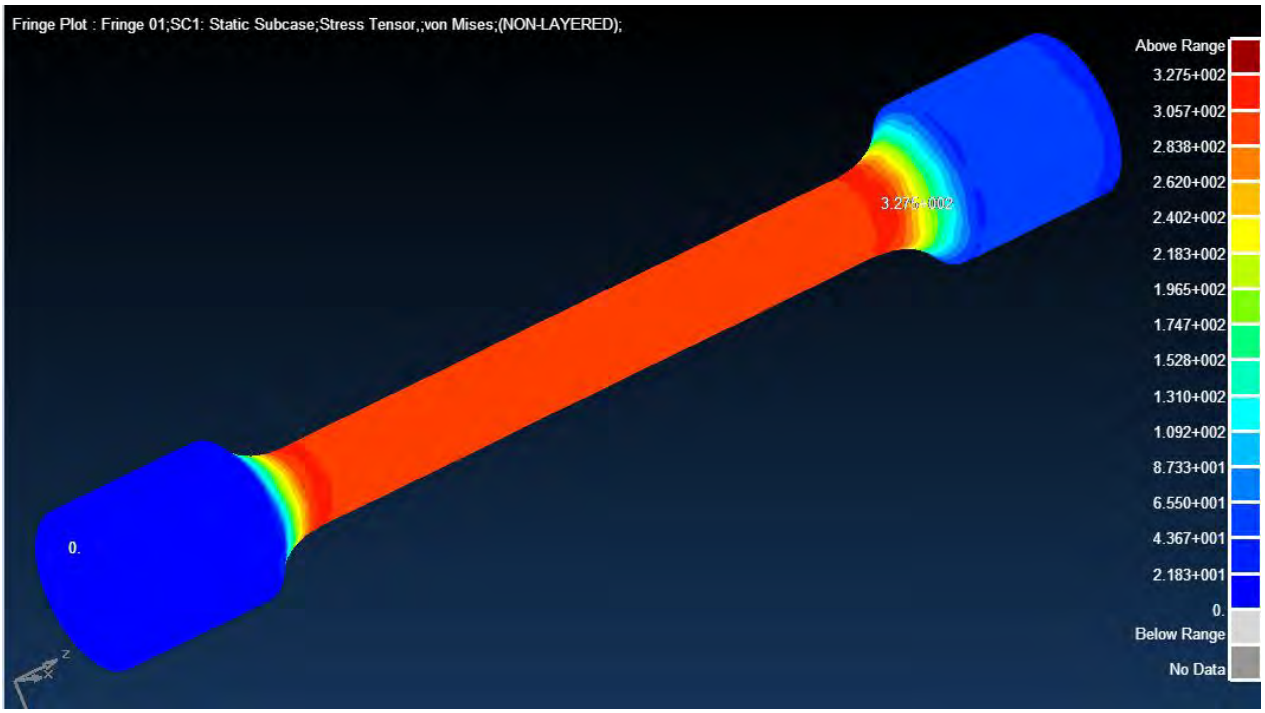

Figure 6-8: Stress Tensor Fringe Plot for Baseline Verification

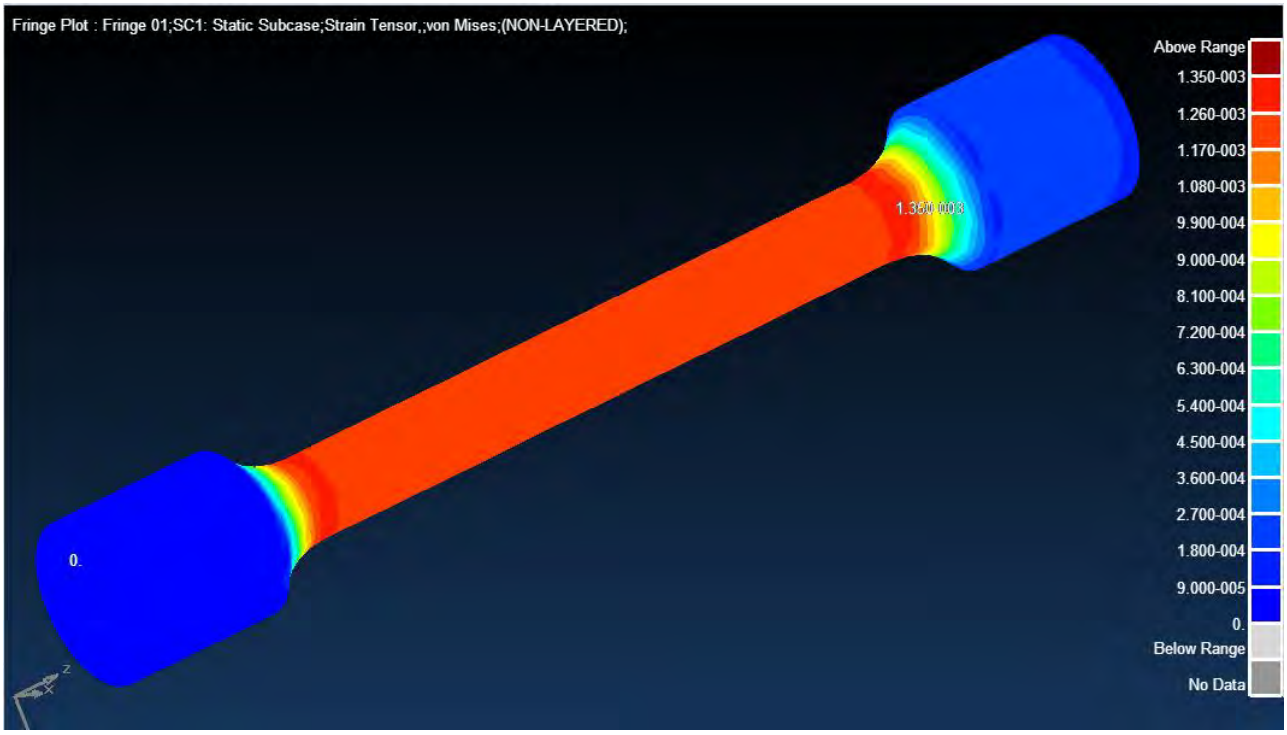

Figure 6-9: Strain Tensor Fringe Plot for Baseline Verification

This was repeated with loads resulting in theoretical stresses of 250MPa and 200MPa. Table 6-1 below summarizes the collected data. Please refer to Appendix I for corresponding fringe plots. These stress-strain points fit on the stress strain curve suggested in the Eurocode standard and featured in the Helsinki Study [51] quite closely as expected. It can be concluded that the model is adequate to replicate the stress strain data in the linear range for simple geometry at room temperature. Figure 6-10 below shows the comparison of this model with the results from Helsinki.

Table 6-1: Comparison to EC model at Room Temperature

Stress (N/mm^2)	Strain (%)	Stress EC3 (N/mm^2)	Strain EC3 (%)
306	0.13	300	0.15
255	0.11	250	0.12
204	0.08	200	0.10

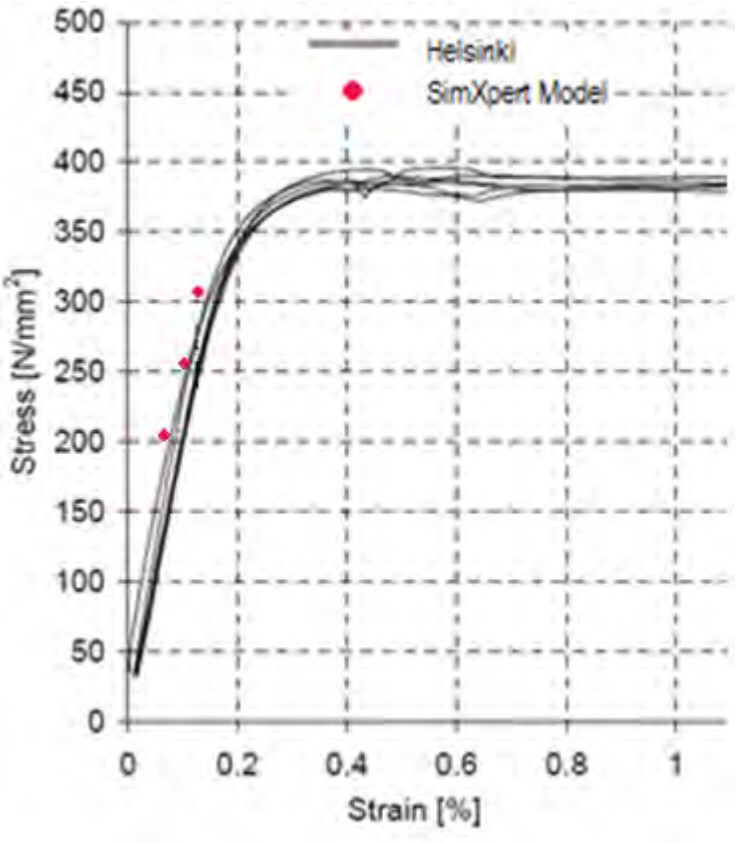

Figure 6-10: Comparison of Model with Helsinki Data at Room Temperature

6.3.7. Temperature Dependence Verification

In order to determine the confidence of this model when dealing with different temperatures, a linear static analysis was again done. However, this time a temperature load was specified. In order to ensure that the scope of application falls within the proportional range, a maximum temperature of 400°C was used and an applied load of 2945N was calculated to result from a stress of 150MPa. There after this scenario was repeated at the same stress for room temperature as well as 300°C. The resultant data is summarized in Table 6-2 below. Please see Appendix I for fringe plots of these simulations.

Table 6-2: Comparison of Temperature Dependant Model to Eurocode

Temperature (C)	Stress (N/mm^2)	Strain (%)	Stress EC3 (N/mm^2)	Strain EC3 (%)
25	153	0.06	150	0.06
300	153	0.08	150	0.09
400	153	0.09	150	0.11

From these results a clear trend can be seen. An increase in temperature results in an increase in strain at constant stress as expected. Below in Figure 6-11 is a graph adapted from the Helsinki study comparing the model results at 300°C and 400°C. The values fit very close to the Eurocode and Helsinki test results. It is observed that as the temperature increased, so the deviation from the Eurocode increased slightly, but still at an acceptable standard. This demonstrates the reason why this linear analysis is only valid for the proportional range of the material. At a constant stress an increase in temperature will move the scenario closer to the proportional limit.

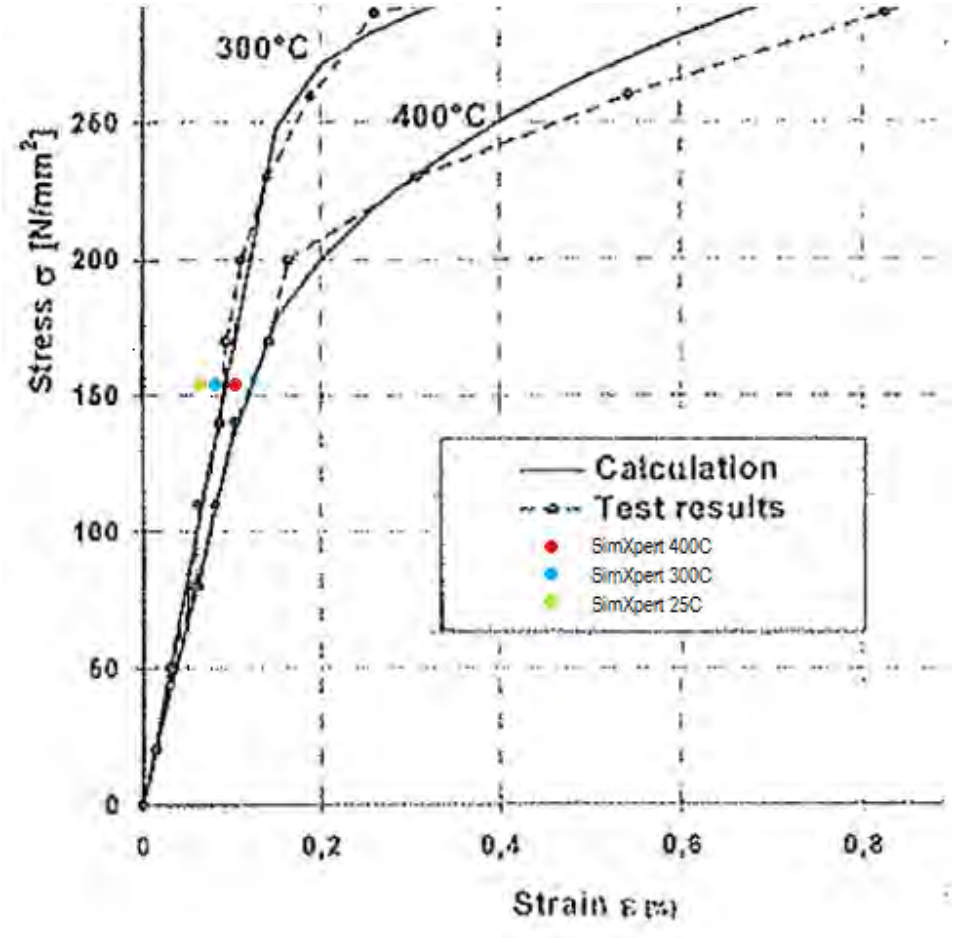

Figure 6-11: Comparison of Helsinki tests, Eurocode and SimXpert model at 150MPa

6.3.8. Non-linear Verification

The last aspect of this model to be verified consists of the prior capabilities of this model, but within the non-linear range. In order for this model to produce beneficial information, the yield point will be of main concern. Theoretically this is within the non-linear range and is the determining factor in designs. Behaviour beyond this point becomes relevant when permanent deformation and fracture analysis is required which does not form part of this study.

Using a very crude approximation that the yield point occurs near a strain of 0.2% throughout the temperature range, one can evaluate the changes with temperature. In practice this value varies with temperature. However, this will ensure that all behaviour is within the non-linear range and demonstrate the ability of this model to replicate non-linear behaviour around the vicinity of the yield point. Table 6-3 below shows a summary of the data gathered from the simulations.

Table 6-3: Summary of Data from Non-linear Simulation

Temperature (C)	Stress (N/mm^2)	Strain (%)	Reduction factor	Stress EC3 (N/mm^2)	Strain EC3 (%)	EC3 Reduction Factor
25	350	0.18	-	344	0.2	-
300	255	0.18	0.73	250	0.2	0.73
400	208	0.18	0.59	204	0.2	0.59

From the data it can be seen that the model produces results which fit the Eurocode3 graphs well as seen in the linear analysis. Figure 6-12 below is taken from the Helsinki study [51] with the SimXpert data superimposed. The more important factor to consider is that the reduction factors for the stresses at a strain of 0.2% are identical. This demonstrates the ability of the model to replicate the temperature dependant behaviour in the non-linear range. Please refer to Appendix J for fringe plots.

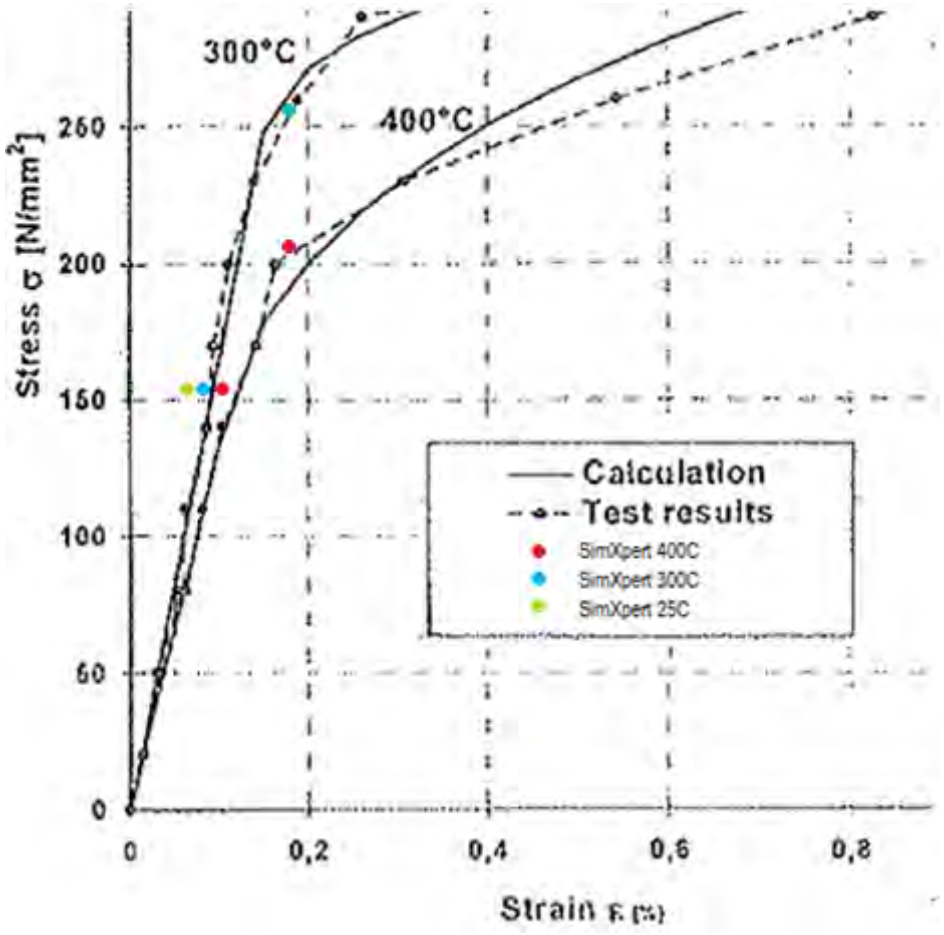

Figure 6-12: Comparison of Helsinki tests, Eurocode and Simulations

7. SIMULATION APPLICATION

7.1. 350W COMPRESSION MODEL

This model will be built upon the frame work of the previous S355 model. In this way we have already verified that this model can successfully replicate the input material data and that for all intents and purposes of this study its accuracy with simple geometry is acceptable. This model will demonstrate the parametric capabilities of simulations which can then be extended to numerous investigations not included in this study. The experimental procedure laid out by Wellmanns [40] is used in this model. Columns of all lengths are characterized by this model even though stub columns are used as an example.

7.1.1. Geometry

Using the specifications obtained from the South African Institute of Steel Construction [56], both the 90x90x8 angle and 152x76x18 channel sections were modelled as used for the experimental investigation done by Wellmanns [40]. See Appendix F for geometry dimensions. Various column lengths were modelled including stub columns. Stub columns are characterized as having low slenderness ratios to assure no buckling takes place when tested. The stub columns have a slenderness ratio of 10. Guidelines for testing by Galambos [57] were followed with regards to the lengths of the stub columns. Creating and importing the geometry was carried out in the same fashion as the previous model. Figures 7-1 and 7-2 show the imported geometry for both cross sections.

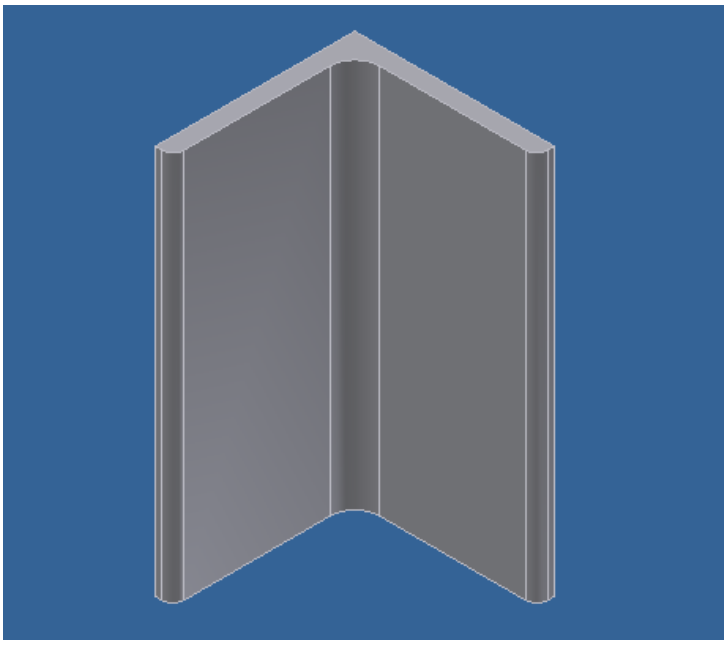

Figure 7-1: Equal Angle90x90x8 Stub Column

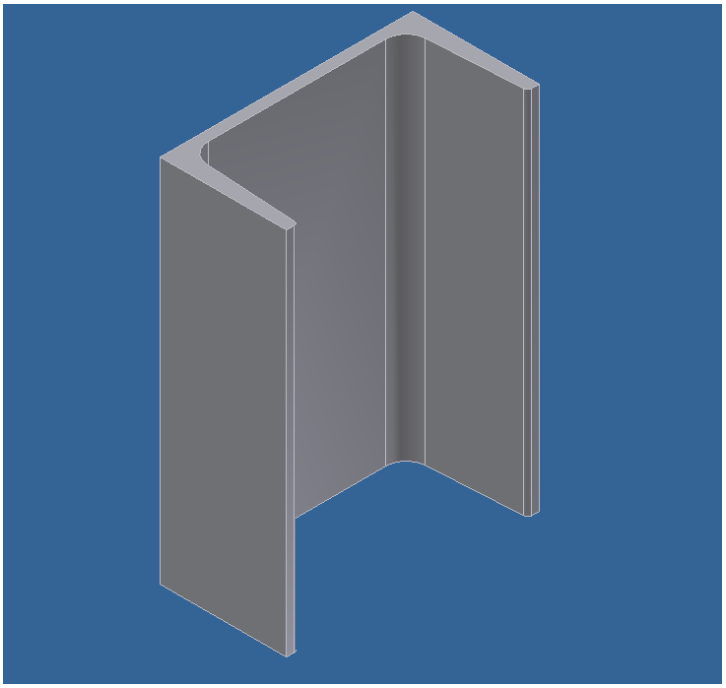

Figure 7-2: Channel 152x76x18 Stub Column

7.1.2. Material Definition

The data input to this model is taken from [40]. Representative stress strain curves were used. This is in keeping to the previous model and will produce results with acceptable accuracy for all dimensions. The Input method is the same as described in the previous model using an isotropic material with an elasto-plastic constitutive model. Figures 7-3 and 7-4 below show the graphs of the representative stress strain curves. See Appendix H for table of values. For linear analysis a Young's Modulus of 205.8GPa and 212.8GPa was used for Equal angle 90x90x8 and Channel 152x76x18 sections respectively. A Poisson's ratio of 0.3 was used for both sections.

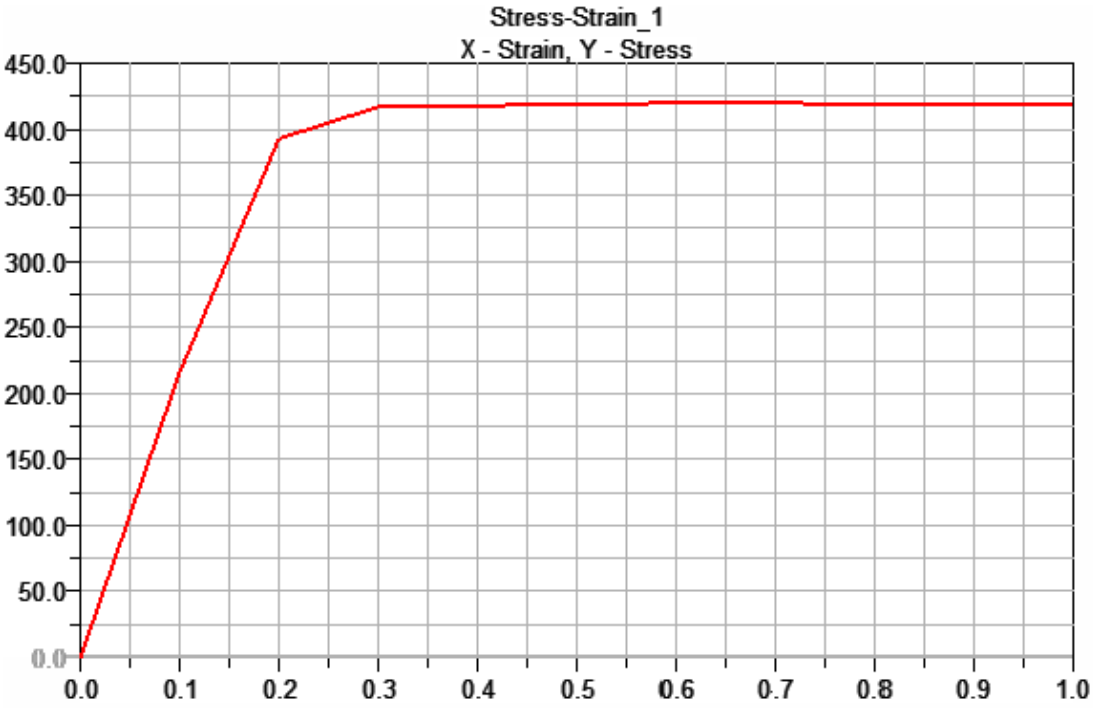

Figure 7-3: Model Input for Stress Strain Data of 350W Equal Angle 90x90x3

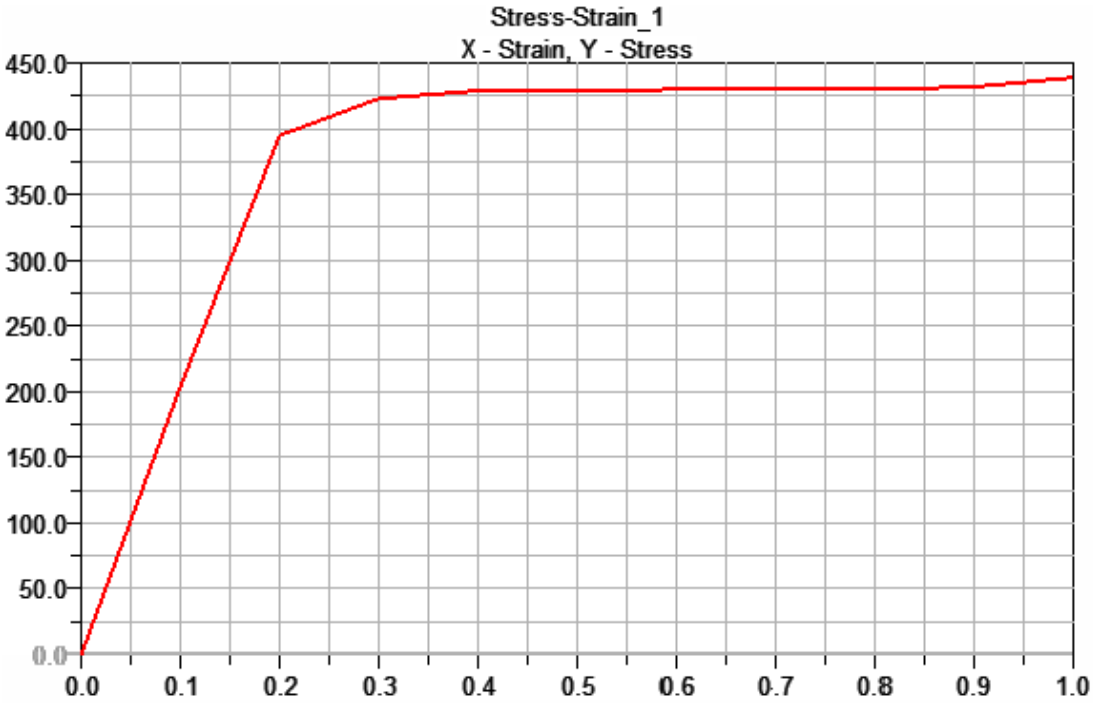

Figure 7-4: Model Input for Stress Strain Data of 350W Channel 152x76x18

7.1.3. Meshing

A solid mesh was chosen which incorporated quadratic elements as before. The relative element size was set at a value of 31. The chordal deviation, minimum length and maximum length ratios were set at values of 0.1, 0.2 and 2 respectively as before. Figures 7-5 and 7-6 below shows the final mesh wire frame superimposed on the transparent geometry for both cross sections.

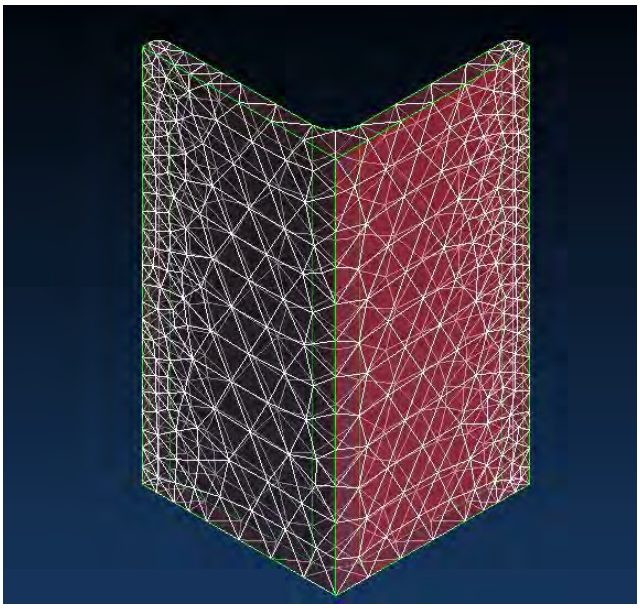

Figure 7-5: Finite Element Wire Mesh 90x90x8 Equal Angle

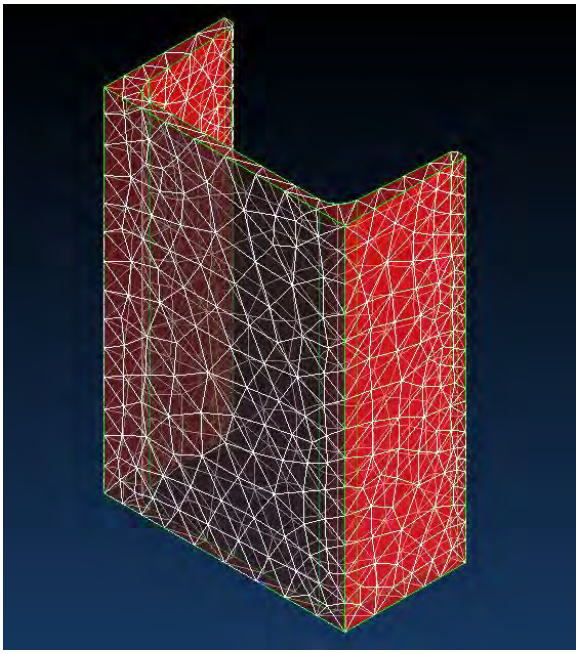

Figure 7-6: Finite Element Wire Mesh 152x76x18 Channel

The tet meshing method was used and internal coarsening was applied to the mesh. The quality analysis gave an overall rating of 80% for both geometries. Looking at Figures 7-7 and 7-8 below one can see that the mesh quality of the equal angle cross section is uniform throughout, but the channel cross section showed lower quality elements within the web. However, this is only a small area of concern in comparison to the mesh quality of the geometry as a whole. Therefore it can be ignored while still producing an acceptable standard of accuracy for the purposes of this study.

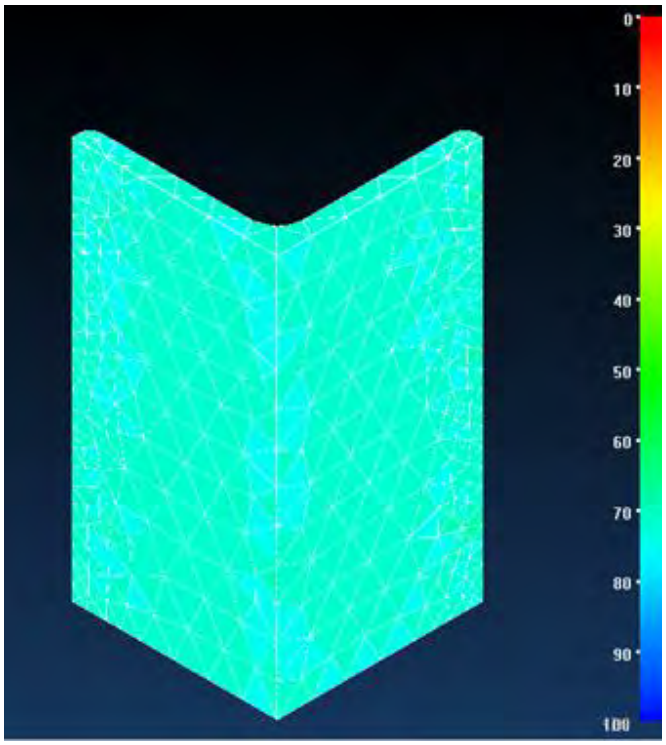

Figure 7-7: Quality Index for 90x90x8 Mesh

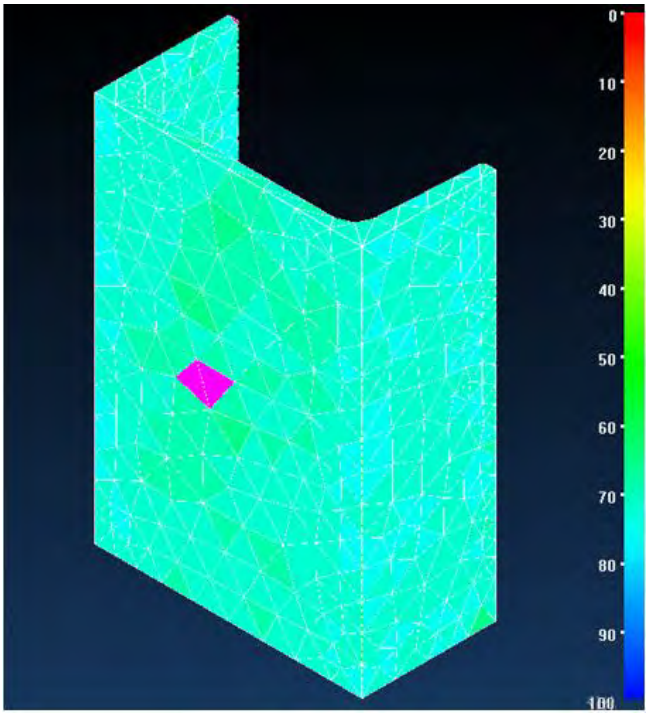

Figure 7-8: Quality Index for 152x76x18 Mesh

7.1.4. Loads and Constraints

With this model the end conditions differ slightly from the previous model. In the experimental procedure this test piece would have been held in a compression testing machine. In order to allow for buckling mechanisms without damaging the machine grips, the specimen ends were held using two hardened steel plates on either end which were slightly recessed in the centre to allow for a hardened steel ball to be located between them as conducted by Wellmanns [40]. Therefore a pined constraint was applied to one end of the specimen and an axial pressure load to the other which is seen in Figures 7-9 and 7-10 below.

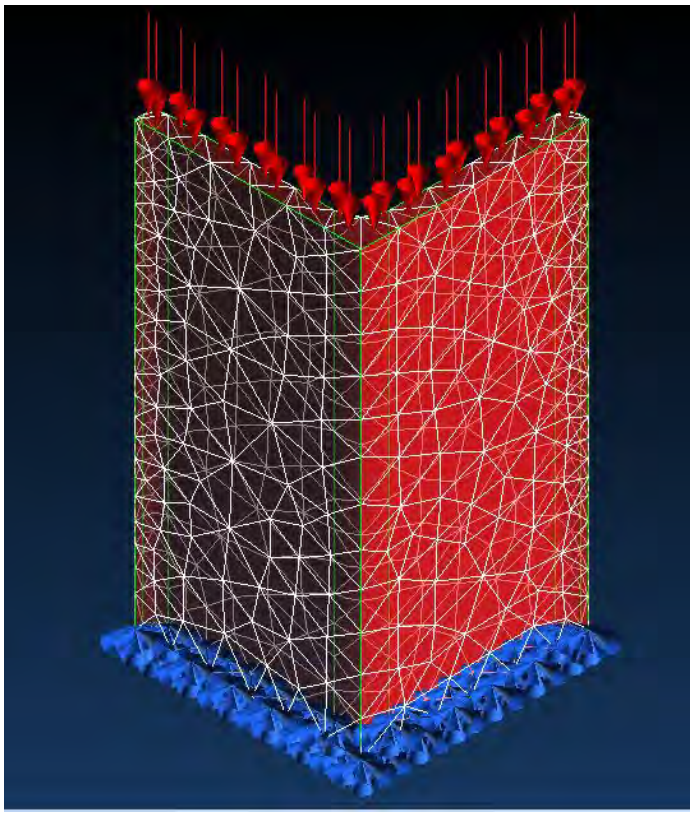

Figure 7-9: Loads and Constraints for 90x90x8 Equal Angle

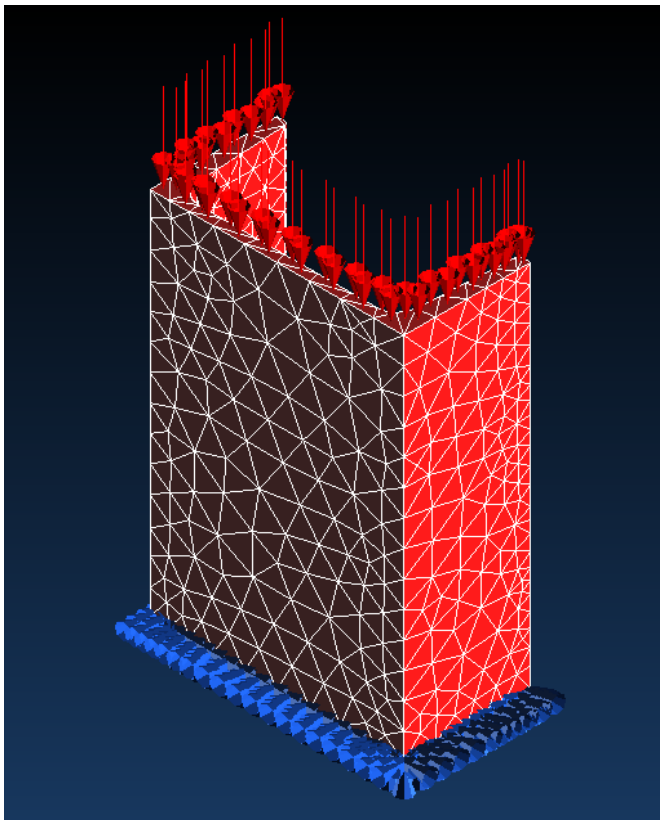

Figure 7-10: Loads and Constraints for 152x76x18 Channel

7.1.5. Assumptions and Limitations

The basic assumptions of the previous model hold true here as well, which assumes the material of concern is completely isotropic and homogeneous. Once again the load is not gradually applied as occurs in practice but acts as a static force. Room temperature was assumed to be 25°C at which the tests were done. For a linear solution this model can only be applied in situations below the proportional limit of the material.

It is assumed that the input stress strain data is valid uniformly throughout the specimen's cross section. The minor difference between the behaviour of the web and flange sections is ignored. Moreover this input data is assumed to be independent of slenderness ratio to enable wider application of this model. The input data and meshing characteristics are constant irrespective of the column length modelled.

7.1.6. Stub Column Geometry Dependence

In order to ensure an accurate resemblance of real life behaviour when dealing with compression, the use of stub columns helps to eliminate the effects of the buckling mechanism on the actual compressive load bearing capacity. In this simulation a pressure load was applied as opposed to a force in order to ensure the same load on each cross section. Likewise, the lengths of the angle and channel sections differed to ensure an equal slenderness ratio. For this instance a slenderness ratio of 10 was used which is typical of stub columns. An applied pressure of 250MPa was applied which resulted in a total deformation of 0.211 and 0.262mm for the angle and channel sections respectively. Figures 7-11 and 7-12 below shows the resulting fringe plots super imposed on the un-deformed geometry.

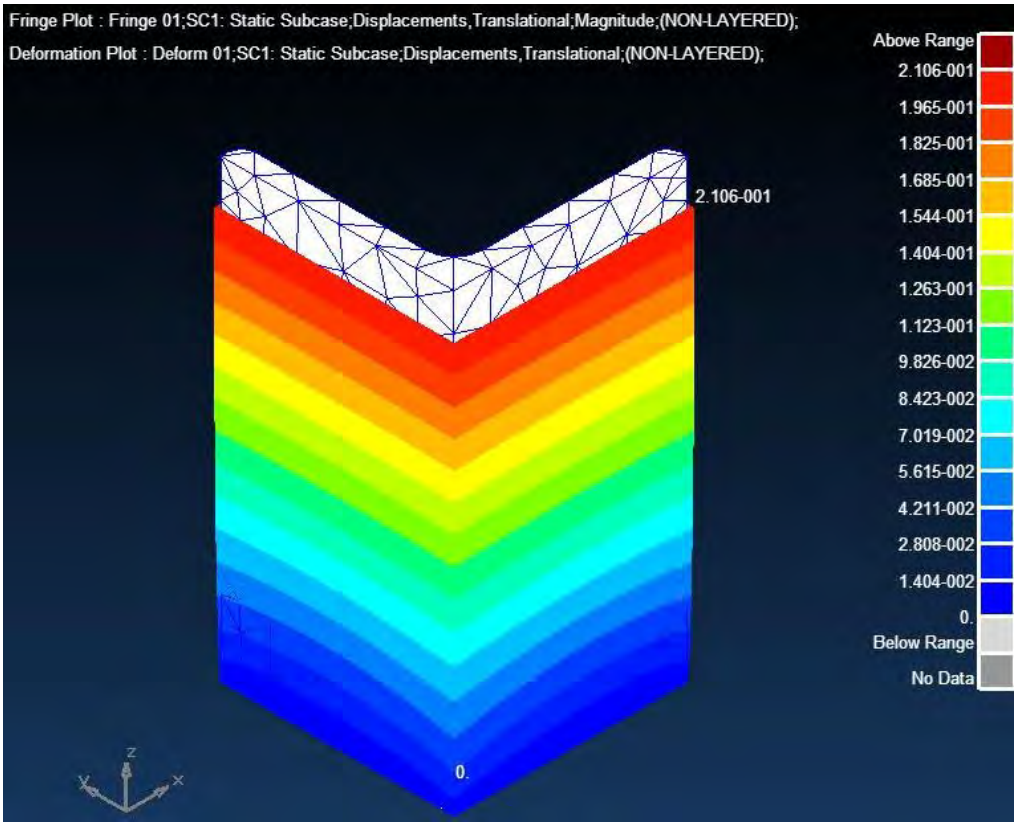

Figure 7-11: 90x90x8 Total Compressive Displacement at 250MPa

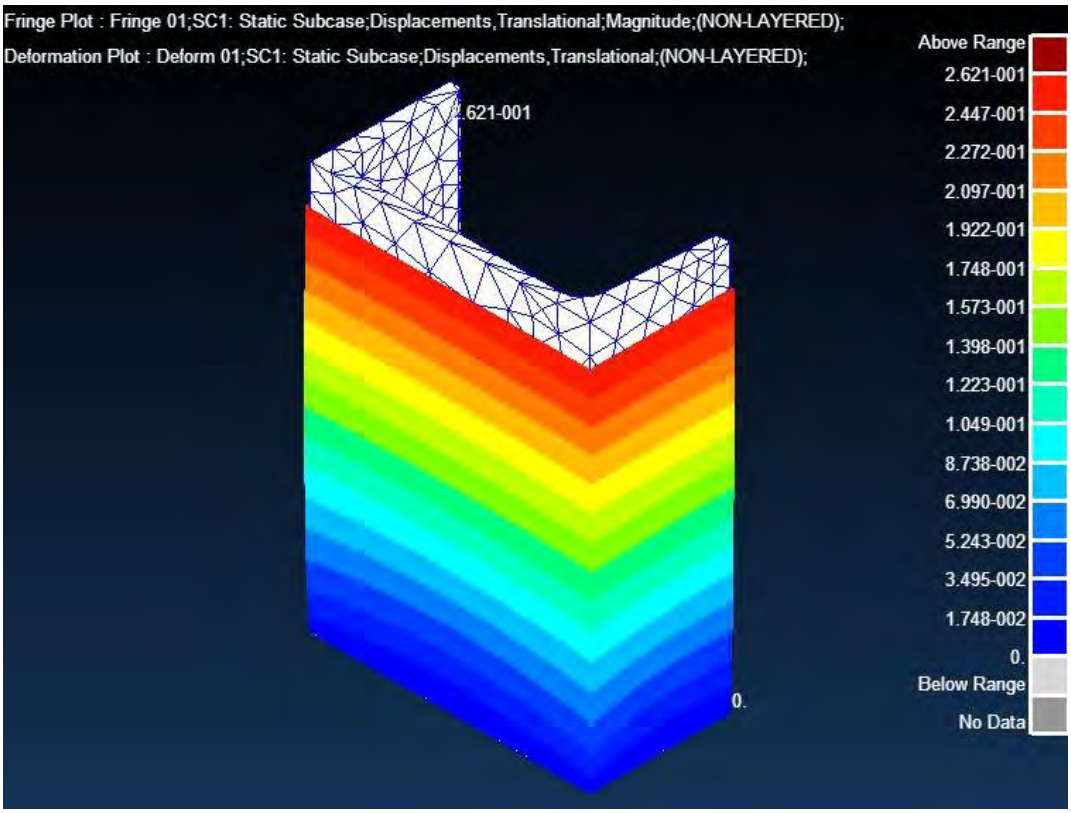

Figure 7-12: 152x76x18 Total Compressive Displacement at 250MPa

The simulation was repeated on both cross sections at pressure loads of 350 and 400MPa. The lateral displacements were also captured. Please see Appendix K for all fringe plots. The displacements observed are summarized in the Table 7-1 below.

Table 7-1: Displacements of Stub Columns

Geometry	**90x90x8**			**152x76x18**		
Displacement (mm)	X	Y	Total	X	Y	Total
@400MPa	0.029	0.028	0.337	0.034	0.044	0.419
@350MPa	0.025	0.025	0.295	0.030	0.039	0.367
@250MPa	0.018	0.018	0.211	0.022	0.028	0.262

Looking at the angle section, the deformation in both the x and y directions are very close if not the same. The channel section shows more variation between the deformations in the x and y directions due to its geometry. These values are very small and can be

neglected which is expected from a stub column. However, the total deformation can be linked with the yield strength. Wellmanns [40] concluded that the 152x76x18 channel section had a lower yield strength than the 90x90x8 angle section. This can be correlated with the higher compressive deformation in the channels section in Figure 7-13 as compared to the angle section. It must be noted that this is only observed for equal slenderness ratios categorized as stub columns. No conclusion can be drawn about the stability of the geometries when using equal lengths. Furthermore it is clear that the channel section experienced a higher applied load due to its greater cross sectional area as compared to the angle section, when keeping the applied stress constant.

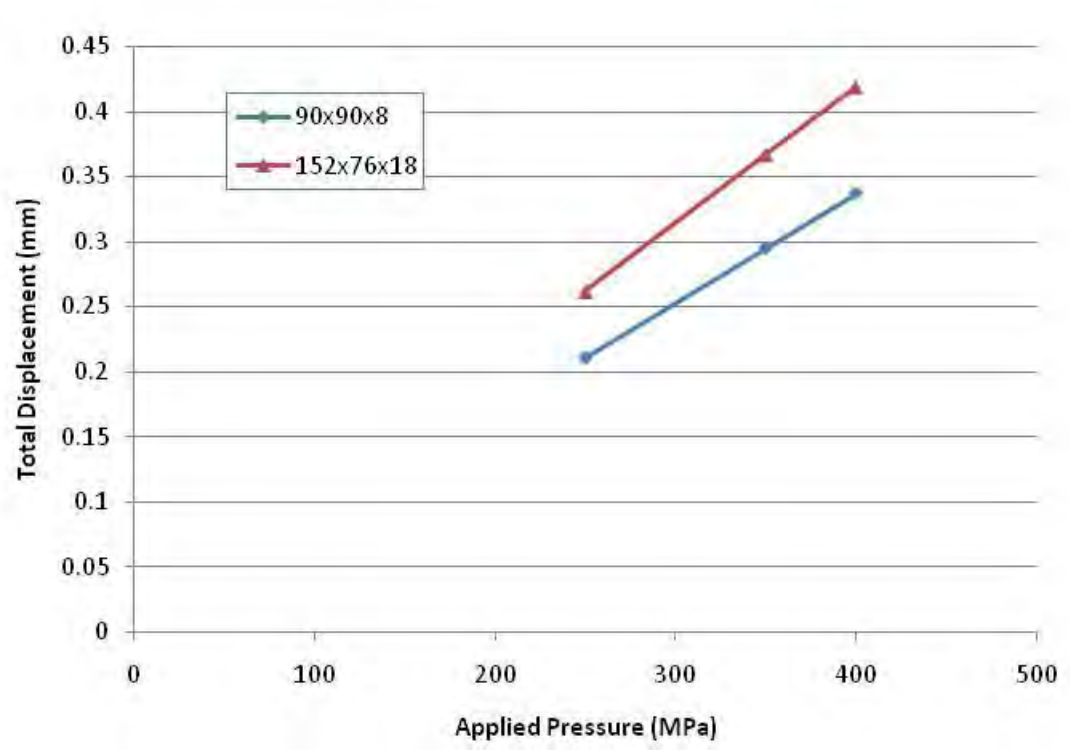

Figure 7-13: Graph of Compressive Displacement Vs Applied Pressure

7.1.7. Slenderness Ratio Dependence

In these simulations the specimens will be modelled within the elastic region which will allow for a linear analysis to be conducted. The area of concern is the susceptibility to buckling while below the proportional limit. Plastic deformation indicates that the specimen has been crushed rather than buckled. An applied pressure of 300MPa was

applied to both cross sections at slenderness ratios of 50, 75, 100, 180 and 200.The results are tabulated in Table 7-2 below.

Table 7-2: Comparison of displacements and slenderness ratios

Geometry	Channel 152x76x18			Equal Angle 90x90x8		
Slenderness Ratio	X-Axis (mm)	Y-Axis (mm)	Total Displacement (mm)	X-Axis (mm)	Y-Axis (mm)	Total Displacement (mm)
50	0.0224	0.0355	1.572	0.0238	0.0243	1.281
75	0.0249	0.0345	2.358	0.0259	0.0279	1.922
100	0.0225	0.0335	3.143	0.0295	0.0271	2.564
180	0.0974	0.0846	5.681	0.0313	0.0382	4.615
200	0.0715	0.0379	6.285	0.0756	0.0731	5.132

Please see Appendix L for the corresponding fringe plots. From the data it can be seen that the equal angle section shows similar lateral displacement with regards to the X and Y axis. However, the difference in the lateral displacements between the x and y axis of the channel section are much larger in comparison. From Figure 7-14 below it can be seen that these lateral deflections fluctuate with the change in slenderness ratio. No correlation could be found between the lateral displacements and the slenderness ratio from the simulations.

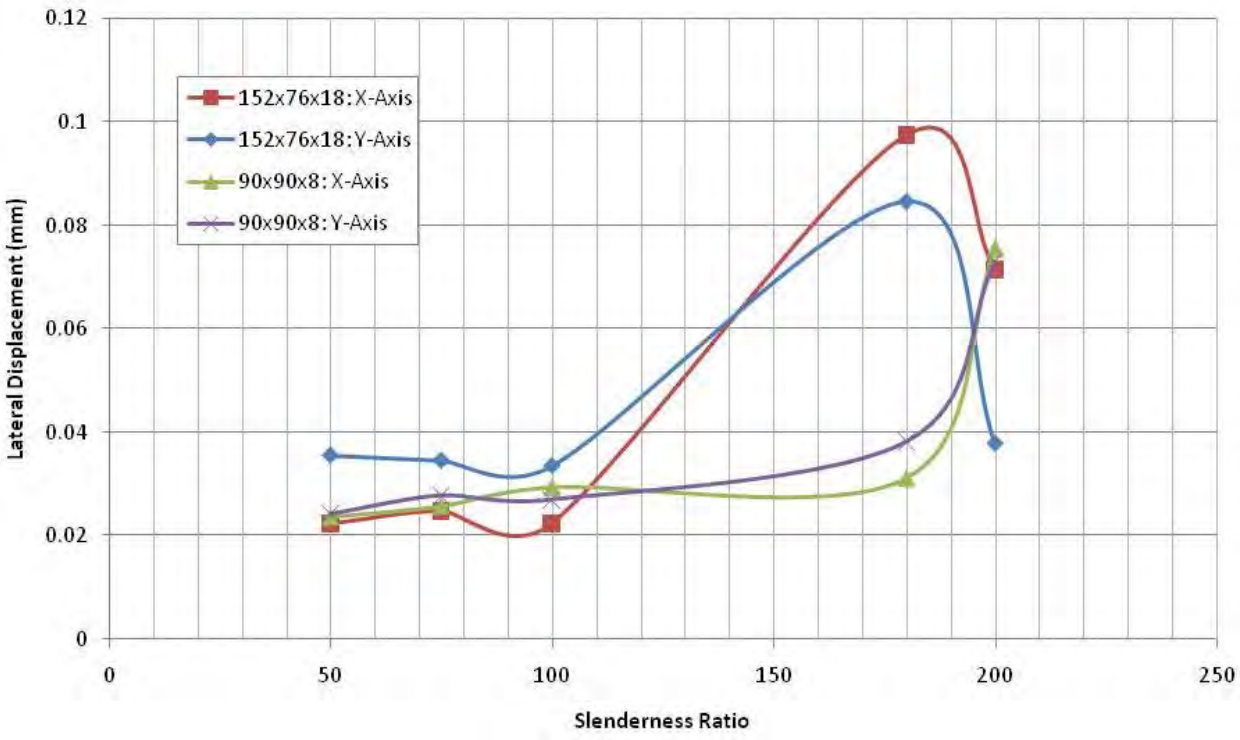

Figure 7-14: Graph of Lateral Displacement Vs Slenderness Ratio @300MPa

The total displacement which incorporates the axial movement was observed to increase with the increase in the slenderness ratio. From Figure 7-15 below it can be seen that the 152x76x18 Channel section showed higher values of total displacement as compared to the 90x90x8 angle section for a particular slenderness ratio. This must not be taken to correlate with the load bearing capacity differences between the two sections as buckling susceptibility is determined by slenderness ratio. In this case the slenderness ratios are equal and the difference in the total displacement is only a function of the length of the specimen. This data only demonstrates that the rate of change of the total displacement with respect to the slenderness ratio of the channel section is higher than that of the angle section.

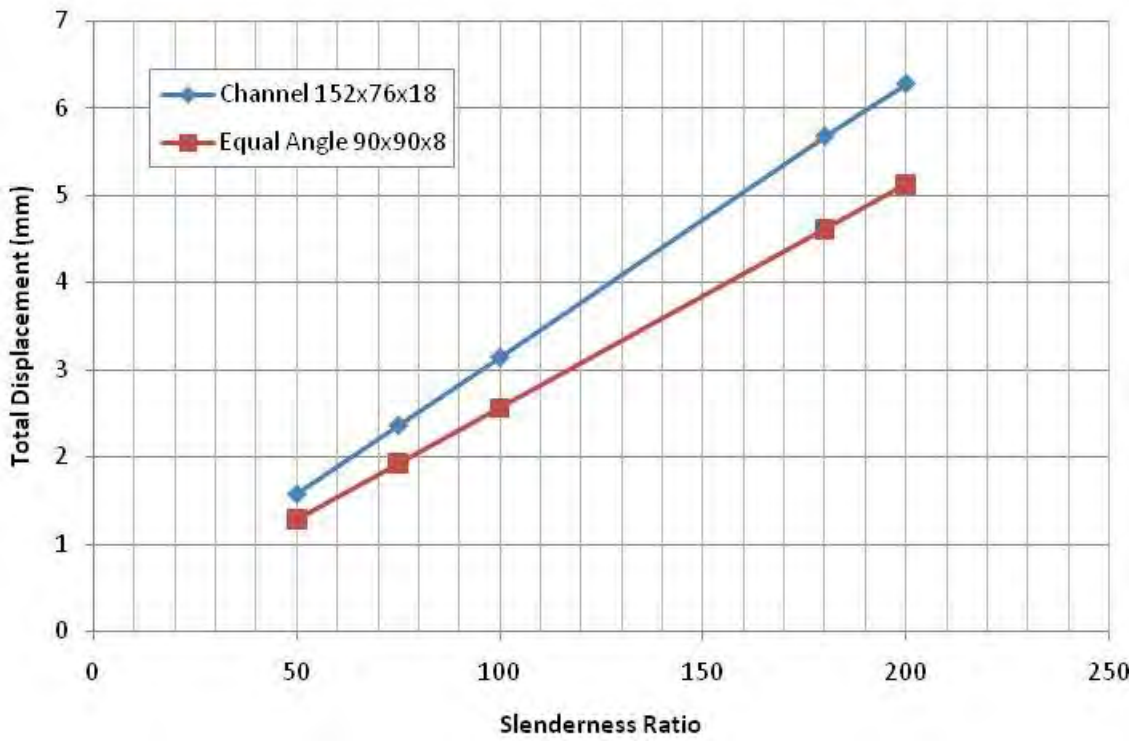

Figure 7-15: Graph of Compressive Displacemnt Vs Slenderness Ratio

8. DISCUSSION OF SIMULATION RESULTS

The development of a computer model for simulation of linear and non-linear static analysis at various temperatures has been outlined. The Data from the Eurocode 3 standard [1] for S355 structural steel has been used to define the material for input in this model to eliminate the possibility of raw data error which would then result in an erroneous model. This took the form of stress strain data points as well as temperature dependant moduli of elasticity and coefficients of thermal expansion. The material geometry was imported via a CAD format and replicated the test pieces used at Helsinki [51]. Within the SimXpert software package [3], the solvers SOL101 and SOL400 were used for the linear and non-linear analysis's respectively. The parameters used in the mesh generation have been presented along with the rationale behind them in order to achieve a mesh quality of 80% and a solvable model. The boundary conditions were constructed as to mimic the conditions typical of a uni-axial testing machine. The model has been verified for application of linear and non-linear static analysis of both S355 and 350W materials at various temperatures. This was done by replicating material behaviour from experimental work outlined in Chapters 3 and 4 in addition to literature [51] and theory. The model was exposed to various loads below the yield strength and successfully predicted the expected strain at room temperature with a linear analysis. Thereafter using a constant load below the yield strength, various temperature loads were applied and again a linear analysis successfully predicted the expected strains.

To verify the non-linear capabilities of the model, various temperatures loads were applied and the corresponding stress to result in a 0.2% strain was found iteratively. This assumed that the yield strength occurred at 0.2% strain regardless of temperature. As was seen in the experimental work, the yield strength decreased with an increase in temperature. This trend corresponded well with the Eurocode 3 standard [1]. However, the framework for this model does have certain restrictions. In a linear analysis the material should be within its proportional range and in a non-linear analysis the material cannot be modelled at the fracture point. Furthermore the load applied in these simulations acts statically as compared to a gradual increasing load seen in practice. One must also bear in mind that this model assume uniform heat distribution and does not cater for transient heating effects.

The basis of this model was then utilized to demonstrate the ease at which parametric studies can be conducted on simple geometry in compression. It was already demonstrated that material behaviour can be successfully predicted by inputting the relevant material data into the model provided the model setup resembles the actual scenario sufficiently. Experimental data obtained from Wellmanns [40] of 350W structural steel was used as input for this model. The model geometry made use of stub columns with a slenderness ratio of 10 which enabled the demonstration of different compressive behaviours for different cross sections, namely channel and angle. The use of stub columns eliminates the buckling mechanism and allows for the compressive strength of the member to be evaluated. It was found that the angle sections showed almost identical deformations in the direction of both axes, whereas the channel section showed greater deformations in the y direction. Overall both cross sections showed an increase in deformation with an increase in applied stress. This was supportive of Wellmanns findings [40]. The channel section experienced the higher deformations which can be attributed to a higher applied force due to the larger cross sectional area and should not be indicative of its strength compared to the angle section. It can be clearly seen that cross section geometry does play a significant role in the behaviour of steel members.

The effects of slenderness ratio on deflection were demonstrated for both types of cross sections by changing the model geometry but preserving the existing material definition taken from Wellmanns [40]. The model geometry included members of varying lengths with slenderness ratios greater than 10 in order to promote buckling. The boundary conditions were adjusted in the model to allow for pined constraints as opposed to fixed as this gave a closer approximation to the experiments conducted by Wellmanns [40]. A constant load of 300MPa was applied irrespective of the slenderness ratio. With the results obtained, a trend could not be seen between lateral deformation and slenderness ratio. This could be due to the different modes of bending in the beams which change with length and hence slenderness ratio. However, the overall deformations in the members were seen to increase with an increase in slenderness ratio. The channel section again showed higher deformations as well as a higher rate of change in deformation with respect to the slenderness ratio. Even though the material behaviour was assumed to be uniform throughout the geometries' cross sections, the results were acceptable for the purpose of this study. No differentiation was made between the behaviour of the web and flange.

Further confidence in this model must still be built by gathering more experimental data and replicating the inputs as done here. This model has shown if used in a similar fashion, it can allow for various other parametric approaches to be studied with regards to the buckling behaviour of steel members. These include parameters such as temperature distributions, end conditions and so forth. The work conducted in this study has included the effects of temperature and geometry separately, thus omitting the simulation of these parameters simultaneously. However, it is clearly possible to incorporate the two by combining the setups for each simulation. This model does not cater for all factors involved when dealing with the effects of fires but is presented as a basis onto which more realistic scenarios can be built upon.

9. CONCLUSION

The aim of this report was to determine the temperature dependant behaviour of structural steels for fire design and their reusability post fire exposure. Additionally, since full scale fire tests were not feasible to conduct, basic computer models were developed to investigate their potential capabilities for application in fire design.

Relevant literature was presented along with theory on full scale fire tests as well as isolated laboratory experiments. This study focused on the material grades S355 and 350W which have near identical chemical compositions. The mechanical behaviour and high temperature failure mechanisms of these steel grades were outlined with consideration for fire design. The behaviour of fires and the modelling thereof were presented which formed a prelude to the effects of fire on steel members after cooling down. This entailed the effects of residual stresses and the various types of heat treatments which could be induced by fires. This directly influenced the hardness of the material and lead to the consideration of hardness degradation as an indicator for remaining service life or simply reusability. From theory it was noted that end conditions and the slenderness of a steel member have a direct effect on the buckling susceptibility. The benchmark full scale fire tests conducted at Cardington [44] were reviewed in order to grasp the major differences between isolated laboratory tests and full scale fire tests on framed structures. Due to the nature of framed structures higher load bearing capacities were observed than that predicted by experimental tests on isolated members.

This then set the platform for the experimental work done in this study. A tensile testing machine coupled with heating tape and insulation material was utilized. Steady state tensile tests were conducted at elevated temperatures and were found to agree well with the Eurocode 3 [1] and other independent studies such as [50]. The yield strength of these steels was confirmed to show a decrease with temperature. A combined loading test rig was built in order to develop tests which were closer to real life situations. Angled cross sections commonly found in building structures were torsionally yielded before a tensile force was applied for various temperatures. This showed that the decrease in yield strength with temperature increase is much more significant for combined loading scenarios.

Thereafter two sets of reusability tests were conducted for 350W and S335 at the University of KwaZulu-Natal and ArcelorMittal SA respectively. This was done by subjecting numerous test specimens to various heating patterns and then obtaining stress

strain data once room temperature had been reached after cooling. It was found that micro structural changes cannot be ignored and therefore temperature and time need to be considered together when determining the reusability of steel after fire exposure. Depending on the exposure time and temperature the yield strength and ultimate tensile strength of the material will either increase or decrease not more than 10% at temperatures below 700°C. Therefore in this temperature range the materials are reusable after fire exposure provided no significant distortions are present which confirms the findings of [52]. With temperatures exceeding 700°C the yield strengths decrease exponentially as temperature is increased and it is therefore recommended that steel members are not reused in this temperature range. It was also found that hardness changes due to heating and cooling cannot be directly used to determine the strength of a material below 600°C. However, using the LMP factor for remaining service life as investigated by [32] which is calculated as a function of temperature and exposure time, hardness degradation can be correlated to it. For temperatures exceeding 600°C the hardness degradation can be directly correlated to the strength of the steel member however, above 700°C the hardness degrades at a much higher rate and should therefore be considered as structural failure.

Computer simulations which form the latter part of this research have been presented to demonstrate the ability to model high temperature behaviour and buckling susceptibility of steel members. Using the software package SimXpert 2010, a model based on the Eurocode 3 [1] standard for S355 has been developed which demonstrates the abilities to model material behaviour at various temperatures. These models have been verified with theoretical expectations and literature such as the study conducted by [51]. Thereafter a similar model for 350W structural steel was built upon this using compression data from published results of [40]. This demonstrated the ability to investigate the basics of buckling at room temperature using computer simulations rather than full scale tests. The results of these simulations agreed with theory that buckling susceptibility increases with an increase in slenderness ratio. Different behaviour between angled and channel sections in compression showed that effects of member geometry can also be investigated using simulations.

With the increasing development of new steel materials, academic research is needed to improve and expand design codes. Experimental data is lacking on residual stresses, compression tests and temperature ranges exceeding that of this research. The standards in many design codes are overly conservative as they are based on isolated laboratory

experiments. In real fire situations end conditions and structural rigidity of a frame consisting of many individual steel members plays an important role.

The outcomes of this study are to be used as a basis to understand the fundamentals of structural fire design and to serve as a platform for more complex models to be developed which can sufficiently simulate full scale fire tests. In addition, it demonstrates the ability of simulations to allow for a wider variety of parameters to be manipulated without additional costs as opposed to large scale experiments. Moreover, it makes clear the need for further research in this field in order to develop more precise design codes and specifications for steel structures and their reusability in light of the high safety risks attributed to building fires.

10. REFERENCES

[1] EN 1993-1-2:2005, Eurocode 3: Design of steel structures, Part 1-2: General rules - Structural fire design.

[2] J. Outinen, "Mechanical Properties of Structural Steels at High Temperatures and after Cooling Down", Ph.D. dissertation, Helsinki University of Technology Laboratory of Steel Structures, Helsinki, 2007.

[3] SimXpert, Education Edition 2010, Copyright 2012, MSC Software Corporation.

[4] J. Ding, G. Li and Y. Sakumoto, "Parametric studies on fire resistance of fire-resistant steel members", *Journal of Constructional Steel Research,* vol. 60, pp. 1007-1027, September 2004.

[5] G. Li and G. Lou, "The principles of fire resistance for steel structures in China", *Proceedings of the International Seminar on Steel Structures in Fire*, Shanghai, 2001, pp. 29-39.

[6] K.T. Ng and L. Gardner, "Buckling of stainless steel columns and beams in fire", *Engineering Structures*, vol. 29, pp. 717-730, June 2007.

[7] H. de Clercq. "South Africa Moves to Grade 350W Steel", *Journal of Steel Construction*, vol. 29, April 2005.

[8] EN 1991-1-2:2002, Eurocode 1: Actions on structures, Part 1-2: General actions – Actions on structures exposed to fire, CEN, Brussels, November 2002.

[9] W.F. Smith and J. Hashemi, *Foundations of Material Science and Engineering*, 4thed.McGraw Hill, 2006.

[10] J.M. Gere, *Mechanics of Materials*, 6thed. Belmont, CA: Thomson, 2004.

[11] SANS 1431:2007, Weldable Structural Steels, Ed 1.8.

[12] EN 10025-2:2004, Hot rolled products of structural steels, Part 2: Technical delivery conditions for non-alloy structural steels.

[13] Key to Metals, (2010, May 21), *Steel Equivalents* [Online], Available: http://www.keytometals.com/page.aspx?ID=SteelEquivalents&LN=EN

[14] P. Masuku, private communication, ArcelorMittal South Africa, April 2012.

[15] *Southern African Steel Construction Handbook*, 5th ed., SAISC, South African Institute of Steel Construction, Johannesburg, 2005.

[16] G. Li, W. Wang and S. Chen, "A simple approach for modelling fire-resistance of steel columns with locally damaged fire protection", *Engineering Structures,* vol. 31, pp. 617-622, December 2009.

[17] C. Bailey. (2010, May 21). *One Stop Shop in Structural Fire Engineering,* University of Manchester [Online]. Available: http://www.mace.manchester.ac.uk/project/research/structures/strucfire/

[18] G. Li and C. Zhang, "Creep effect on buckling of axially restrained steel columns in real fires", *Journal of Constructional Steel Research*, vol. 71, pp. 182-188, April 2012.

[19] D.R. Askeland and P.P. Phulé, *The Science and Engineering of Materials*, 5th ed. Toronto, CA: Thomson, 2006.

[20] M. Kadlec et al., "Thermal fatigue crack growth in stainless steel", *International Journal of Pressure Vessels and Piping*, vol. 98, pp. 89-94, October 2012.

[21] Matco Services Inc. (2012, June 17), *Technical Notes*, Matco Services Inc. [Online] Available: http://www.matcoinc.com/home/technical-notes/254-high-temperature-corrosion

[22] BS 476-20: 1987, Fire Tests on Building materials and structures: Part 20: Method of test for determination of the fire resistance of elements of construction (General principles)

[23] K. Tan et al., "Structural responses of restrained steel columns at elevated temperatures. Part 1: Experiments", *Engineering Structures*, vol. 29, no. 8, pp. 1641-1652, August 2007.

[24] J. Sheperd, (2012, April 19), *Structural Fire Engineering to Eurocodes*, University of Sheffield [Online] Available: https://sites.google.com/site/structuralfire/fire-curves

[25] J.A. El-Rimawi, I.W. Burgess and R.J. Plank, "The treatment of strain reversal in structural members during the cooling phase of a fire", *Journal of Constructional Steel Research*, vol. 37, no. 2, pp.115-135, April 1996.

[26] G. Rein et al., "Multi-storey fire analysis for high-rise buildings", *11th Interflam*, London, September 2007.

[27] P. Wang, G. Li and S. Guo, "Effects of the cooling phase of a fire on steel structures", *Fire Safety Journal*, vol. 43, pp. 451-458, August 2008.

[28] R. Beardmore, (2010, March 12), *Heat Treatment Processes,* RoyMech [Online], Available: http://www.roymech.co.uk/Useful_Tables/Matter/Hardening.html

[29] Callister, *Materials Science and Engineering: An Introduction*, 6Th ed., India, Wiley, 2009.

[30] University of Tennessee (2012, August 21), *Iron-Carbon Phase* Diagram, Dept. of Materials Science and Engineering [Online],

Available: http://web.utk.edu/~prack/MSE%20300/FeC.pdf

[31] R.N. Gosh, (2012, August 4), IIT Kharagpur, Principles of Physical Metallurgy: Lecture 31, NPTEL [Video], Available: http://nptel.iitm.ac.in/courses/113105024/

[32] S.K. Mukhopadhyay, H. Roy and A. Roy, "Development of hardness-based model for remaining life assessment of thermally loaded components", *International Journal of Pressure Vessels and Piping*, vol. 86, pp.246-251, April 2009.

[33] T. B. Quimby, (2012, February 12), *A Beginners Guide to the Steel Construction Manual* (14thed.)[Online]Available: http://www.bgstructuralengineering.com/

[34] Z. Huang, K. Tan and S. Ting, "Heating rate and boundary restraint effects on fire resistance of steel columns with creep", *Engineering Structures*, vol. 28, no. 6, pp. 805-817, May 2006.

[35] J. Seputro, "Effect of Support Conditions on Steel Beams Exposed to Fire", M.S. thesis, Department of Civil Engineering, University of Canterbury, Christchurch, NZ, 2002.

[36] A. Heidarpour and M.A. Bradford, "Generic nonlinear modelling of restrained steel beams at elevated temperatures", *Engineering Structures*, vol. 31, pp. 2787-2796, November 2009.

[37] P.J. Dowling, P.R. Knowles and G.W. Owens, *Structural Steel Design*. Oxford, UK: Butterworth, 1988.

[38] Y. L. Guo, Y. Fukumoto, "Theoretical study of ultimate load of locally buckled stub columns loaded eccentrically", *Journal of Constructional Steel Research*, vol. 38, no. 3, pp. 239-255, July 1996.

[39] SANS 10162-1:2005, The Structural Use of Steel, Part 1: Limit State Design of Hot Rolled Steelwork.

[40] R.G. Wellmanns, "An investigation into the structural behaviour of 350W structural steel axial members", M.S. dissertation, University of Johannesburg, Johannesburg, 2007.

[41] J. Mahachi, "A Concise Comparison of Limit State Structural Steel Design to SABS 0162 and Eurocode", CSIR Building and Construction Technology, Pretoria, 2001.

[42] EN 10002-2:1992, Metallic Materials, Part 2: Tensile Testing - Verification of the force measuring systems of the testing machines

[43] EN 10002-5:1992, Metallic Materials, Part 5: Tensile Testing – Method of testing at elevated temperature.

[44] A.S. Usmani et al., "Behaviour of steel framed structures under fire conditions", University of Edinburgh, Main Report, June 2008.

[45] MSC Software Corporation, (2010, May 10), *Integrated Products* [Online], Available: http://www.mscsoftware.com/Products/CAE-Tools/SimXpert.aspx

[46] ASTM A370–10:2010, Standard Test Methods and Definitions for Mechanical Testing of Steel Products.

[47] SANS 6892:1988, Metallic materials - Tensile testing at ambient temperature, ed. 2.

[48] SANS 7500-1:2009, Metallic materials - Verification of static uniaxial testing machines Part 1: Tension/compression testing machines - Verification and calibration of the force measuring system

[49] SANS 6508-1:2009, Metallic Materials – Part 1: Rockwell Hardness Test – test methods.

[50] J. Chen, B. Young and B. Uy, "Behaviour of high strength structural steel at elevated temperatures", *Journal of Structural Engineering*, vol. 132, no. 12, pp. 1948-1954, December 2006.

[51] J. Outinen, O. Kaitila and P. Makelainen, "A study for the development of the design of steel structures in fire conditions", *Proceedings of the 1st International Workshop of Structures in Fire*, pp. 267-281, Copenhagen, Denmark, 2000.

[52] X. Qiang, F.S.K. Bijlaard and H. Kolstein, "Post-fire mechanical properties of high strength structural steels S460 and S690", *Engineering Structures*, vol. 35, pp. 1-10, February 2012.

[53] S.K. Ghosh, P. Mallick and P.P. Chattopadhyay, "Effect of cold deformation on phase evolution and mechanical properties in an austenitic stainless steel for structural and safety applications", *Journal of Iron and Steel Research*, vol. 19, no. 4, pp. 63-68, April 2012.

[54] M. Macdonald, G.T. Taylor and J. Rhodes, "The effect of cold forming on the yield strength of thin gauge steel—hardness test approach", *Thin-Walled Structures*, vol. 29, pp. 243-256, December 1997

[55] F.O. Sonmez and A. Demir, "Analytical relations between hardness and strain for cold formed parts", *Journal of Materials Processing Technology*, vol. 186, pp. 163-173, May 2007.

[56] South African Institute of Steel Construction, (2012, April 20), *Section properties of steel profiles* [Online], Available: http://saisc.co.za/saisc/struct_sd_profiles.htm

[57] T.V. Galambos, *Guide to Stability Design Criteria for Metal Structures*. 4th ed., United States of America: John Wiley & Sons, 1988.

[58] Constructalia: The Steel Construction Website (2012, April 22), *Steel beams and channels*, ArcelorMittal [Online], Available: http://www.constructalia.com/english/products/structures/steel_beams_and_channels

A. APPENDIX - FR STEEL NUMERICAL MODELS

The following equations were taken from [4]

Thermal expansion coefficient:

$$\alpha_s = (0.0062T_s + 11.48) \times 10^{-6} \ {}^{m}/_{(m\,°C)} \quad \text{(A.1)}$$

Specific heat:

$$c_s = 1.95 \times 10^{-6}T_s^3 - 1.58 \times 10^{-3}T_s^2 + 0.689T_s + 473.1 \ {}^{J}/_{(kg\,°C)} \quad \text{(A.2)}$$

Conductivity:

$$\lambda_s = -0.0256T_s + 54 \ {}^{W}/_{(m\,°C)} \quad \text{(A.3)}$$

Yield strength:

$$\frac{f_{yT}}{f_y} = 1 - {(0.001724 \times T_s - 0.034482)^{3.2}}/{3} \quad \text{(A.4)}$$

Modulus of elasticity:

$$\frac{E_T}{E} = -2.22 \times 10^{-7}T_s^2 - 2.097 \times 10^{-4}T_s + 1.005 \quad \text{(A.5)}$$

Where T_s is the temperature of the steel; and E and E_T are the elastic modulus of steel at normal temperature and elevated temperature respectively.

B. APPENDIX - THERMAL SHOCK PARAMETER

$$R_T = \frac{k\sigma_T(1-\nu)}{\alpha E} \qquad \text{(B.1)}$$

Where,

K *is thermal conductivity,*

σ_T *is maximal tension the material can resist,*

α *is the thermal expansion coefficient*, and

E *is the Young's modulus, and* ν *is the Poisson ratio. [19]*

C. APPENDIX - TEST PIECE DIMENSIONS

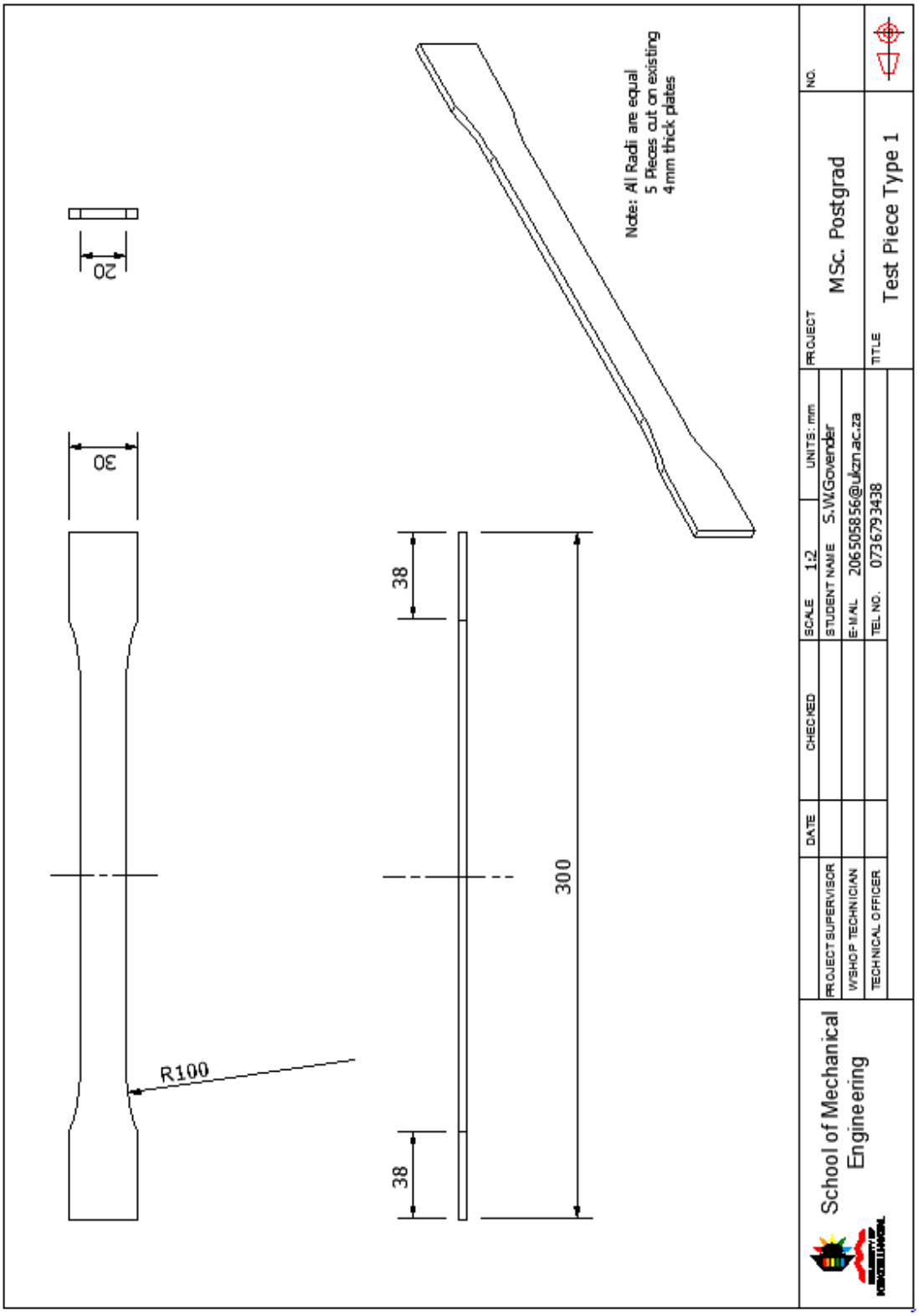

Figure C-1: Detail Drawing of Dog-bone test piece

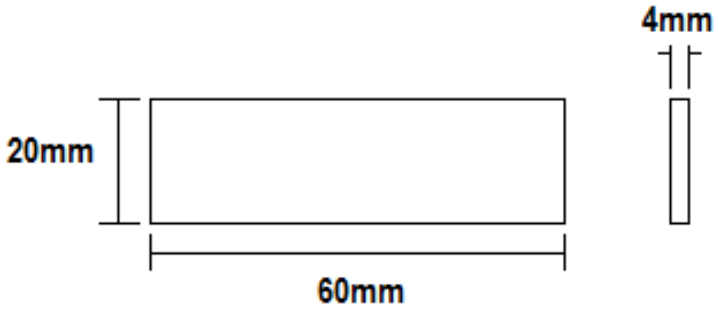

Figure C-2: Dimensions of specimens for hardness testing

D.APPENDIX - HEATING PATTERNS

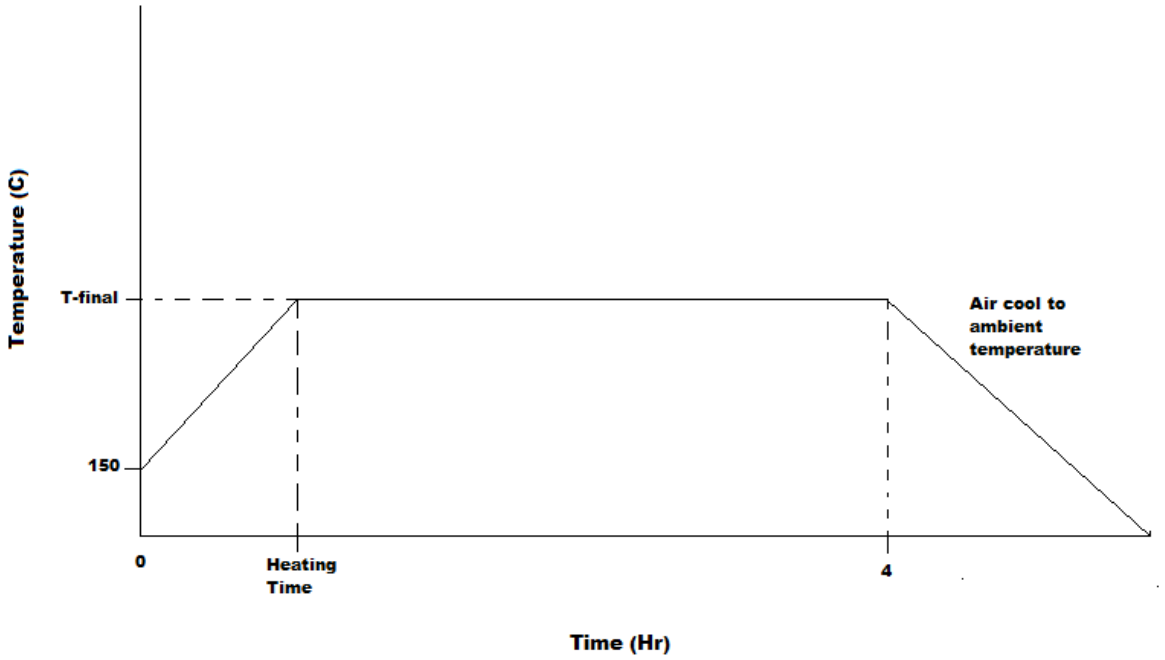

Figure D-1: Heating pattern for reusability tests on 350W

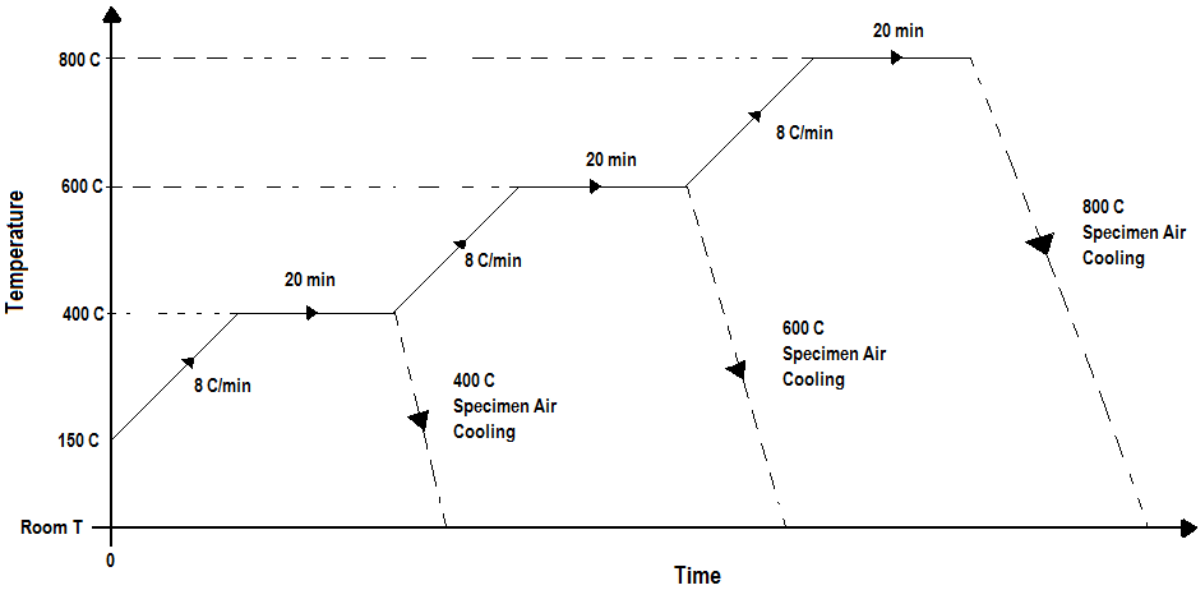

Figure D-2: Heating pattern for reusability tests on S355

E. APPENDIX - YIELD ANGLE CALCULATIONS

Using the torsion formula Eq. (E.1):

$$\tau_{max} = \frac{Tr}{J} \qquad \text{(E.1)}$$

Where, J is the polar moment of inertia.

Using 350MPa as the maximum shear stress, the torque T can be solved for.

The angle of twist can be found using Eq. (E.2),

$$\phi = \frac{TL}{GJ} \qquad \text{(E.2)}$$

Where G is the shear modulus of elasticity,

F. APPENDIX - DIMENSIONS OF MODEL GEOMETRY

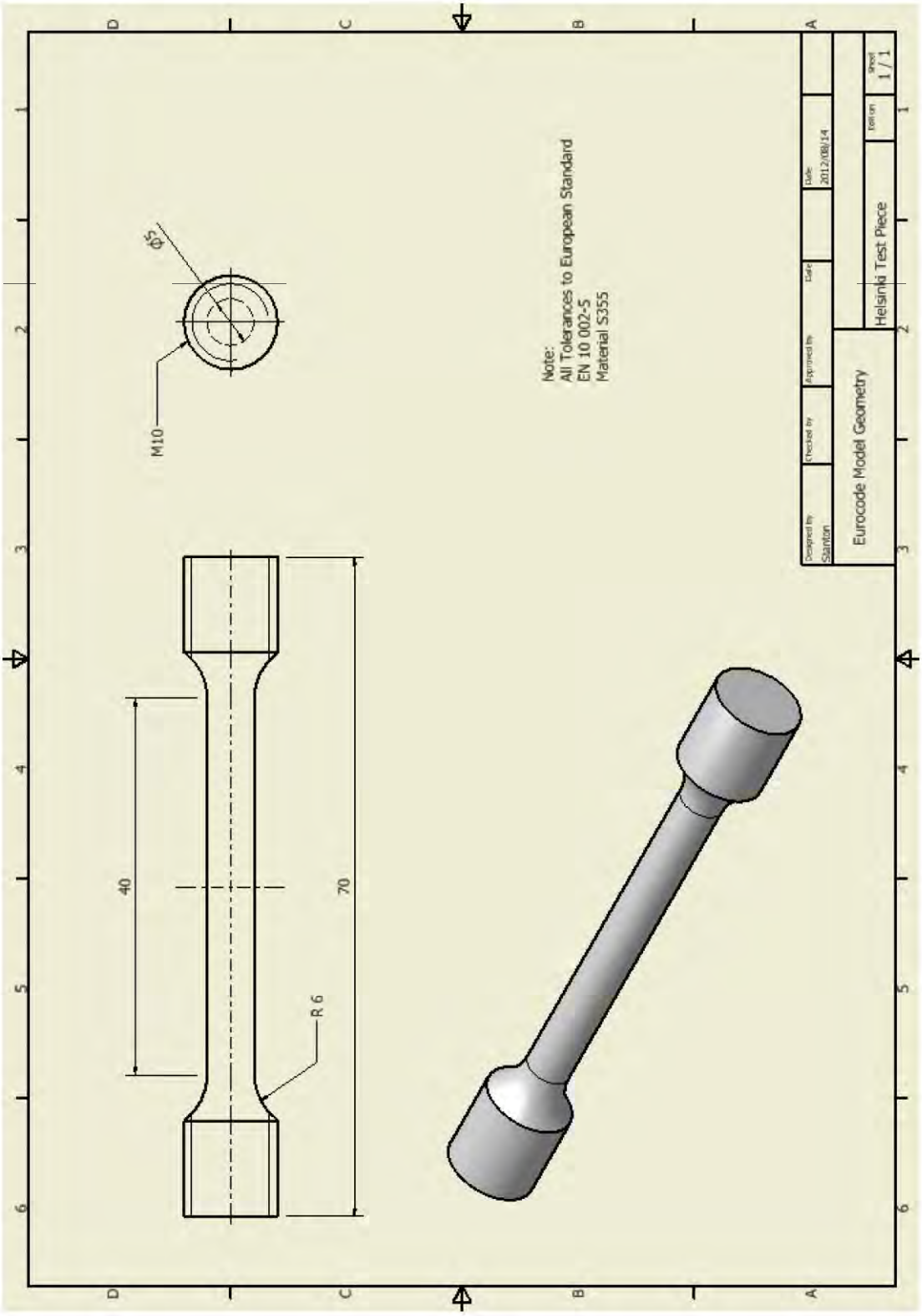

Figure F-1: Dimensions of Helsinki Test Piece

Table F-1: 90x90x8 Dimensional Properties [56]

h=b(mm)	t(mm)	r_1(mm)	r_2(mm)	A(mm^2)	$z_s=y_s$(mm)	v(mm)	u_1(mm)	u_2(mm)	I_v(mm^4)	$I_y= I_z$(mm^4)
90	8	11	5,5	13900	25,0	63,6	35,3	31,7	428900	1044000

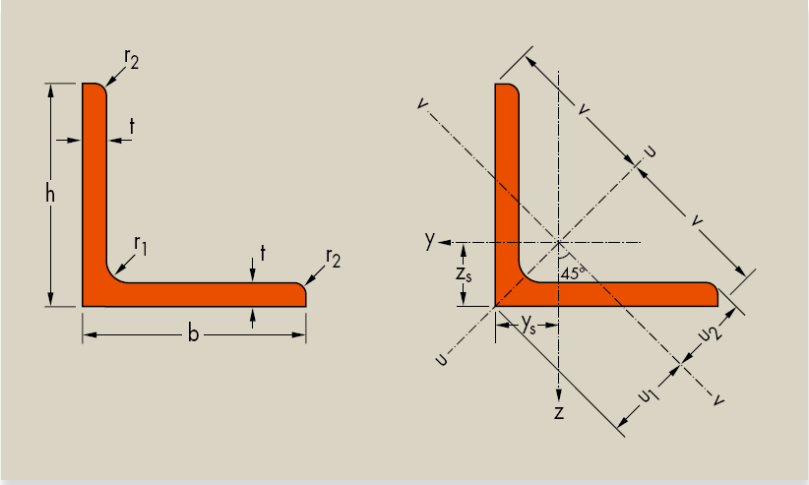

Figure F-2: 90x90x8 Equal Angle Cross Section [58]

Table F-2: 152x76x18 Dimensional Properties [56]

h(mm)	b(mm)	t_w(mm)	t_f(mm)	r_1(mm)	r_2(mm)	d(mm)	A(mm^2)	I_z(mm^4)	y_s(mm)	y_m(mm)
152,4	76,2	6,4	9,0	14,0	7,0	103	2248	1090000	20,4	41,2

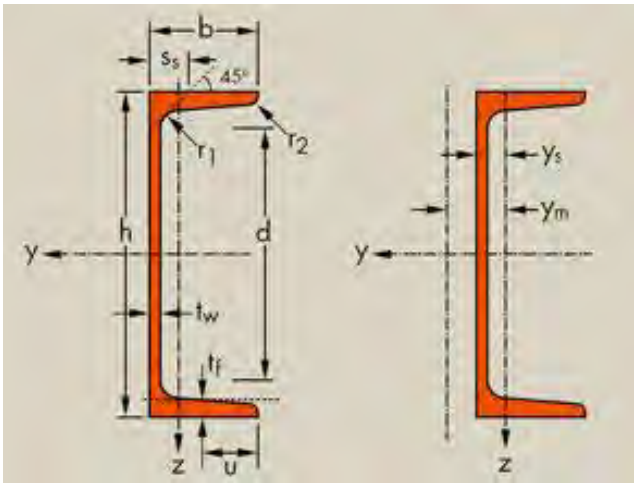

Figure F-3: 152x76x18 Channel Cross Section [58]

G. APPENDIX - EUROCODE INPUT DATA

Table G-1: EC3 – Temperature Dependant Young's Modulus for S355

Temperature [°C]	Modulus of Elasticity [N/mm^2]
0	210345
100	210000
200	189655
300	171034
400	146896
500	125517
600	63448
700	29655
800	18621
900	13103
1000	8275

Table G-2: EC3 – Temperature Dependant Thermal Expansion Coefficient for S355

Temperature [°C]	Thermal Coefficient of Expansion [1/°C]
0	0.00E+00
50	2.00E-05
100	1.60E-05
150	1.44E-05
200	1.43E-05
250	1.42E-05
300	1.42E-05
350	1.42E-05
400	1.44E-05
450	1.46E-05
500	1.47E-05
550	1.49E-05
600	1.50E-05
650	1.50E-05
700	1.53E-05
750	1.50E-05
800	1.42E-05
850	1.33E-05
900	1.35E-05
950	1.38E-05
1000	1.42E-05

Table G-3: EC3 – Stress Vs Strain at Room Temperature for S355

Strain [%]	Stress [N/mm^2]
0	25
0.1	225
0.2	344
0.3	378
0.4	388
0.5	391
0.6	388
0.7	384
0.8	384
0.9	384
1	388
1.1	384
1.2	388
1.3	384
1.4	384
1.5	388
1.6	394
1.7	397
1.8	397
1.9	398
2	399

Table G-4: Stress Vs Strain at 300C for S355

Strain[%]	Stress [N/mm^2]
0	0
0.1	169
0.2	250
0.3	273
0.4	286
0.5	296
0.6	307
0.7	315
0.8	323
0.9	327
1	332
1.1	338
1.2	342

1.3	344
1.4	348
1.5	349
1.6	350
1.7	352
1.8	354
1.9	355
2	355

Table G-5: Stress Vs Strain at 400C for S355

Strain[%]	Stress [N/mm^2]
0	0
0.1	146
0.2	204
0.3	232
0.4	252
0.5	269
0.6	282
0.7	294
0.8	305
0.9	313
1	323
1.1	327
1.2	335
1.3	339
1.4	344
1.5	346
1.6	350
1.7	352
1.8	354
1.9	355
2	355

H.APPENDIX - 350W COMPRESSION INPUT DATA

Table H-1: 350W Stress Vs Strain Equal Angle 90x90x8

Strain[%]	Stress [N/mm^2]
0	0
0.1	216
0.2	393
0.3	417
0.4	418
0.5	419
0.6	420
0.7	420
0.8	419
0.9	419
1	419

Table H-2: 350W Stress Vs Strain Channel 156x76x18

Strain[%]	Stress [N/mm^2]
0	0
0.1	204
0.2	395
0.3	423
0.4	429
0.5	429
0.6	430
0.7	430
0.8	430
0.9	432
1	439

I. APPENDIX - S355 LINEAR MODEL FRINGE PLOTS

ROOM TEMPERATURE

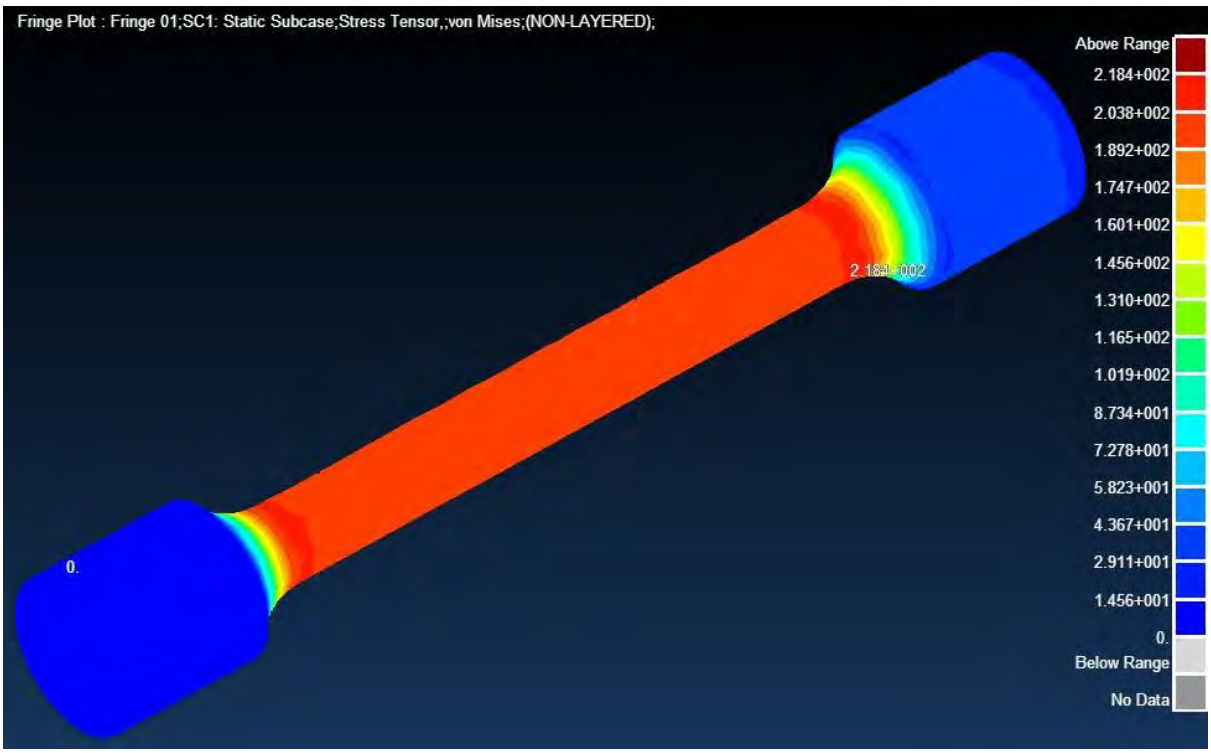

Figure I-1: Stress fringe plot at 200MPa

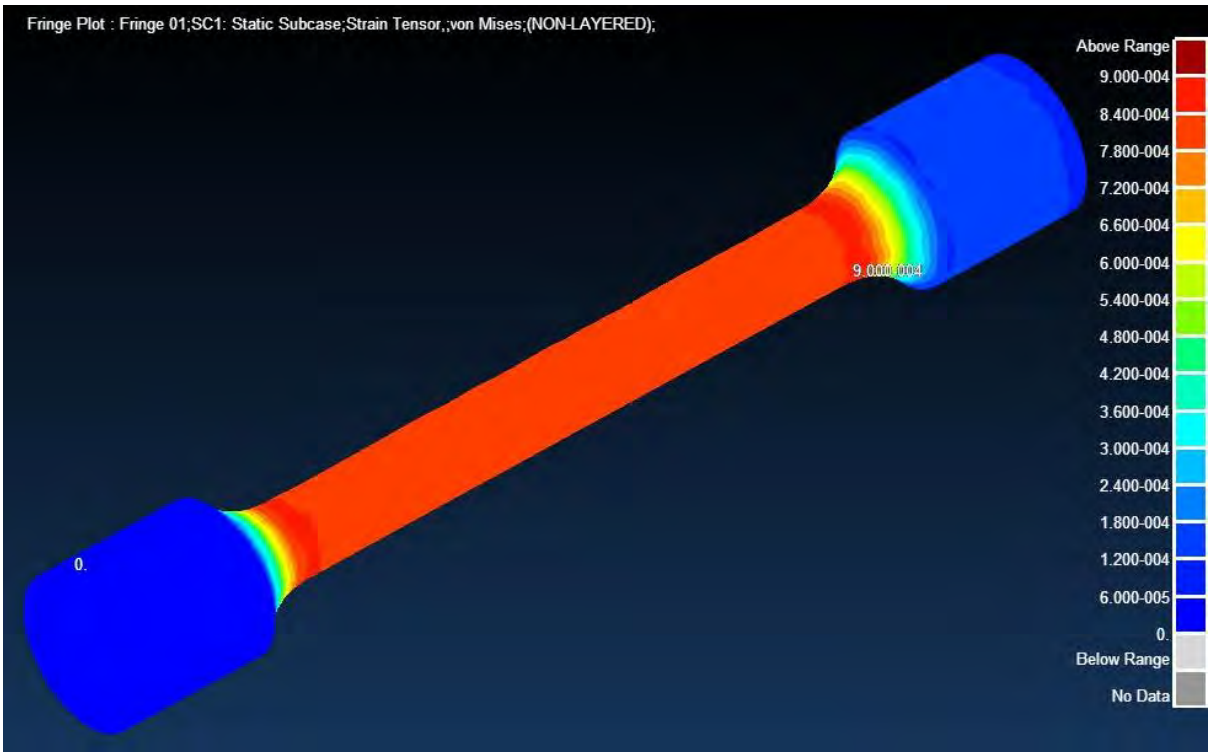

Figure I-2: Strain fringe plot at 200MPa

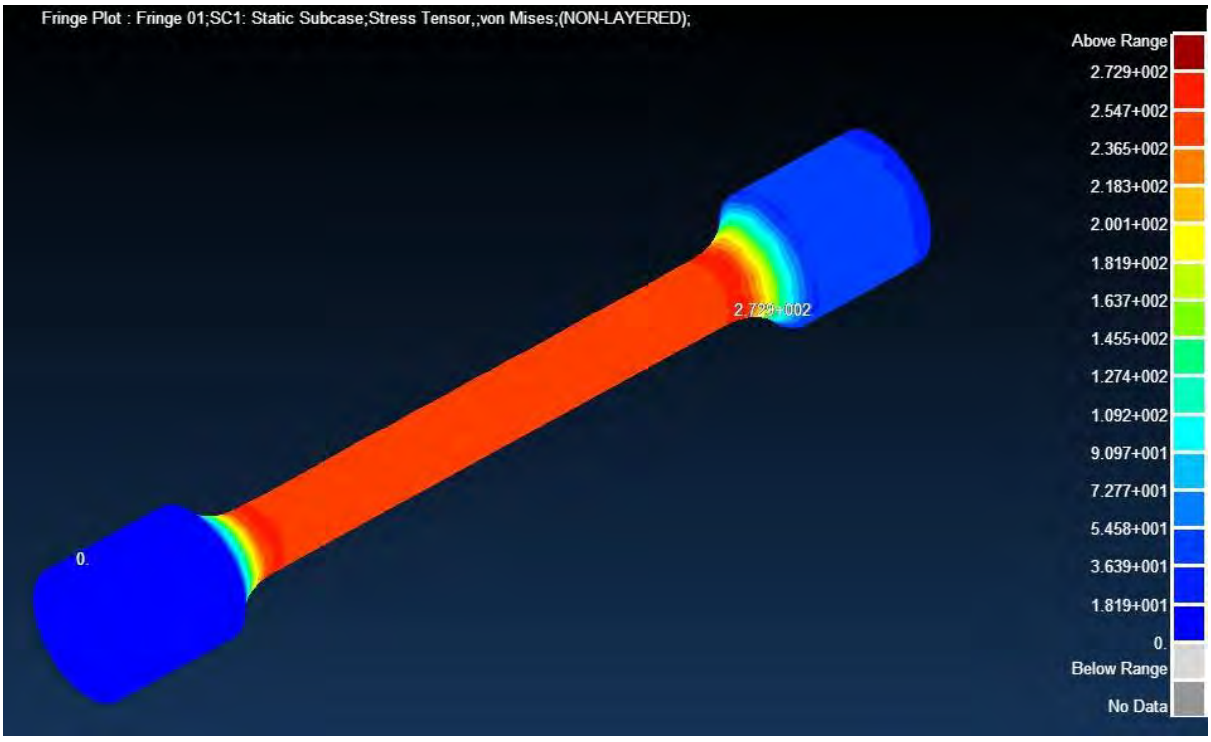

Figure I-3: Stress fringe plot at 250MPa

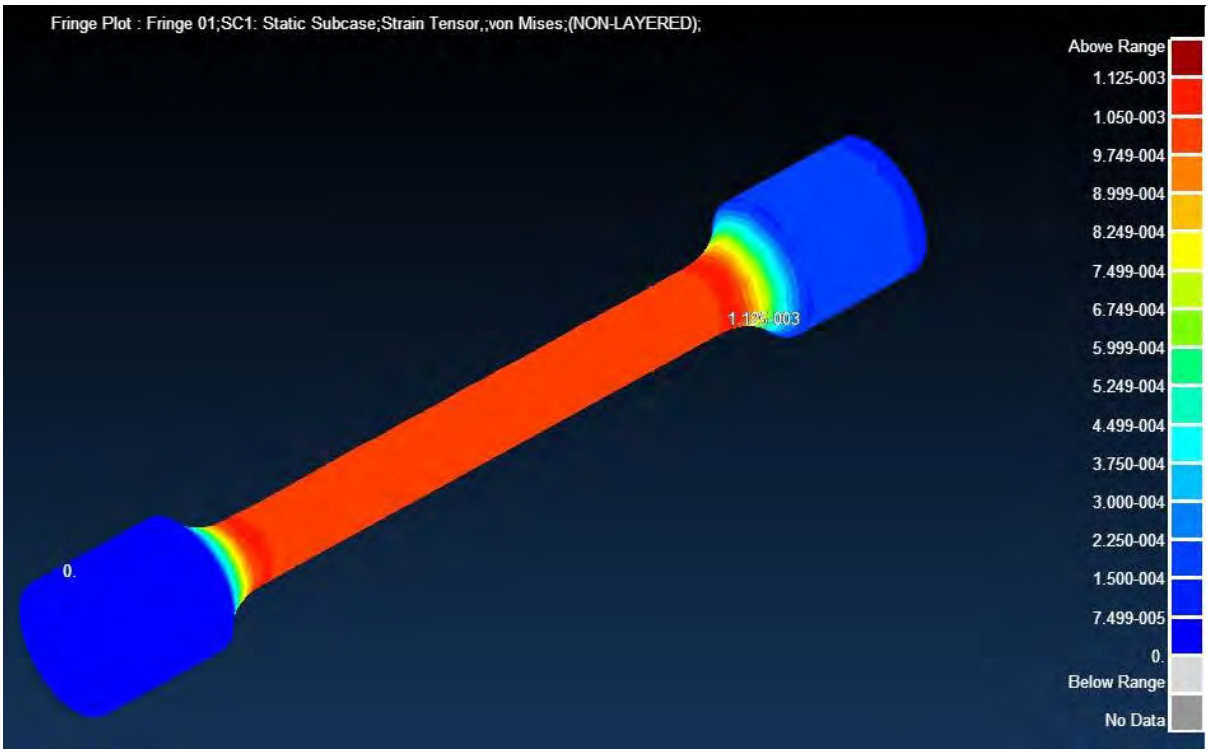

Figure I-4: Strain fringe plot at 250MPa

TEMPERATURE DEPENDENCE AT 150MPA

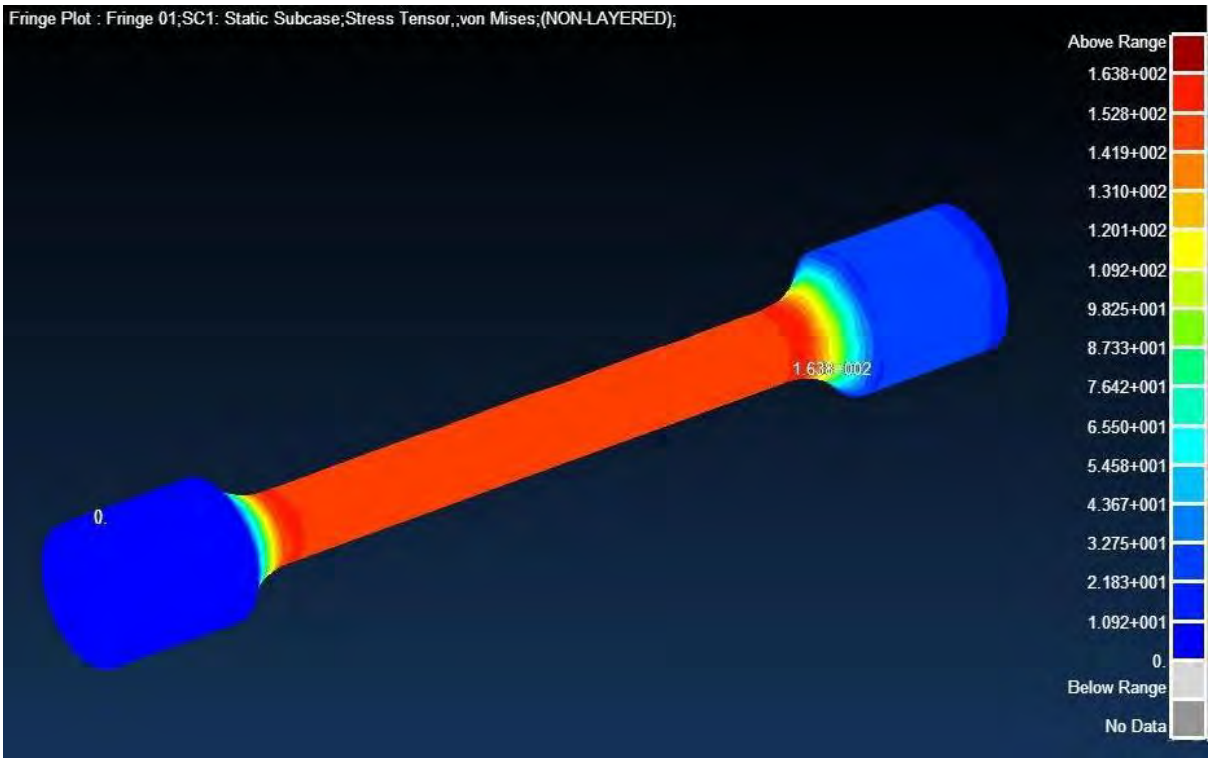

Figure I-5: Stress Fringe Plot for S355 Linear Model at Room Temperature

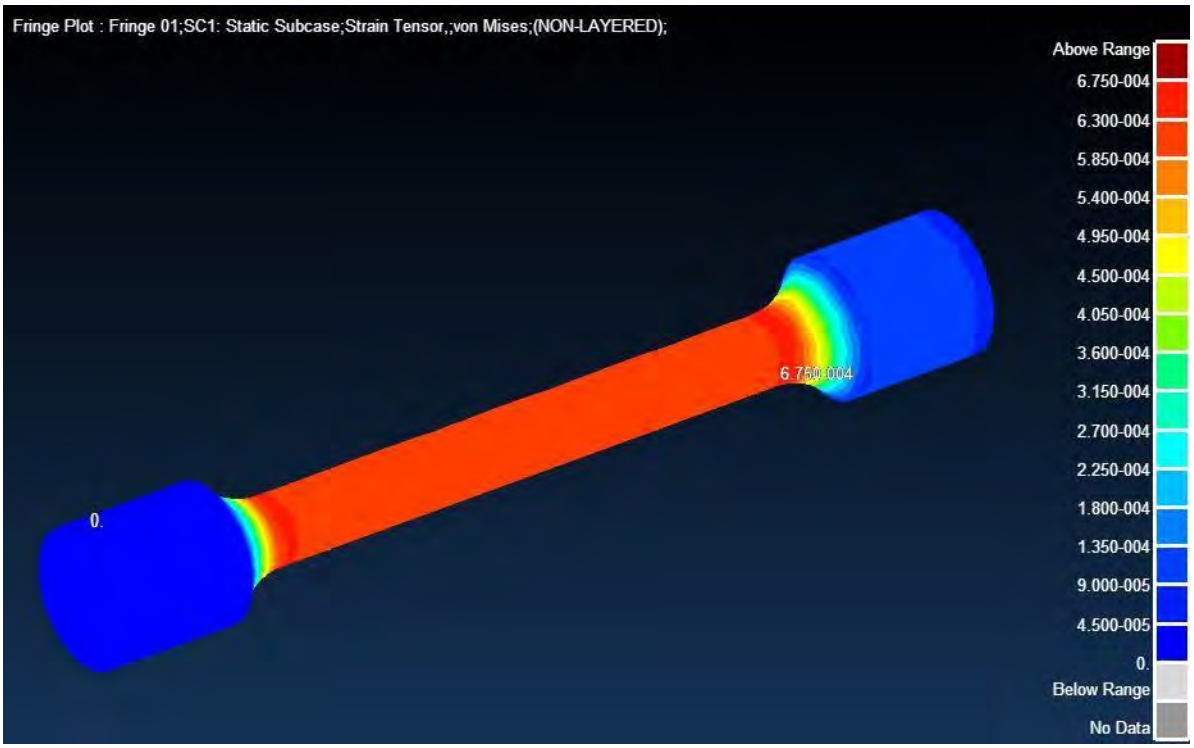

Figure I-6: Strain Fringe Plot for S355 Linear Model at Room Temperature

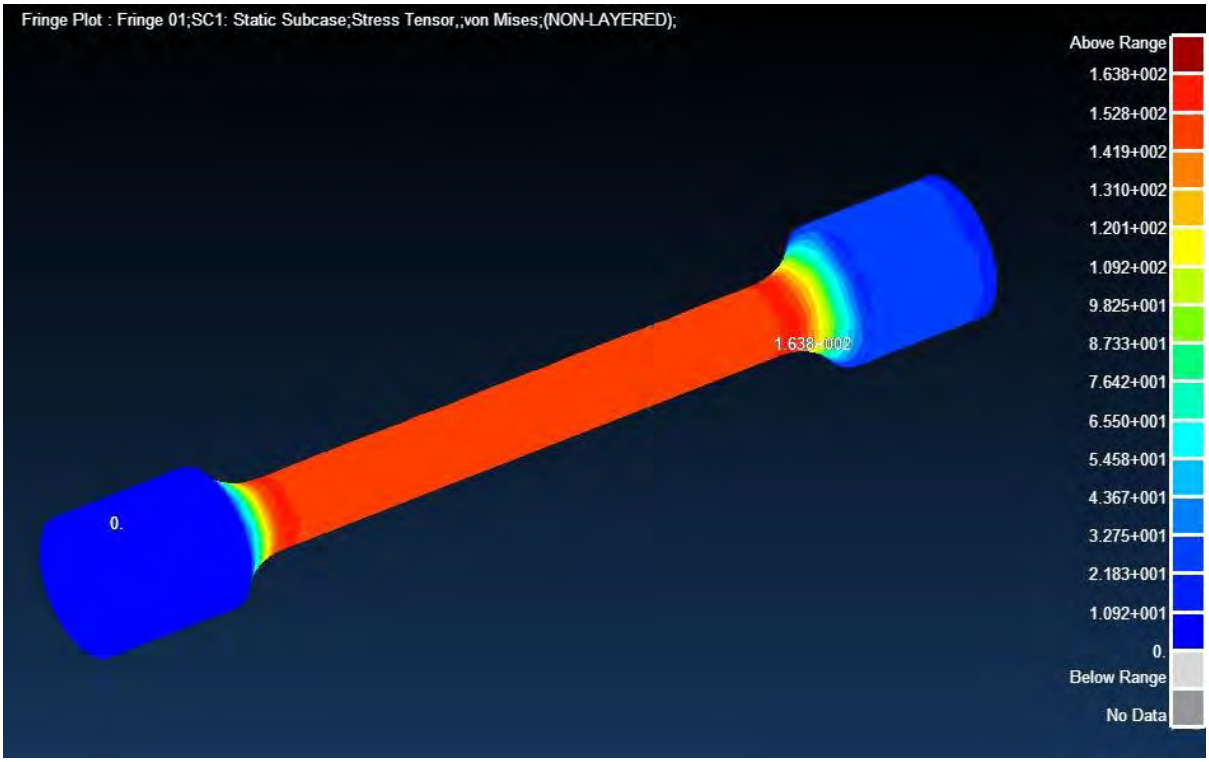

Figure I-7: Stress Fringe Plot for S355 Linear Model at 300°C

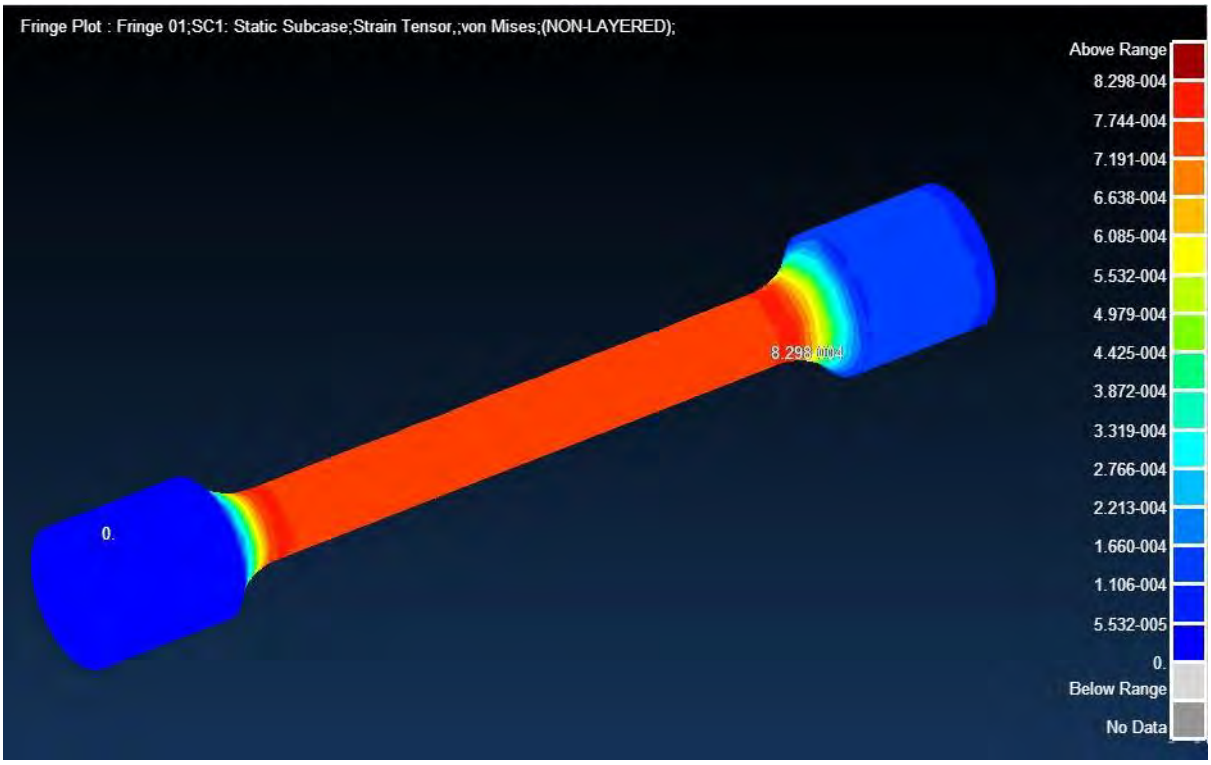

Figure I-8: Strain Fringe Plot for S355 Linear Model at 300°C

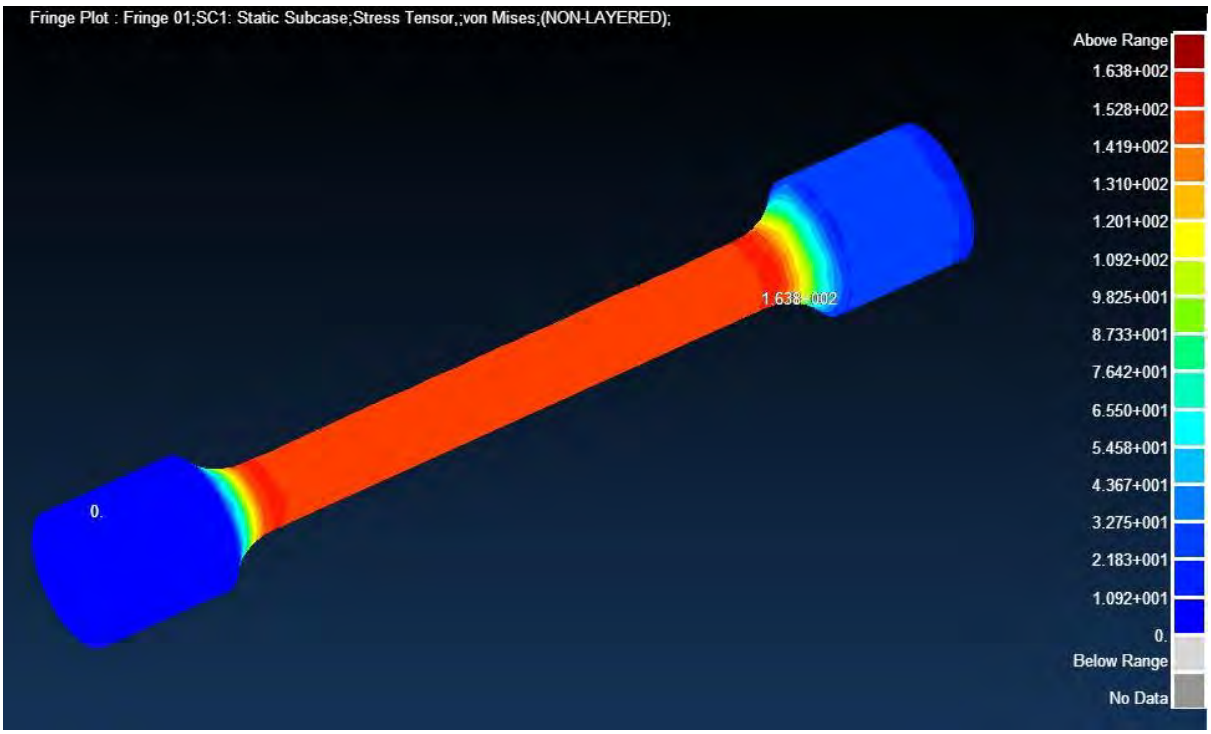

Figure I-9: Stress Fringe Plot for S355 Linear Model at 400°C

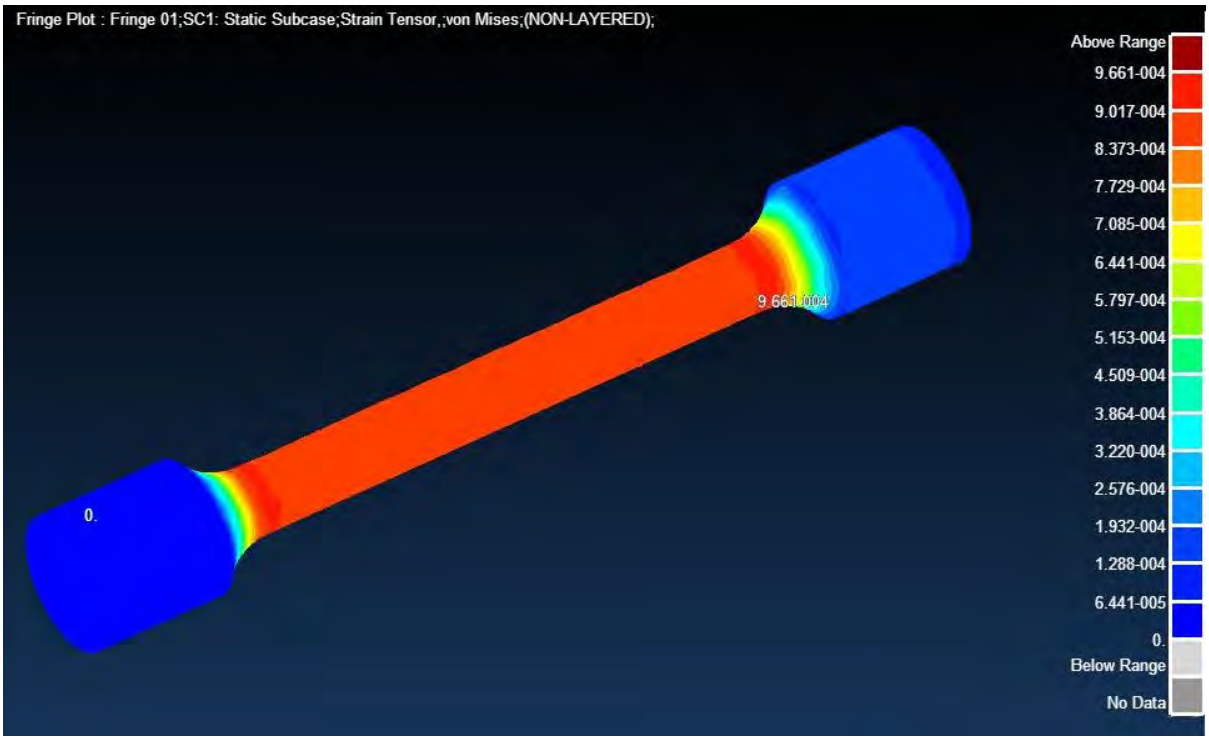

Figure I-10: Strain Fringe Plot for S355 Linear Model at 400°C

J. APPENDIX - S355 NON-LINEAR FRINGE PLOTS

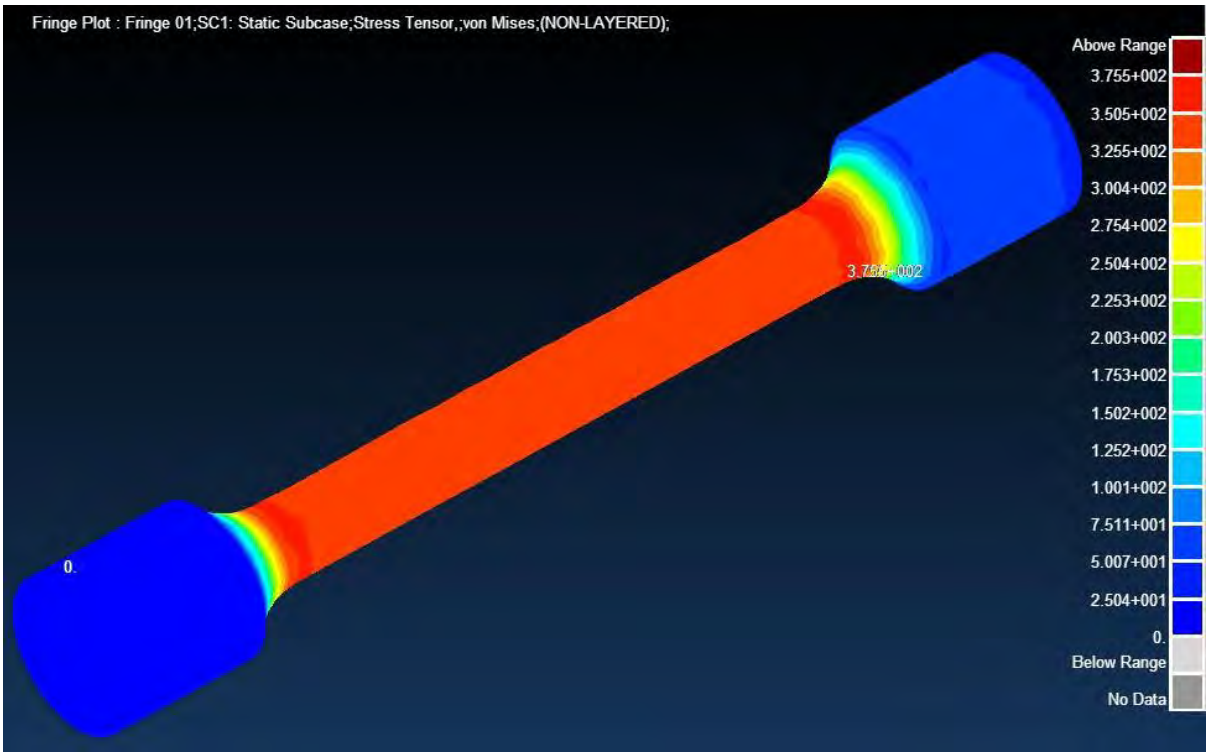

Figure J-1: Stress fringe plot for S355 Non-linear Model at 25°C

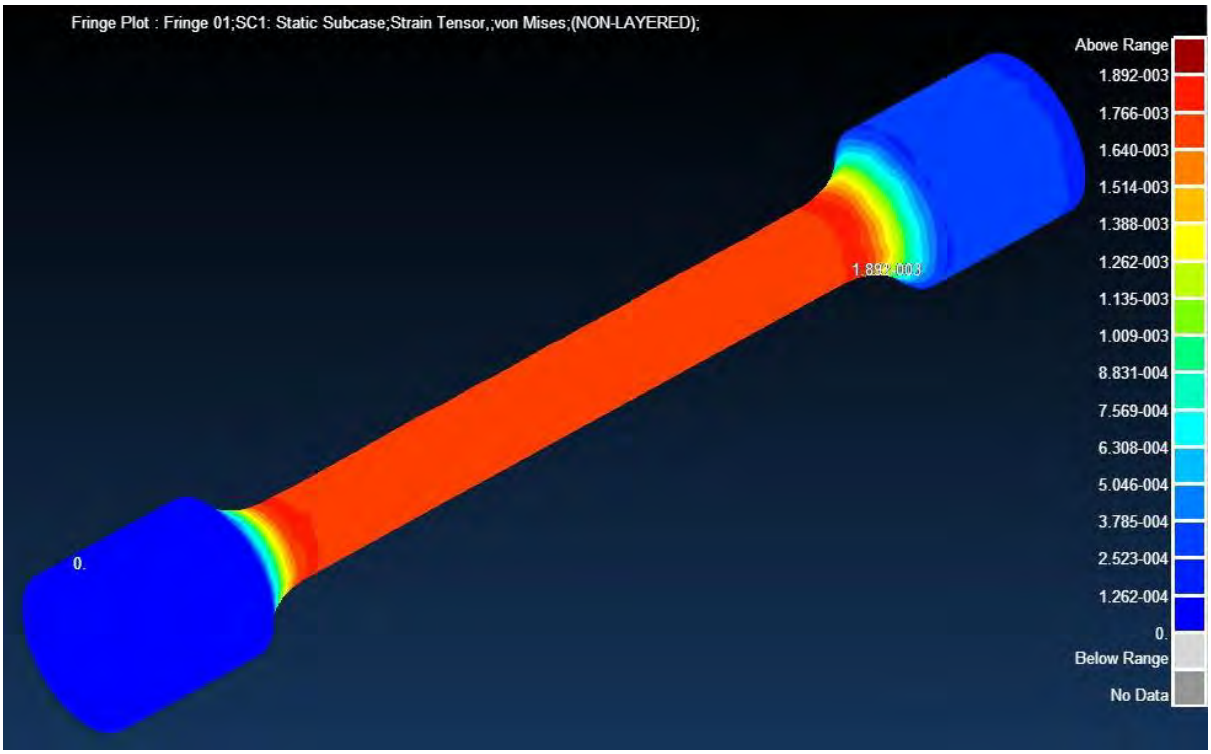

Figure J-2: Strain fringe plot for S355 Non-linear Model at 25°C

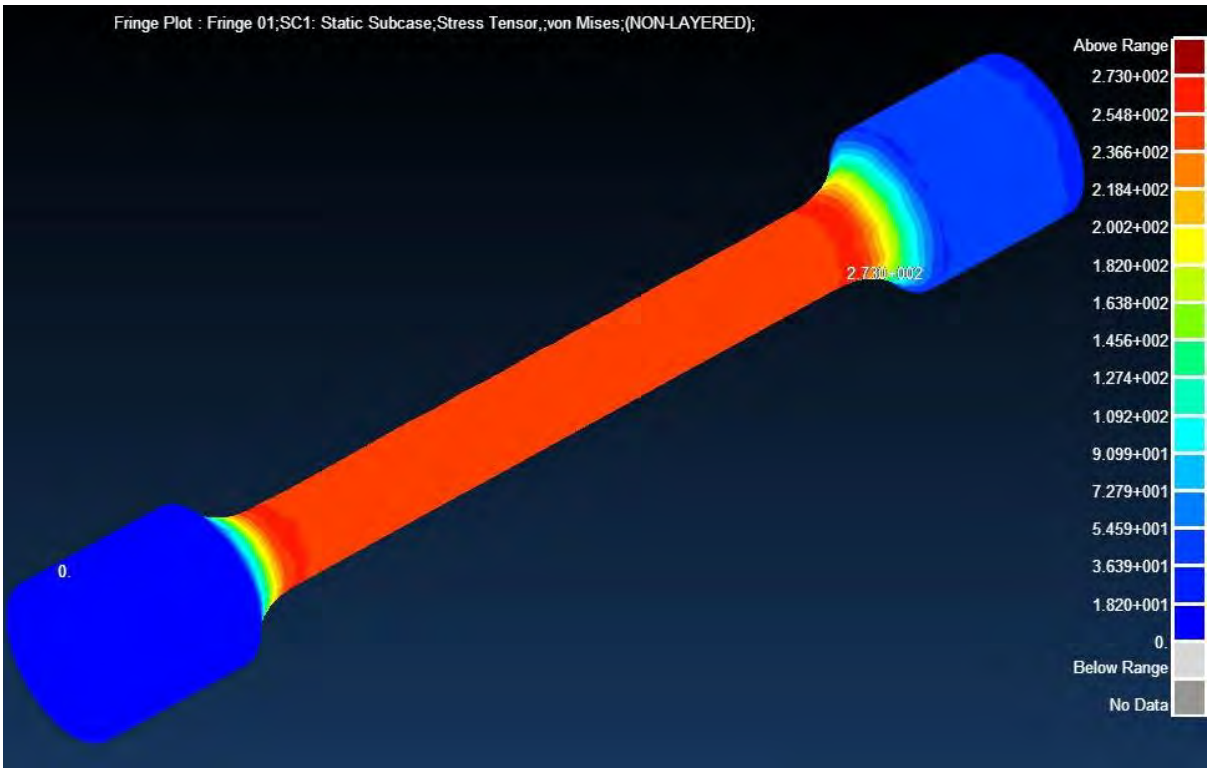

Figure J-3: Stress fringe plot for S355 Non-linear Model at 300°C

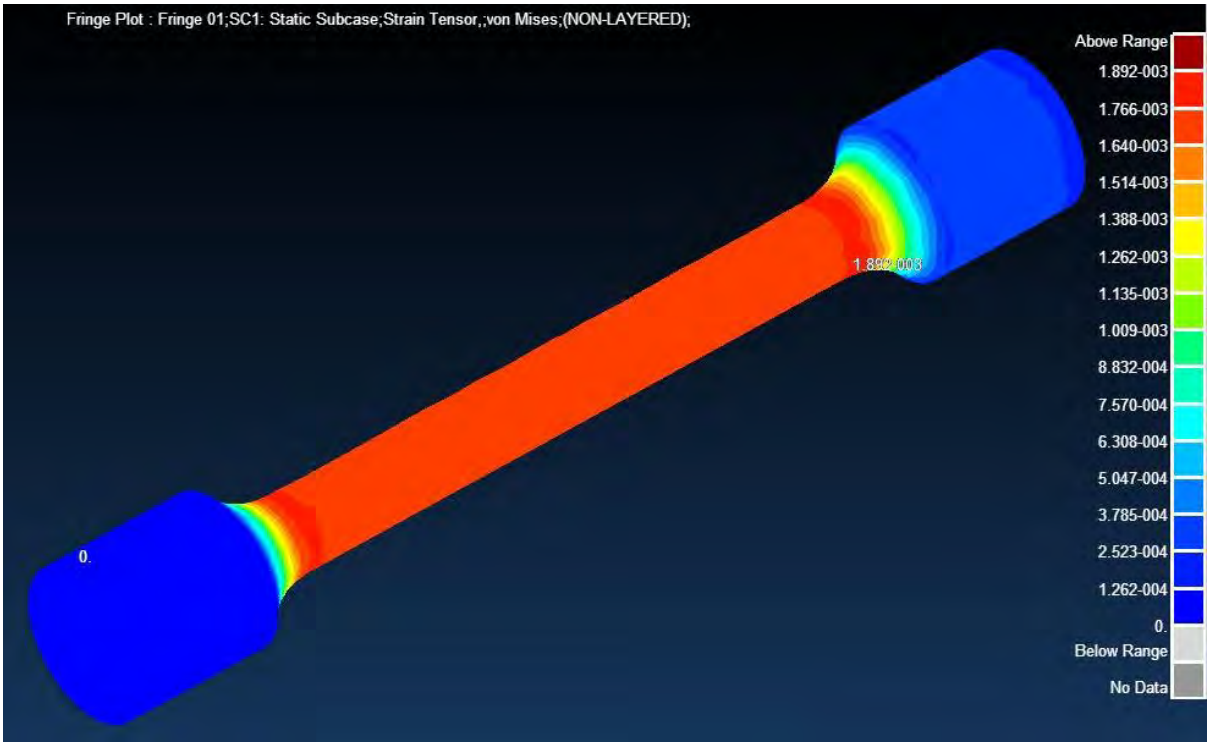

Figure J-4: Strain fringe plot for S355 Non-linear Model at 300°C

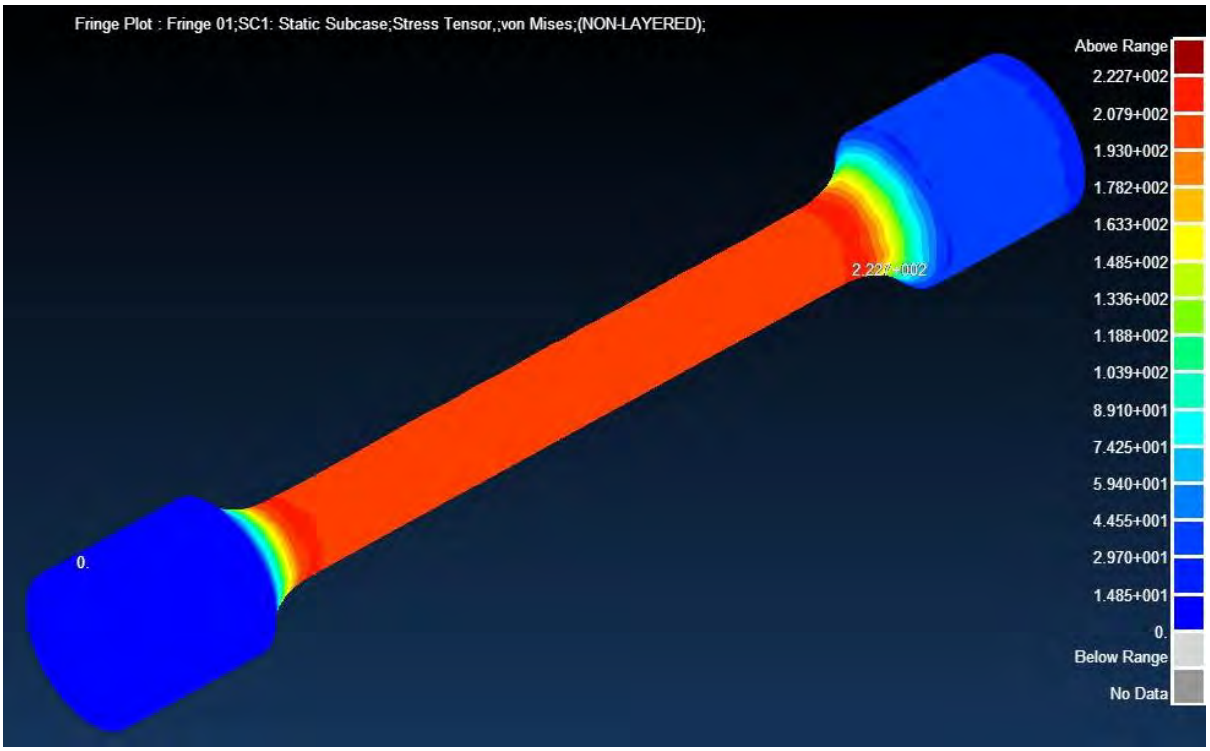

Figure J-5: Stress fringe plot for S355 Non-linear Model at 400°C

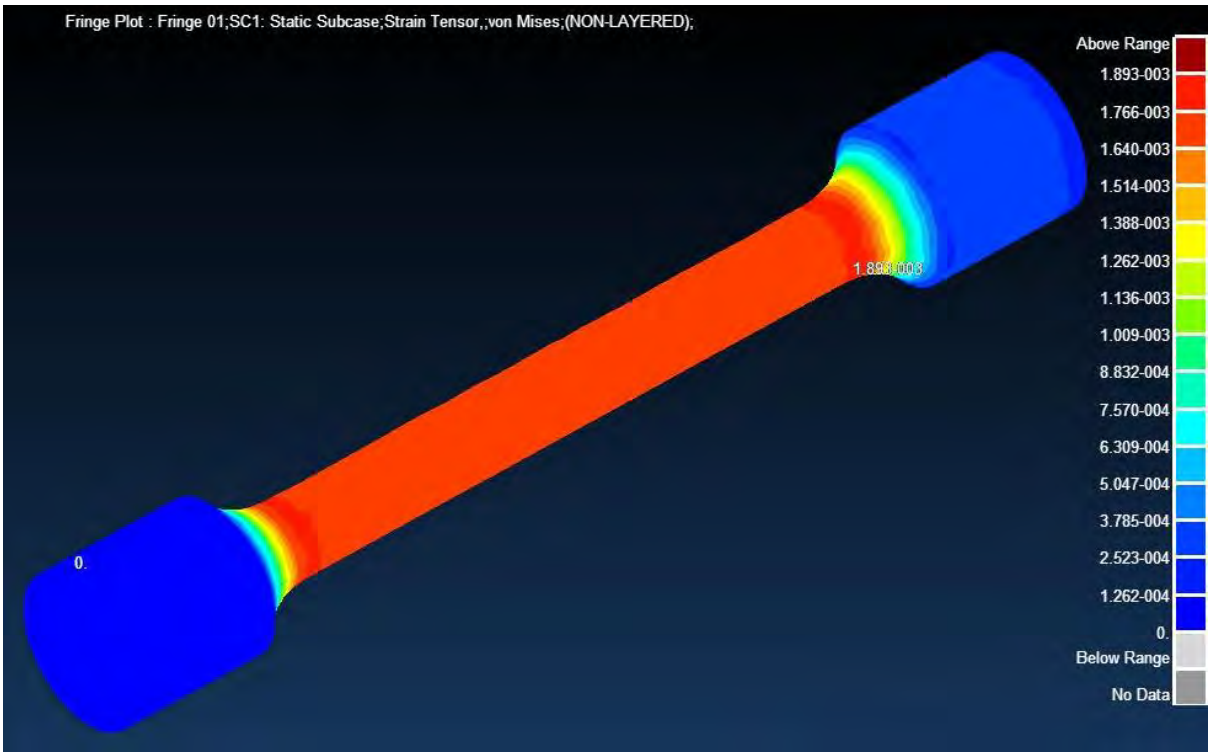

Figure J-6: Strain fringe plot for S355 Non-linear Model at 400°C

K. APPENDIX - 350W STUB COLUMN FRINGE PLOTS

EQUAL ANGLE 90X90X8

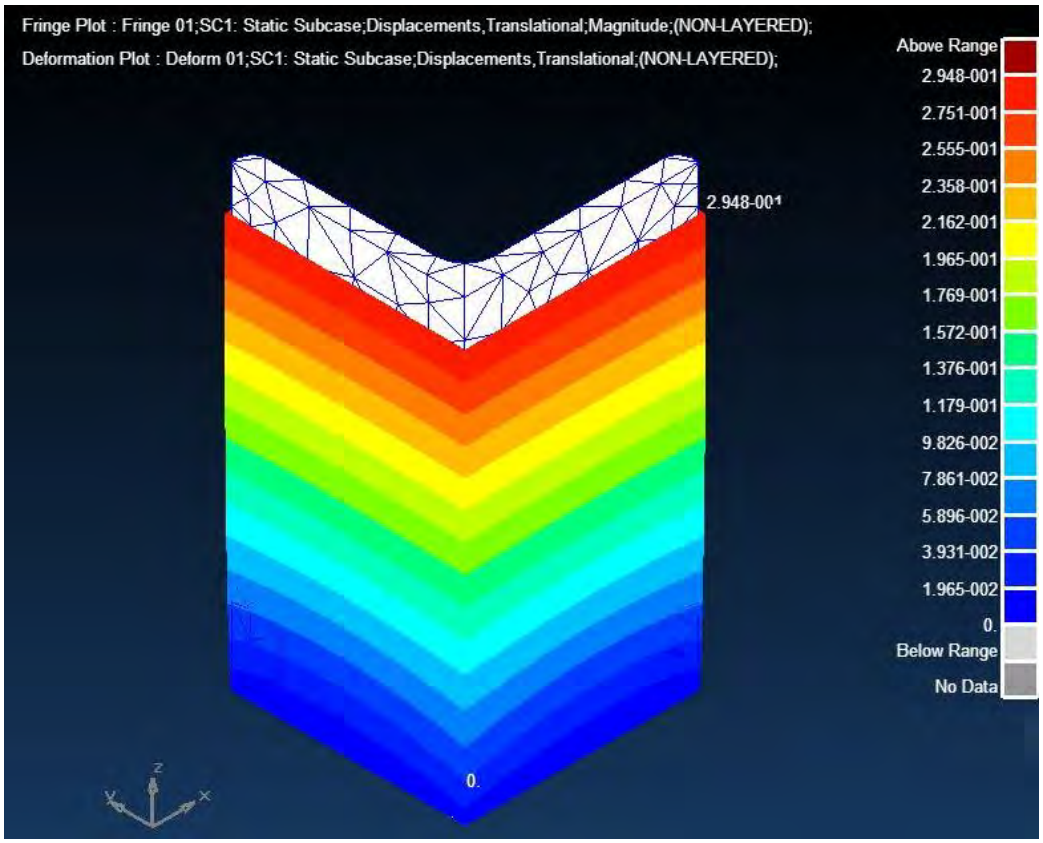

Figure K-1: 90x90x8 Total Compressive Displacement at 350MPa

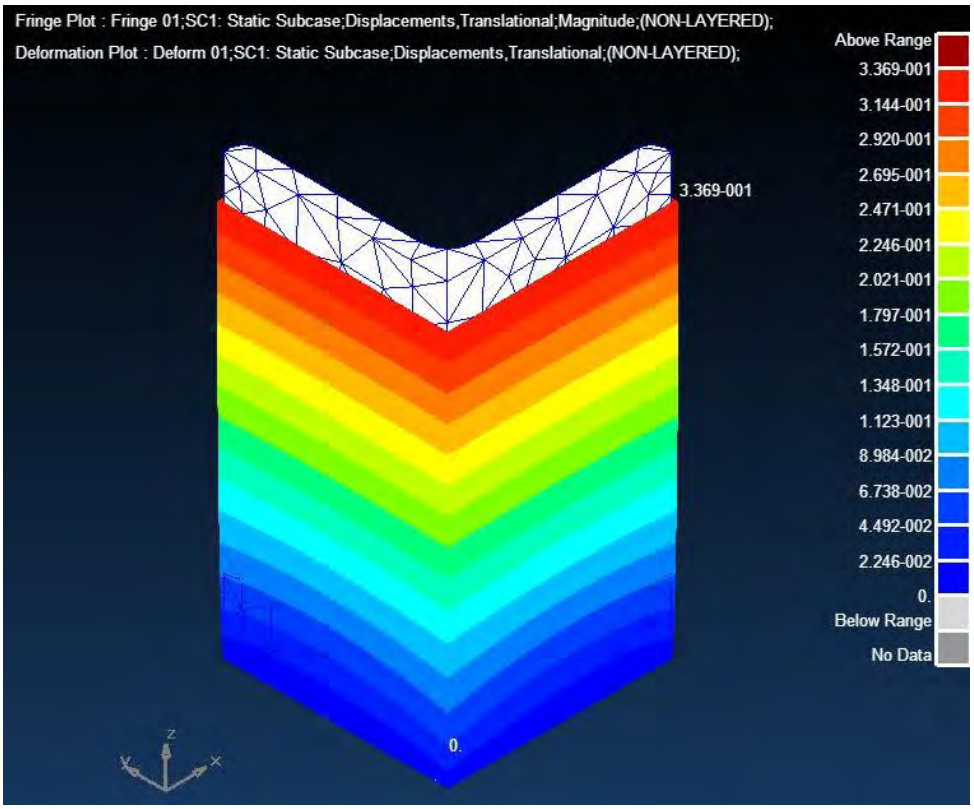

Figure K-2:90x90x8 Total Compressive Displacement at 400MPa

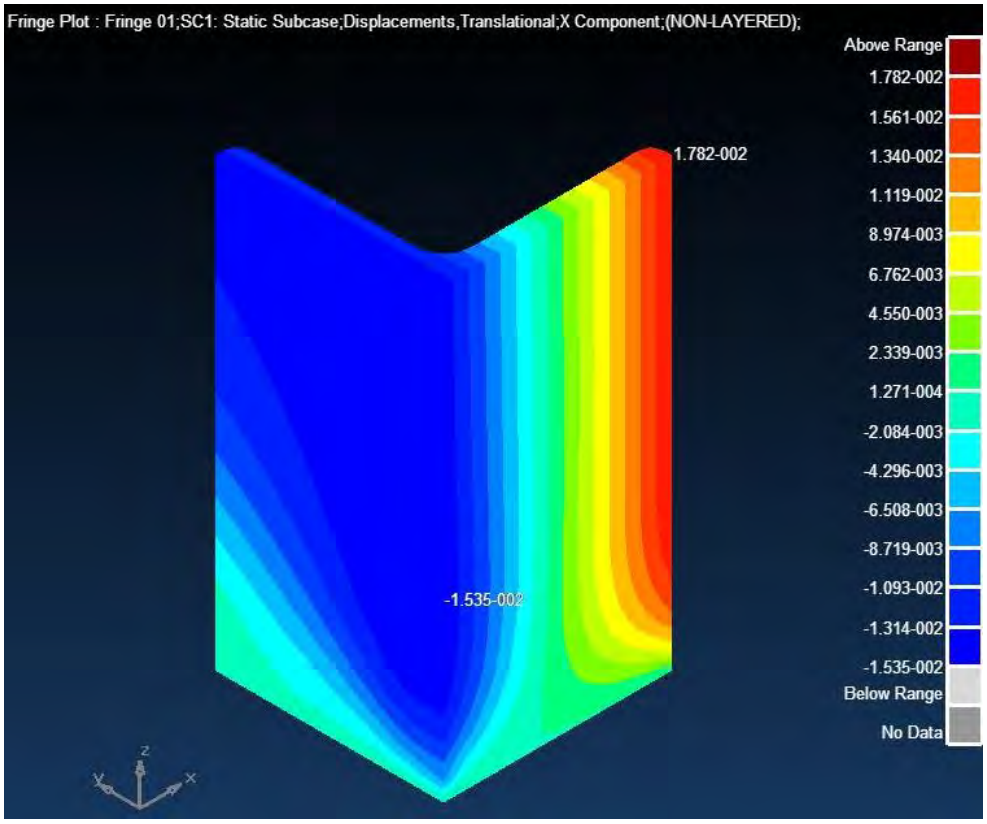

Figure K-3:90x90x8 X Displacement at 250MPa

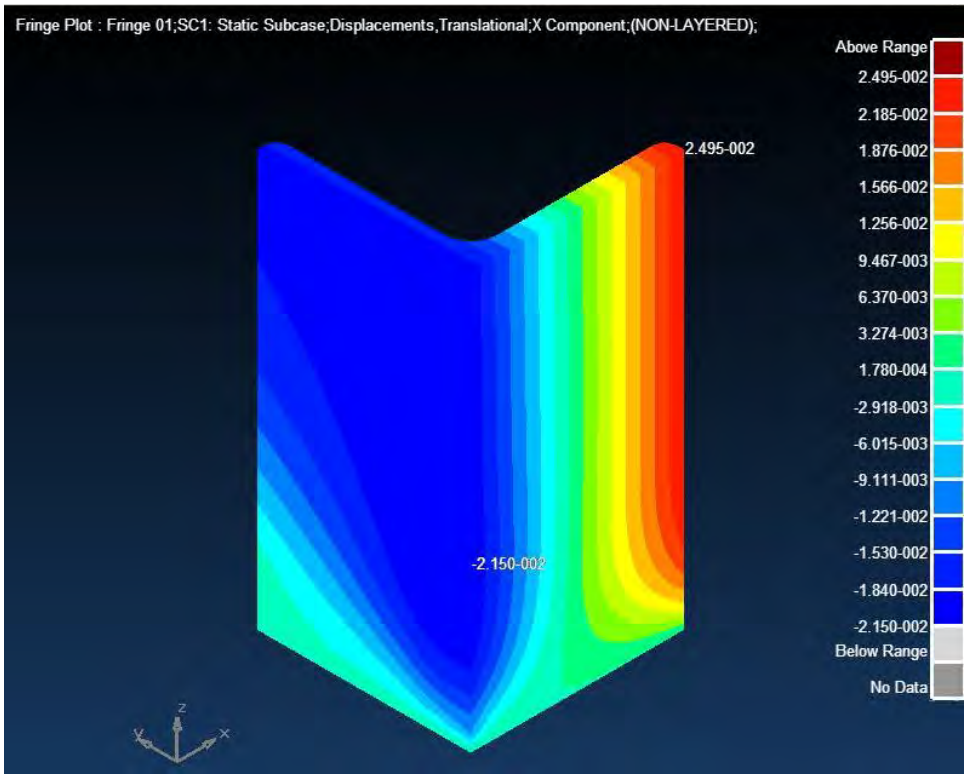

Figure K-4: 90x90x8 X Displacement at 350MPa

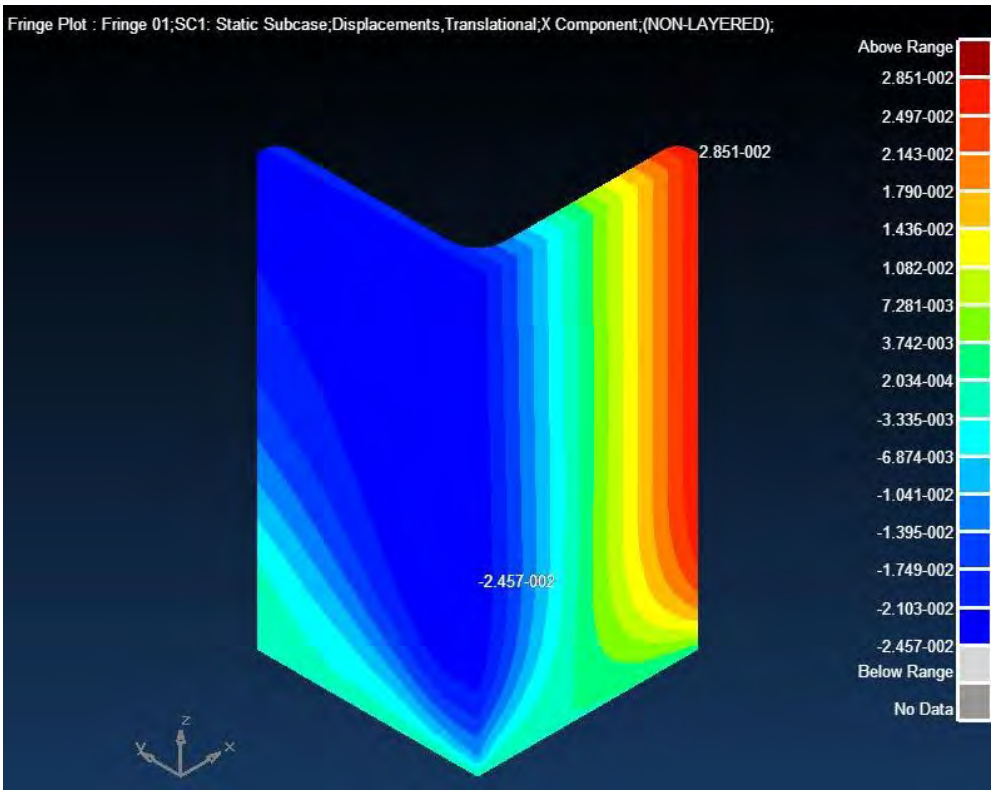

Figure K-5:90x90x8 X Displacement at 400MPa

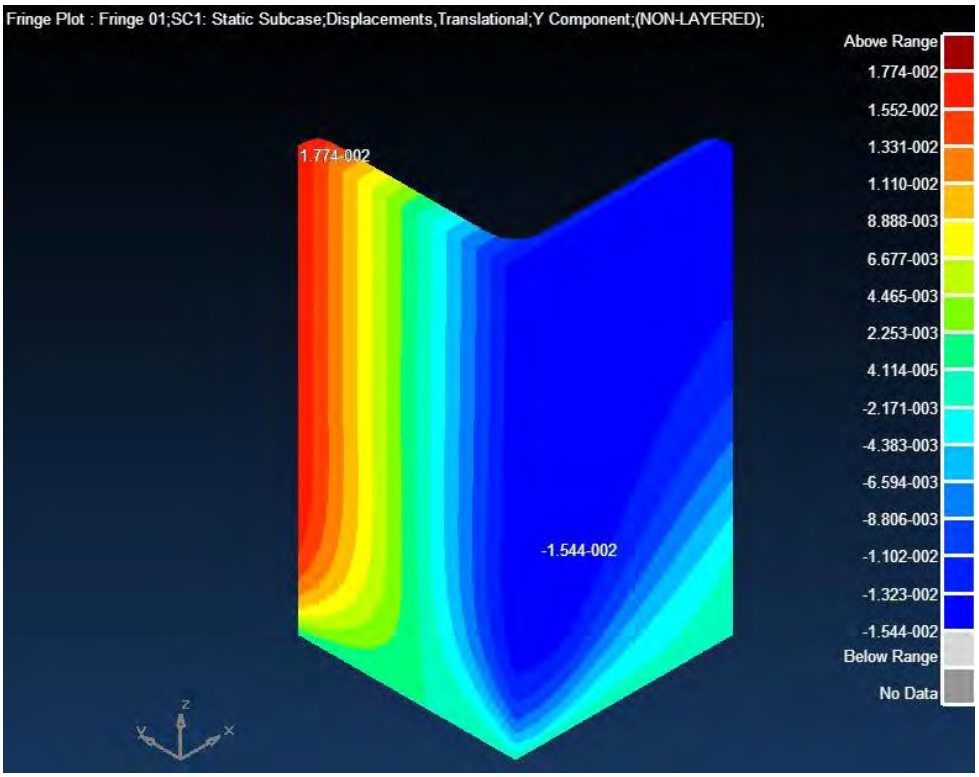

Figure K-6: 90x90x8 Y Displacement at 250MPa

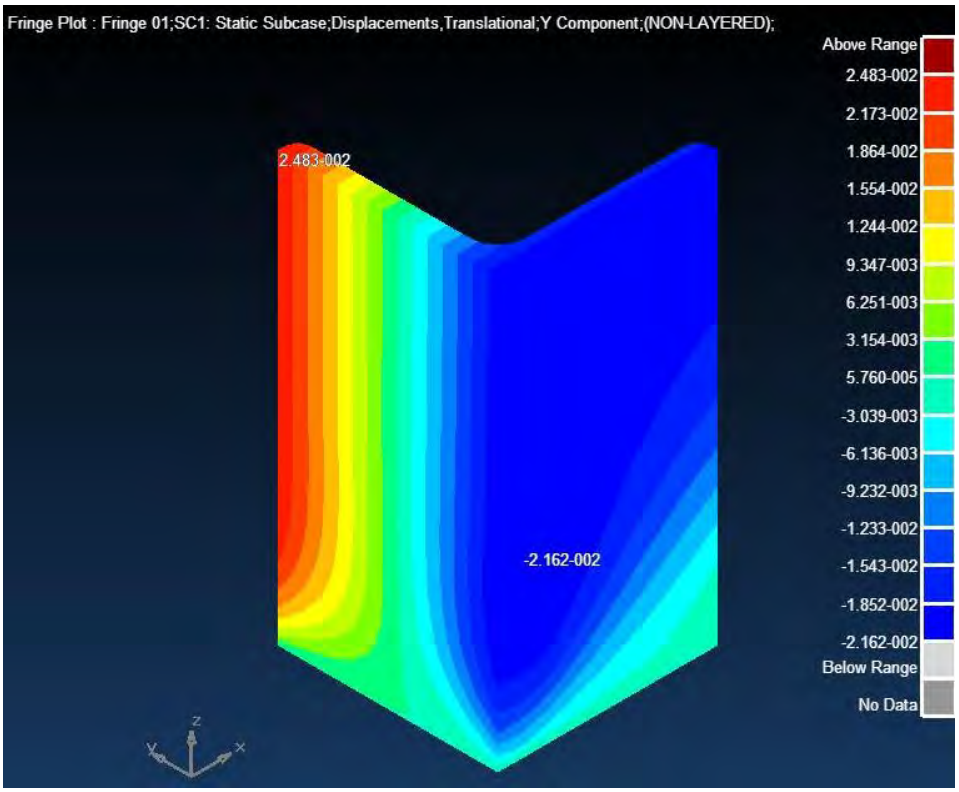

Figure K-7: 90x90x8 Y Displacement at 350MPa

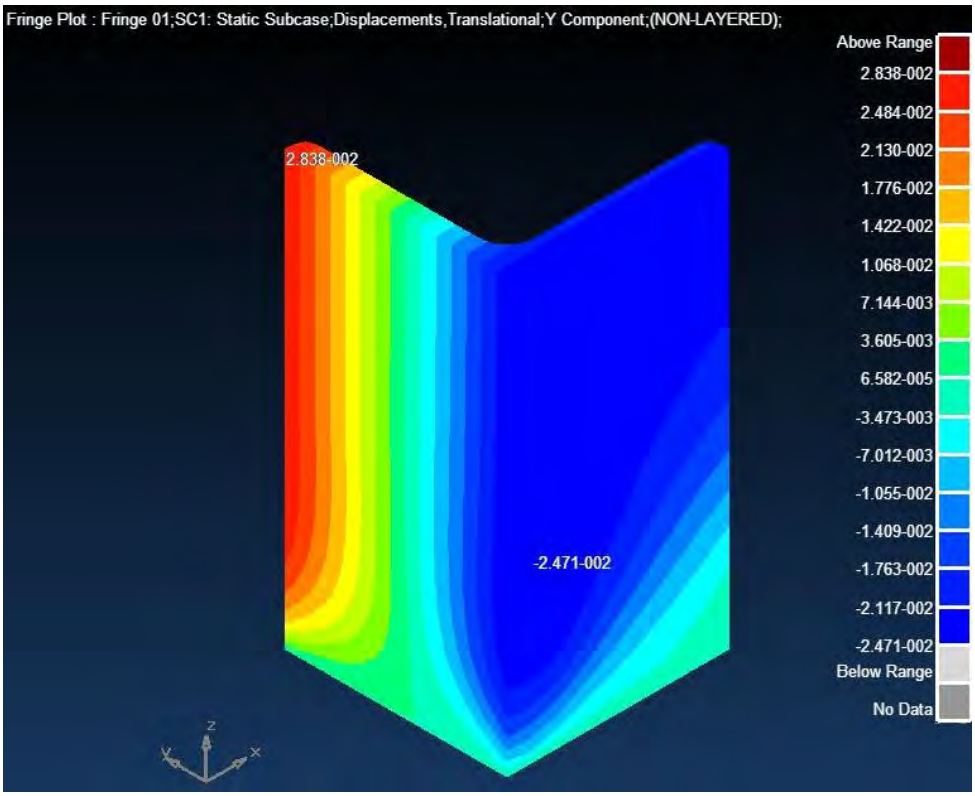

Figure K-8:90x90x8 Y Displacement at 400MPa

CHANNEL 152X76X18

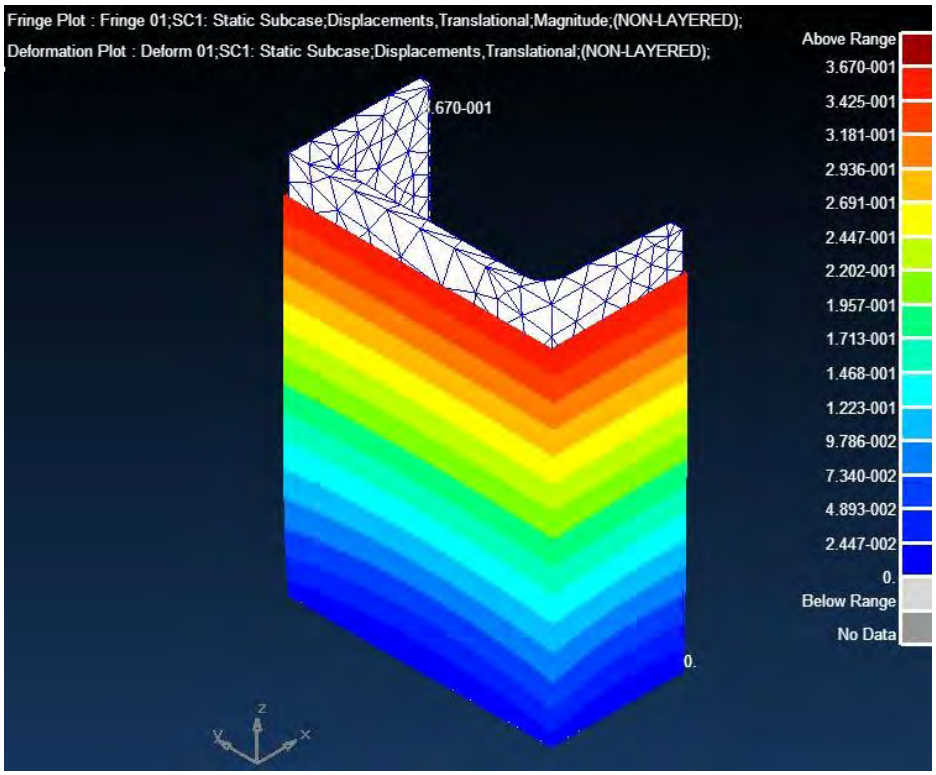

Figure K-9:152x76x18 Total Compressive Displacement at 350MPa

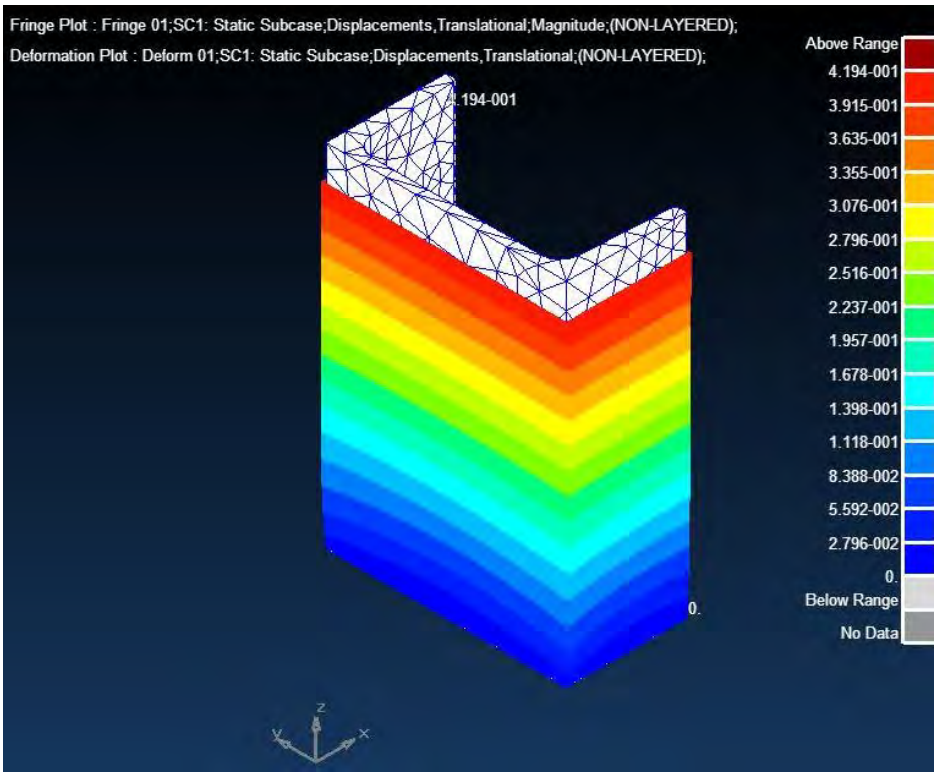

Figure K-10: 152x76x18 Total Compressive Displacement at 400MPa

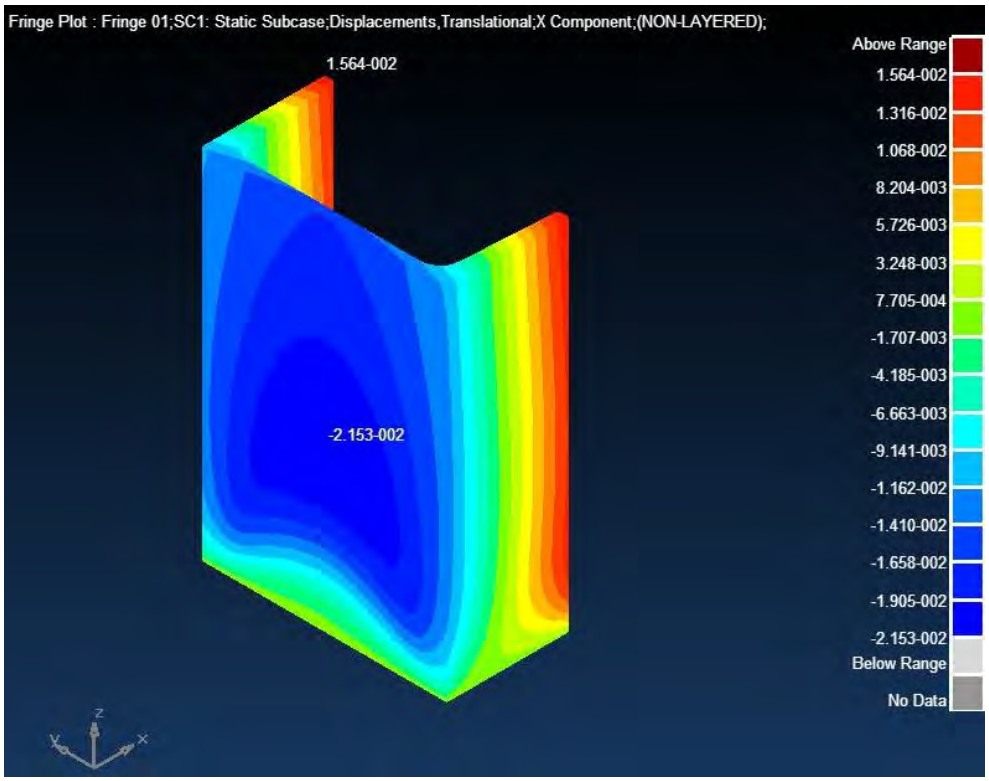

Figure K-11:152x76x18 X Displacement at 250MPa

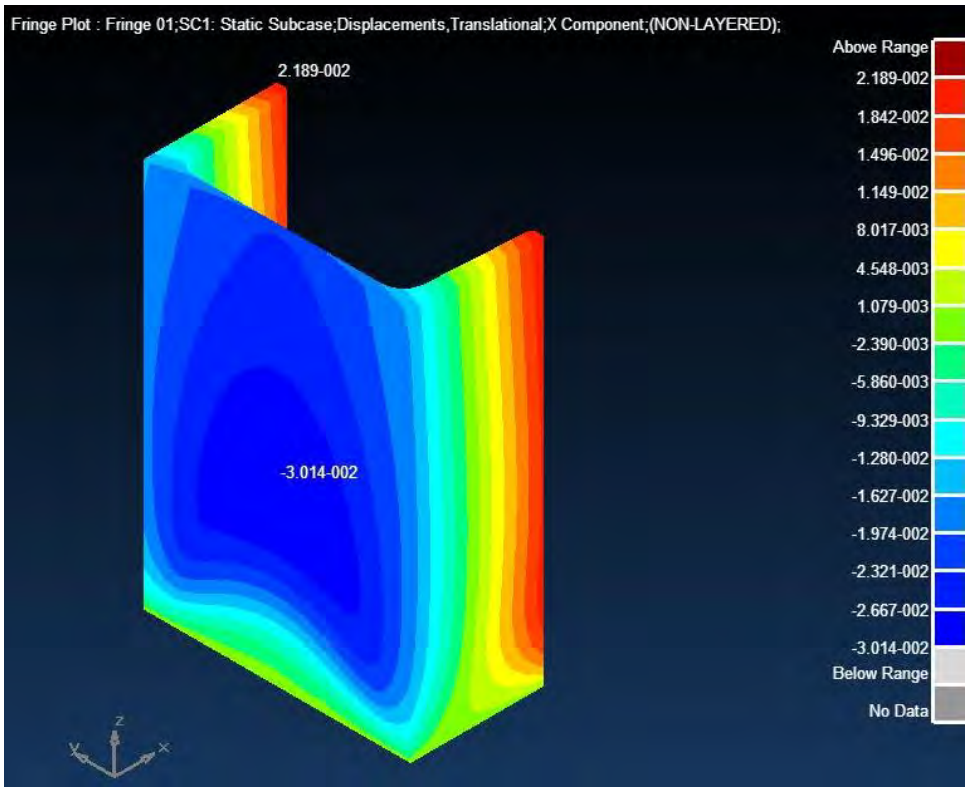

Figure K-12:152x76x18 X Displacement at 350MPa

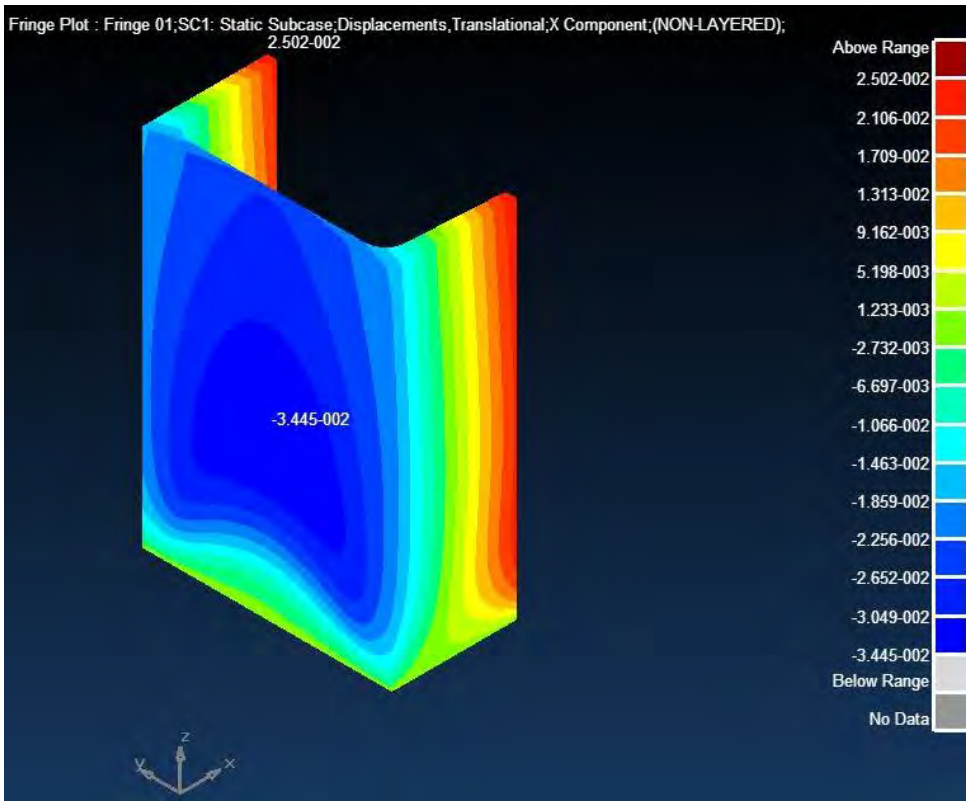

Figure K-13:152x76x18 X Displacement at 400MPa

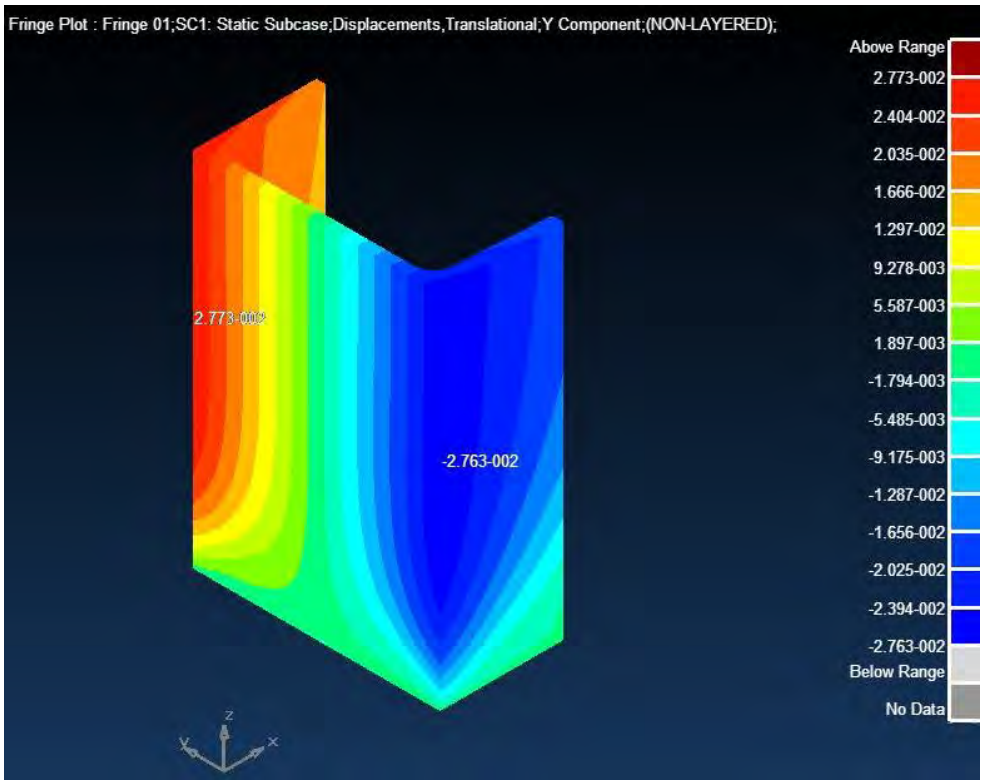

Figure K-14:152x76x18 Y Displacement at 250MPa

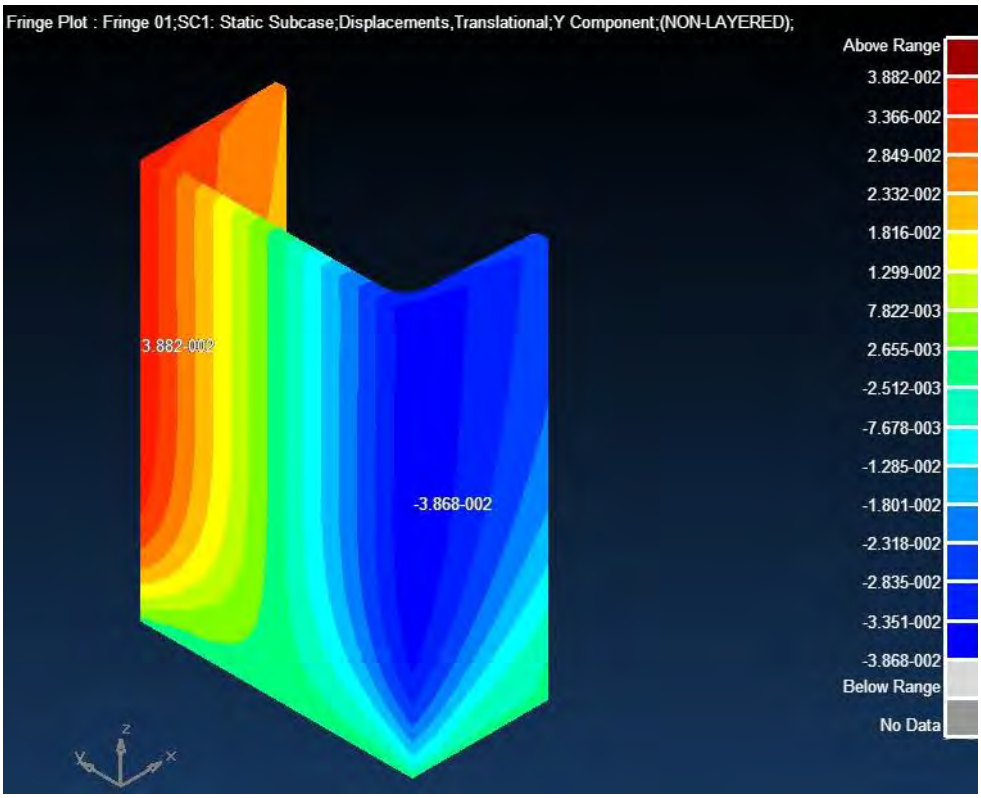

Figure K-15:152x76x18 Y Displacement at 350MPa

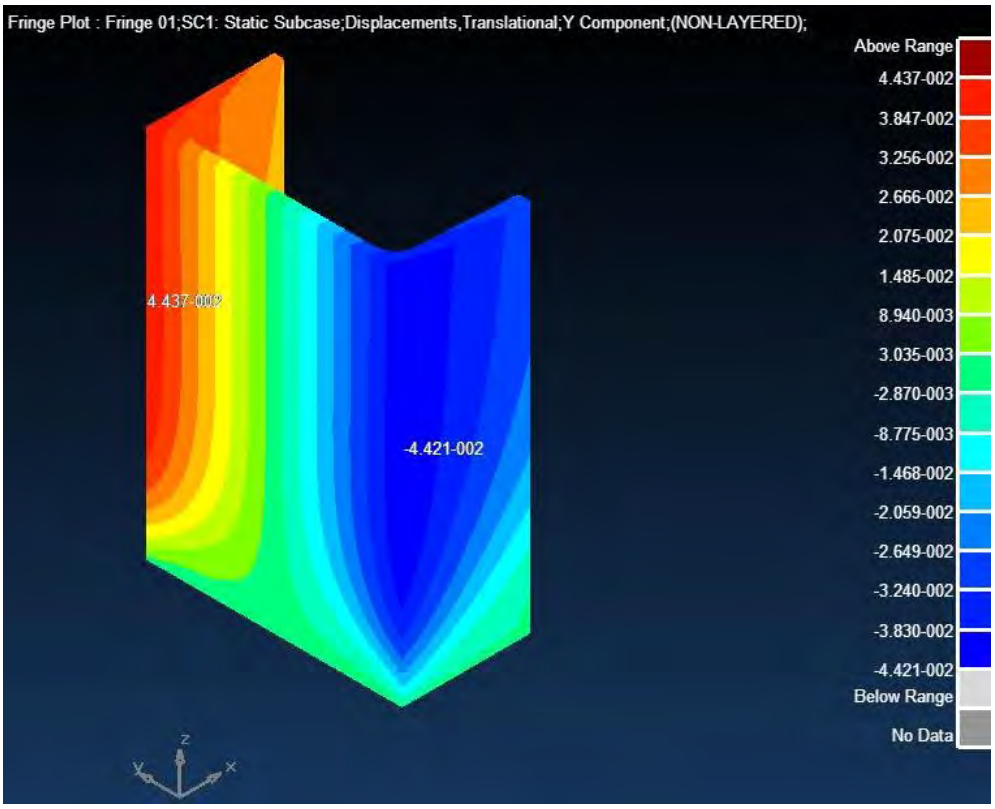

Figure K-16:152x76x18 Y Displacement at 400MPa

L. 350W SLENDERNESS DEPENDANT FRINGE PLOTS

EQUAL ANGLE 90X90X8

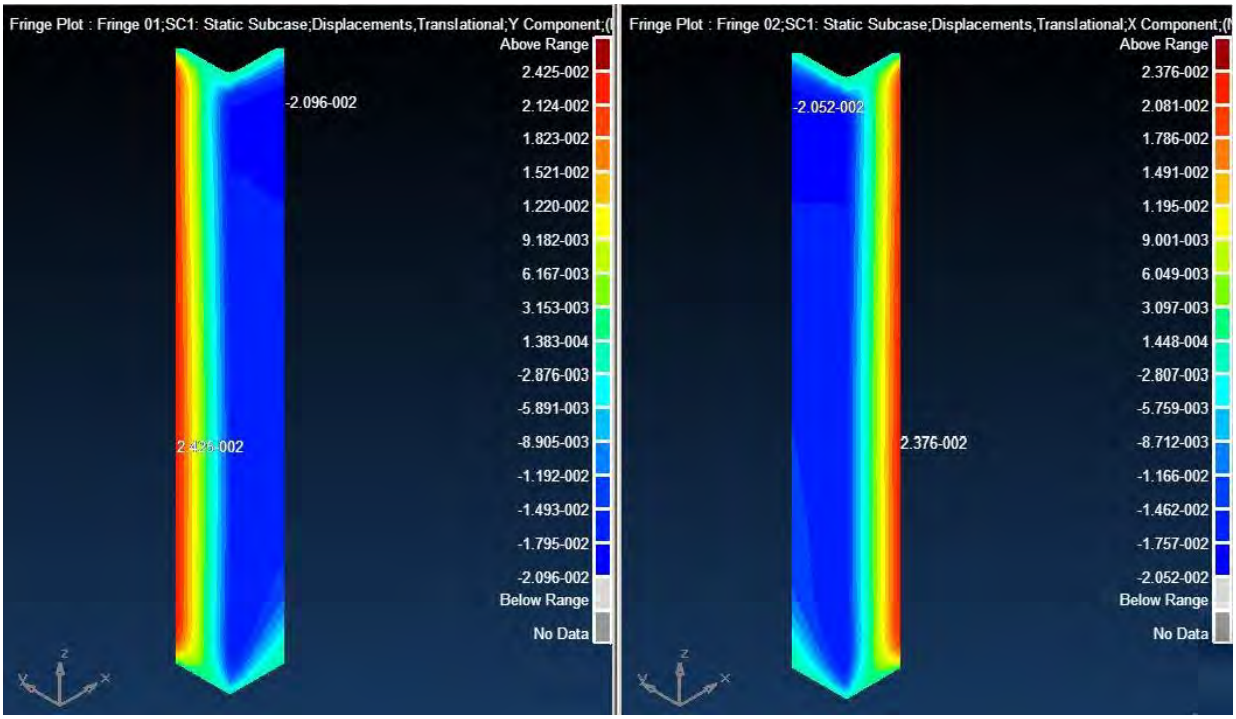

Figure L-1: Angle Section Lateral Displacements with SR=50

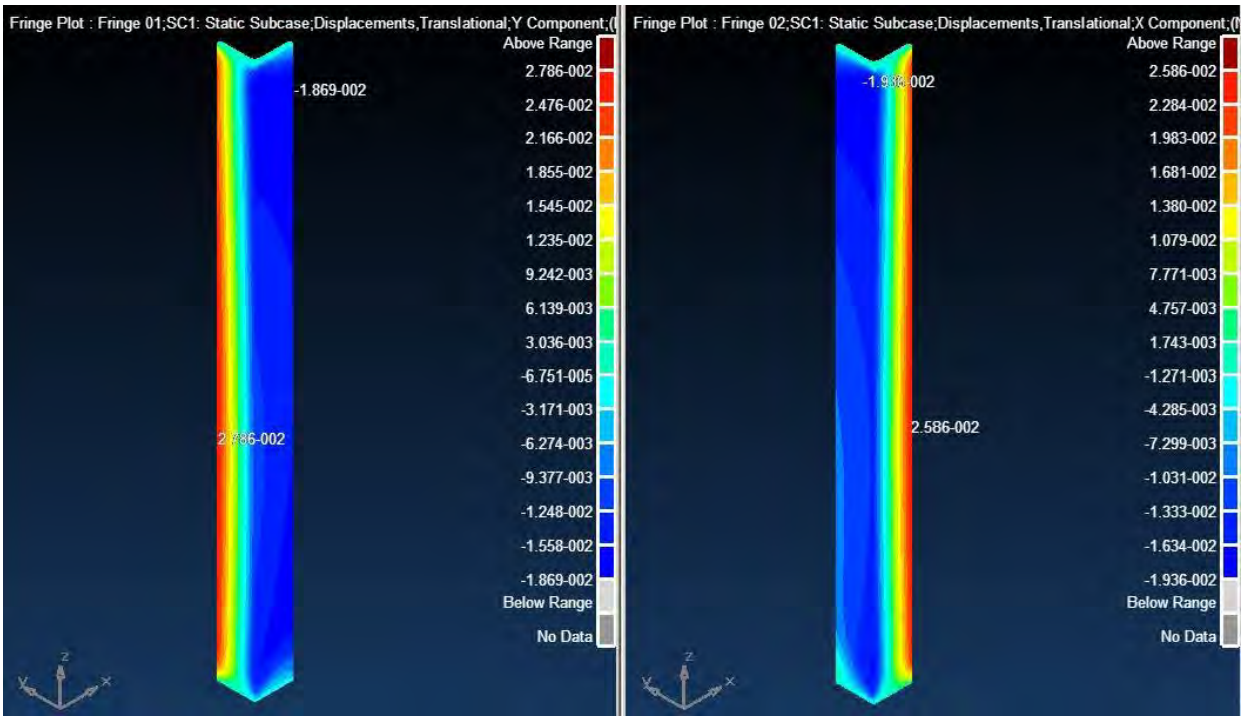

Figure L-2: Angle Section Lateral Displacements with SR=75

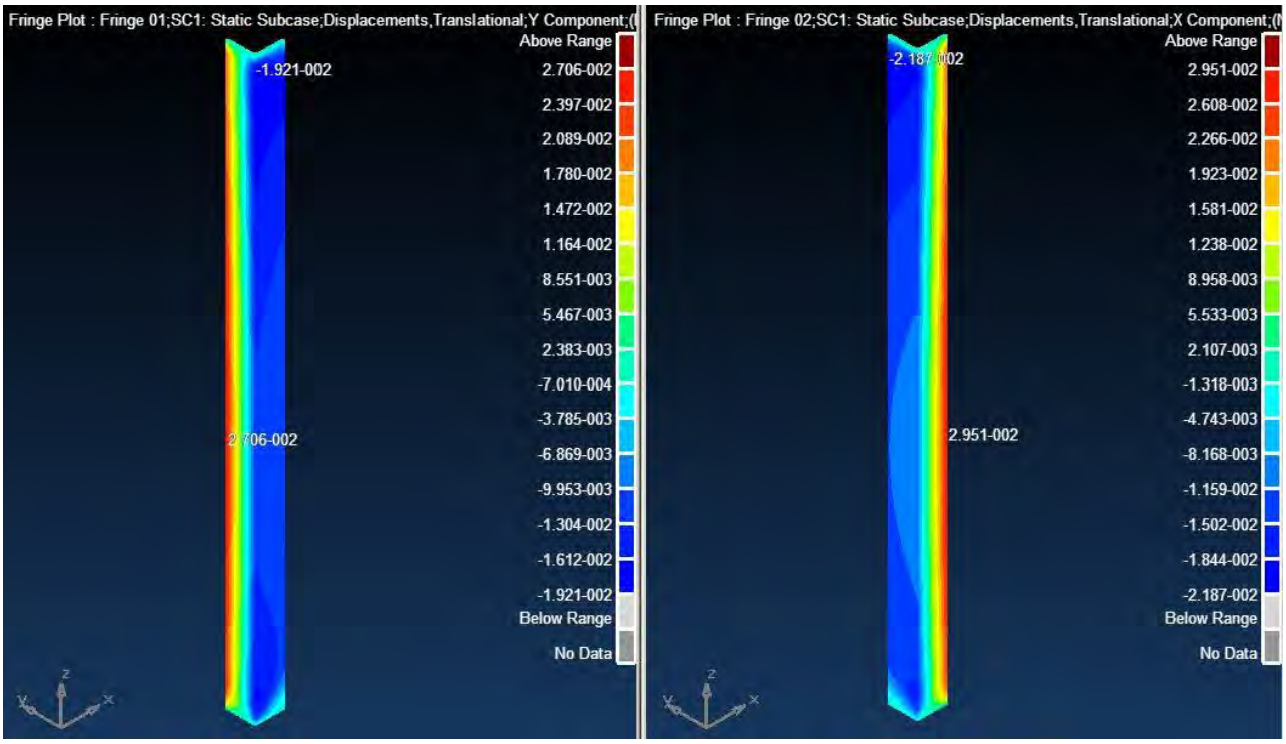

Figure L-3: Angle Section Lateral Displacements with SR=100

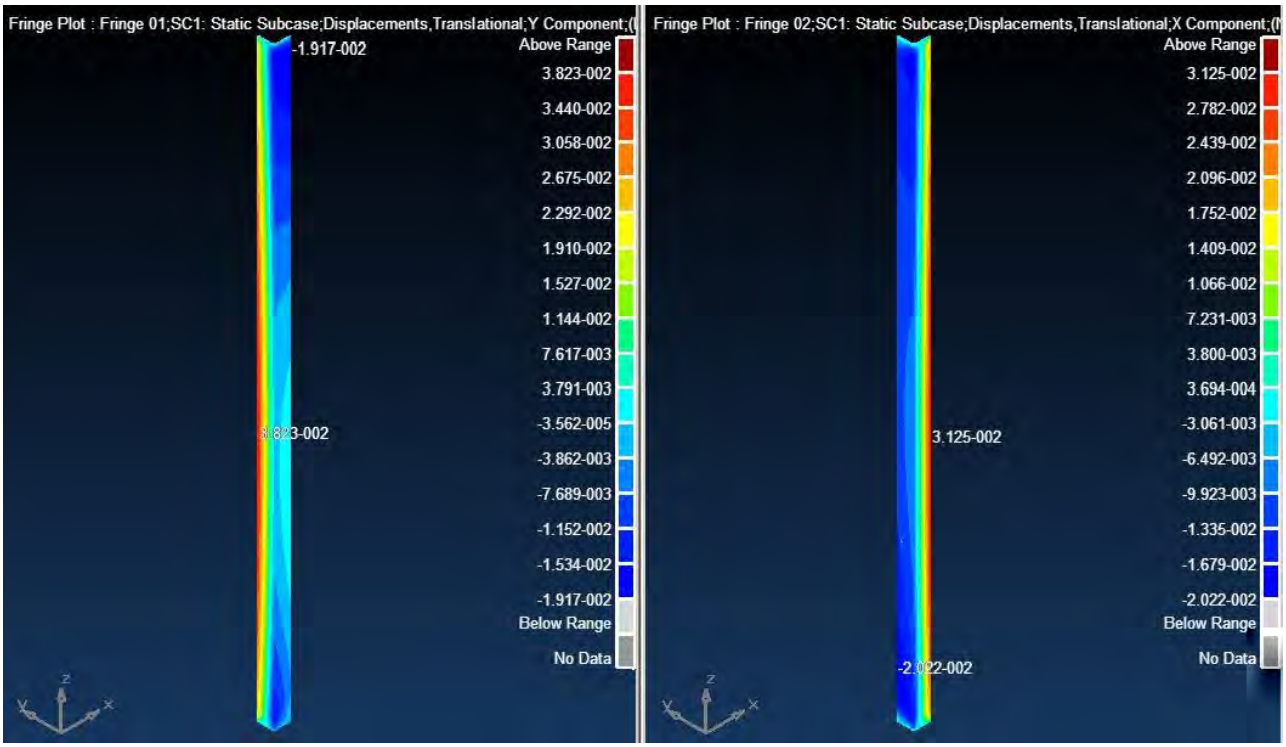

Figure L-4: Angle Section Lateral Displacements with SR=180

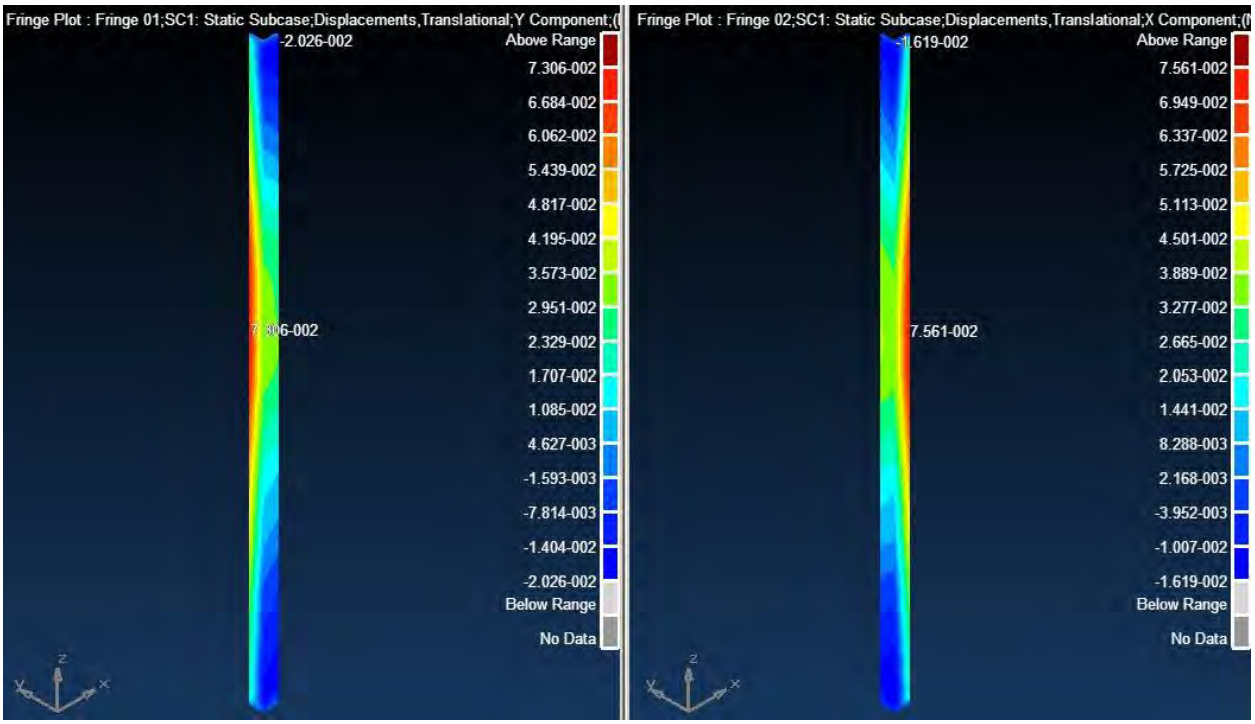

Figure L-5: Angle Section Lateral Displacements with SR=200

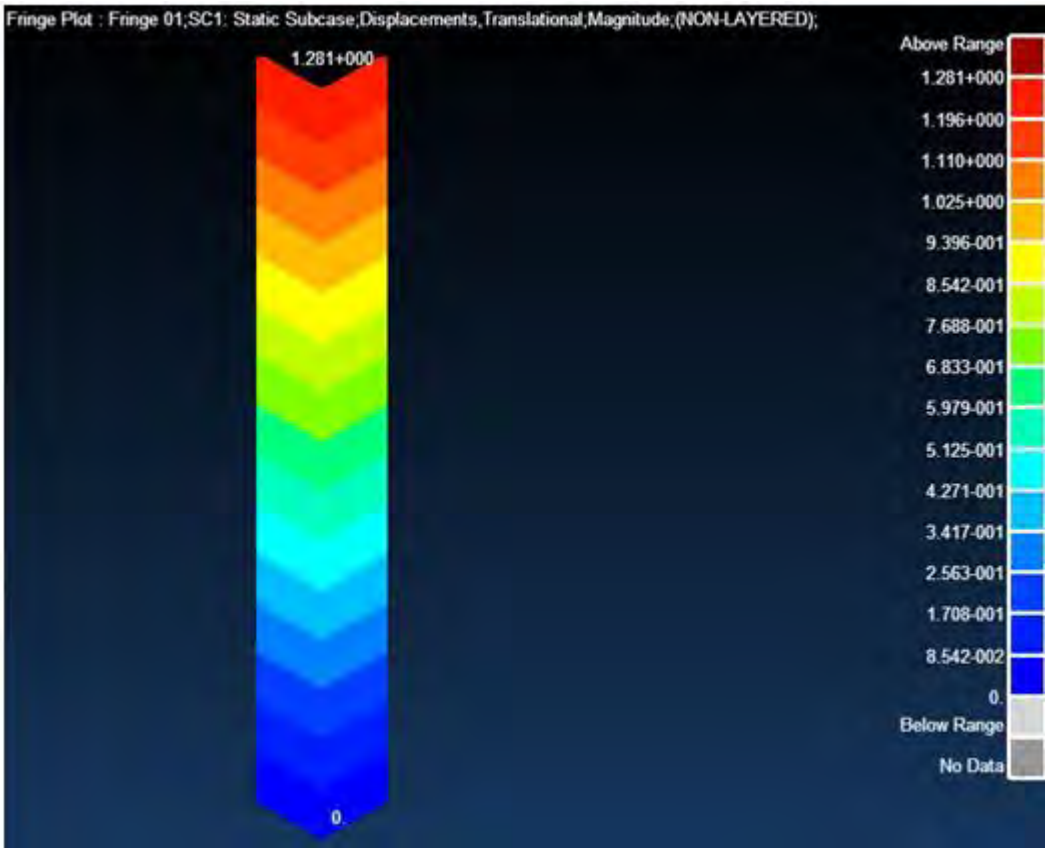

Figure L-6: Angle Section Total Displacement with SR=50

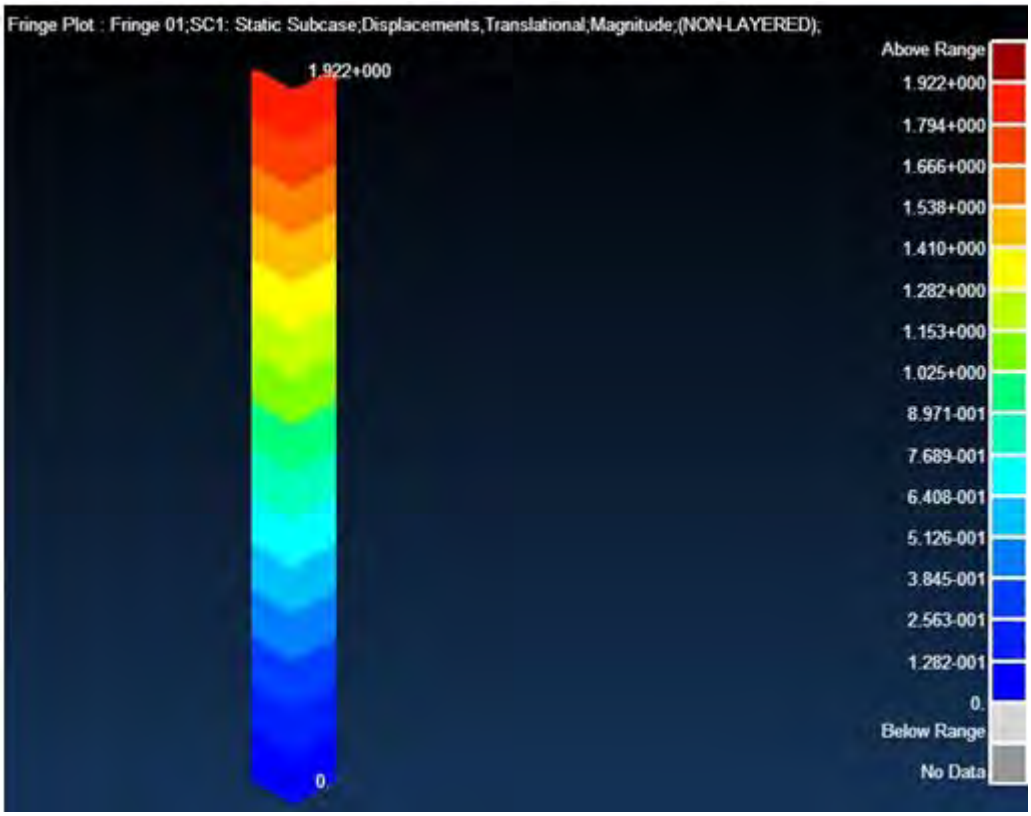

Figure L-7: Angle Section Total Displacement with SR=75

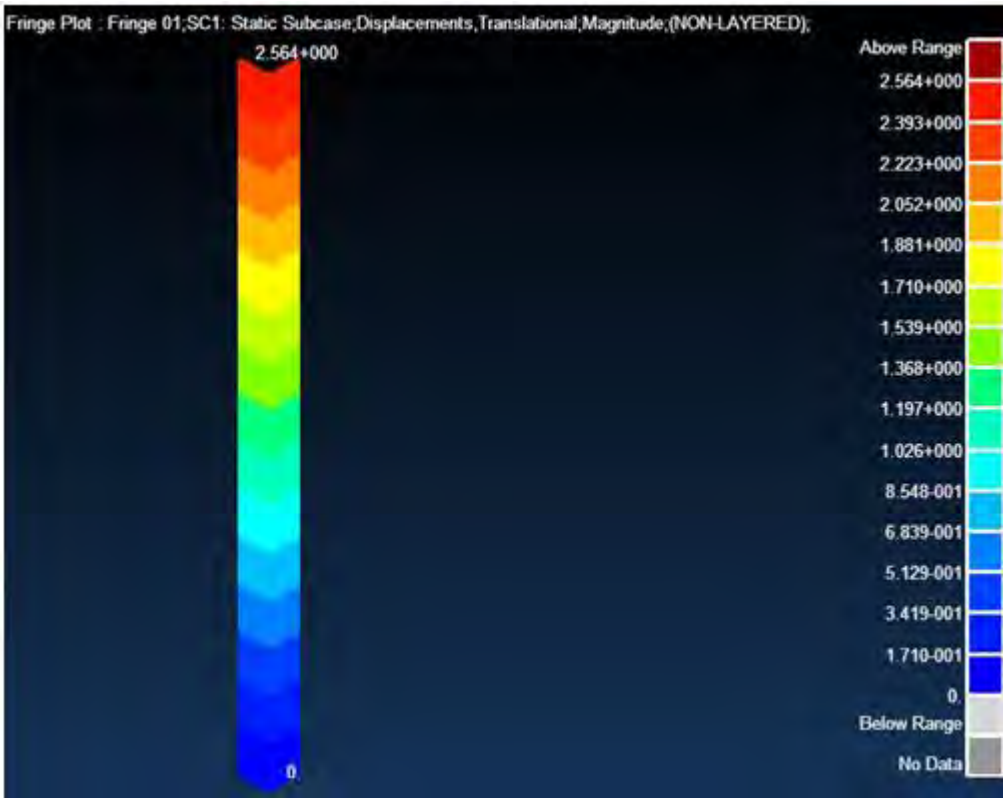

Figure L-8: Angle Section Total Displacement with SR=100

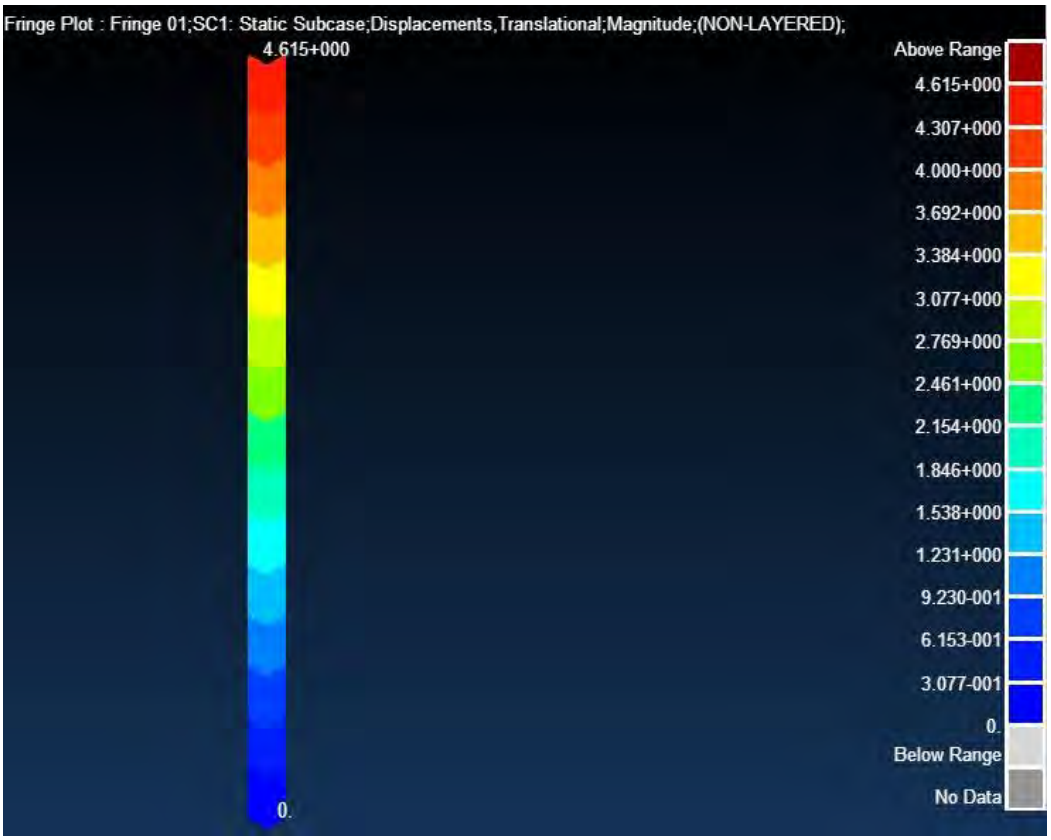

Figure L-9: Angle Section Total Displacement with SR=180

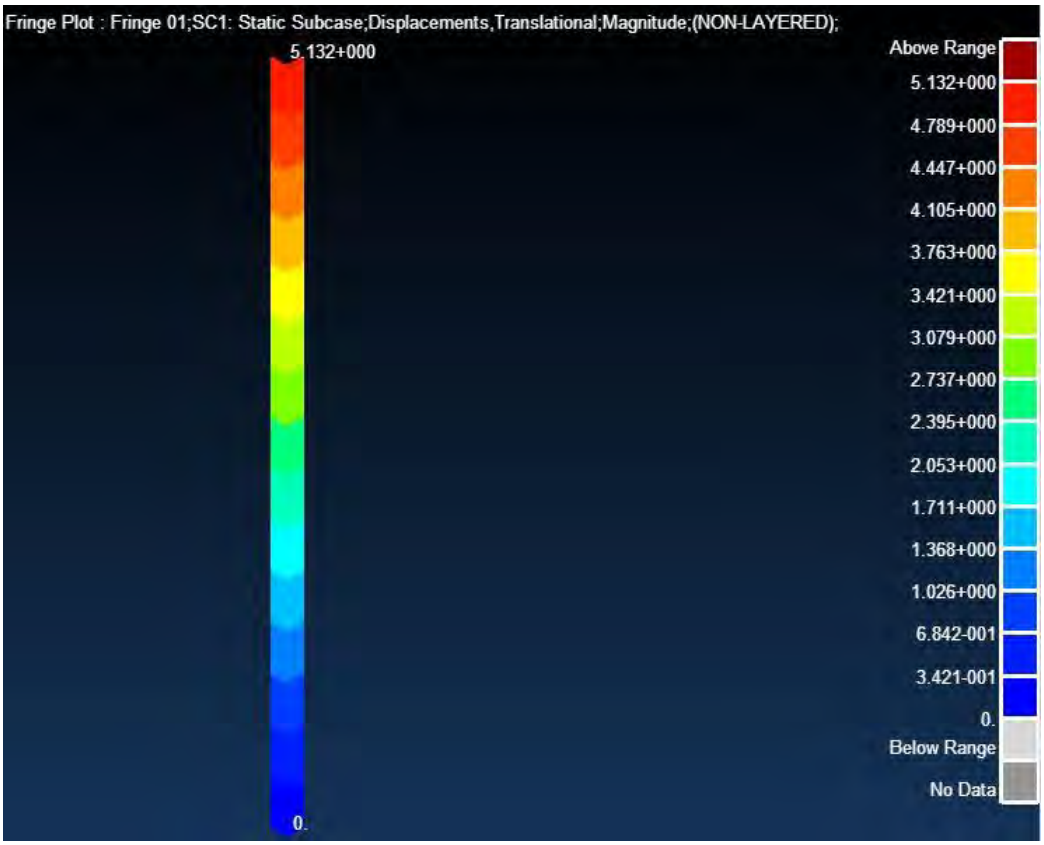

Figure L-10: Angle Section Total Displacement with SR=200

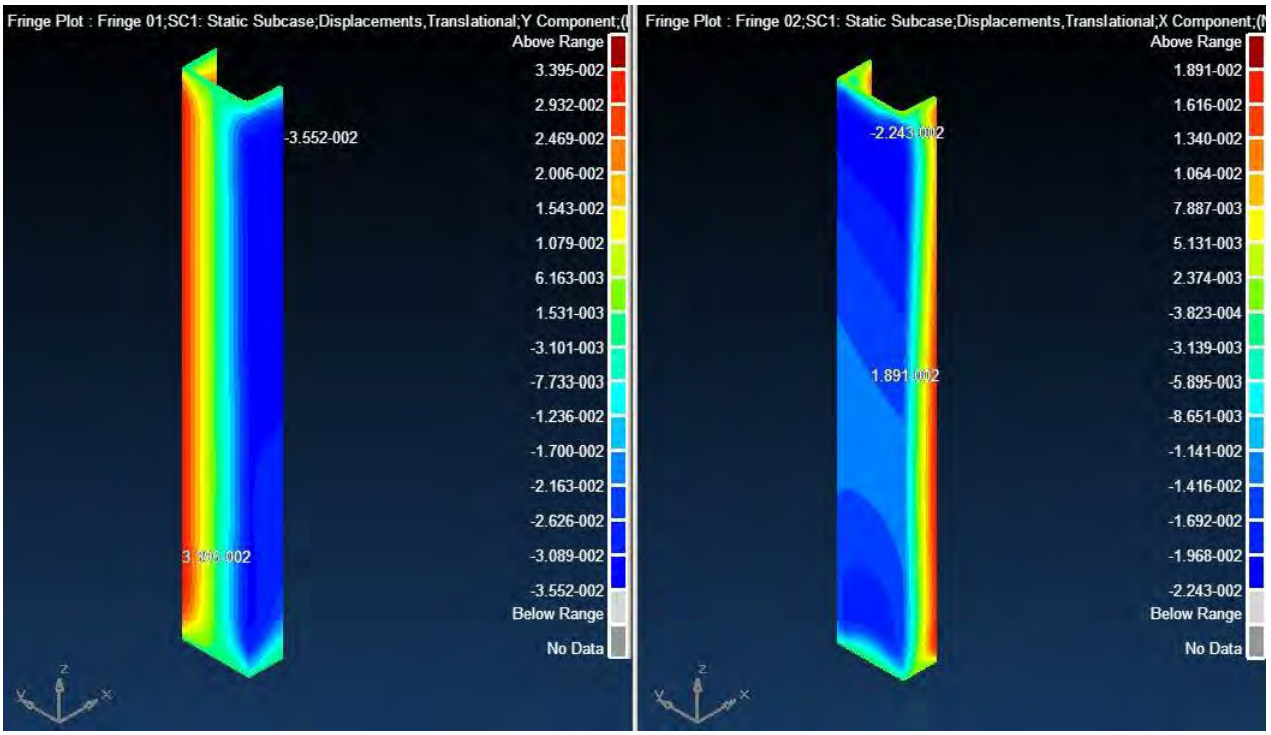

Figure L-11: Channel Section Lateral Displacements with SR=50

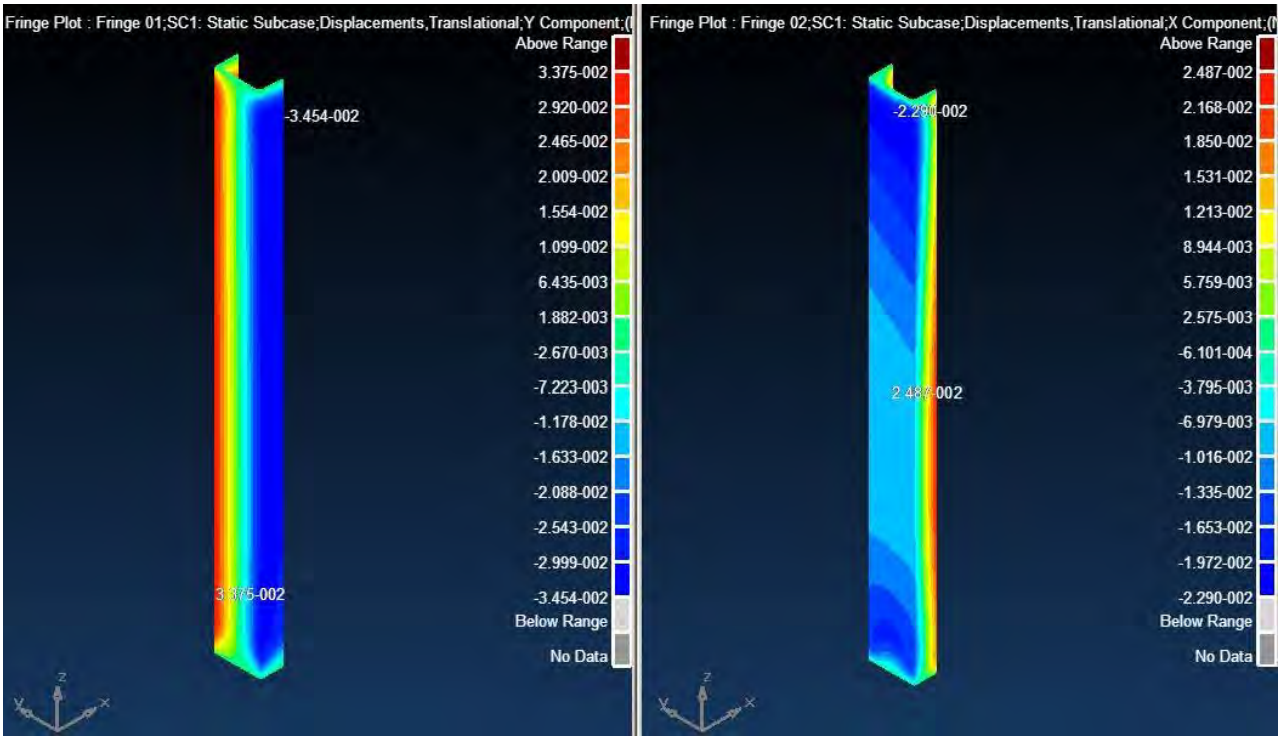

Figure L-12: Channel Section Lateral Displacements with SR=75

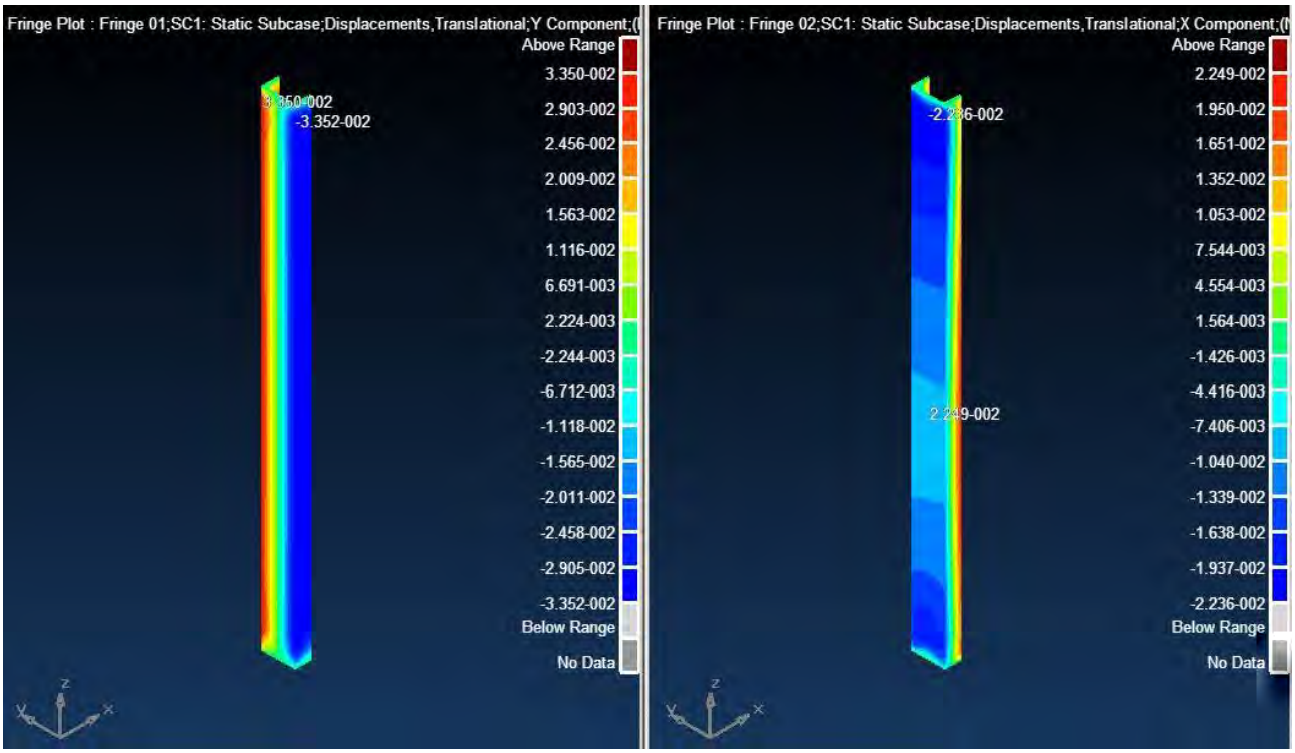

Figure L-13: Channel Section Lateral Displacements with SR=100

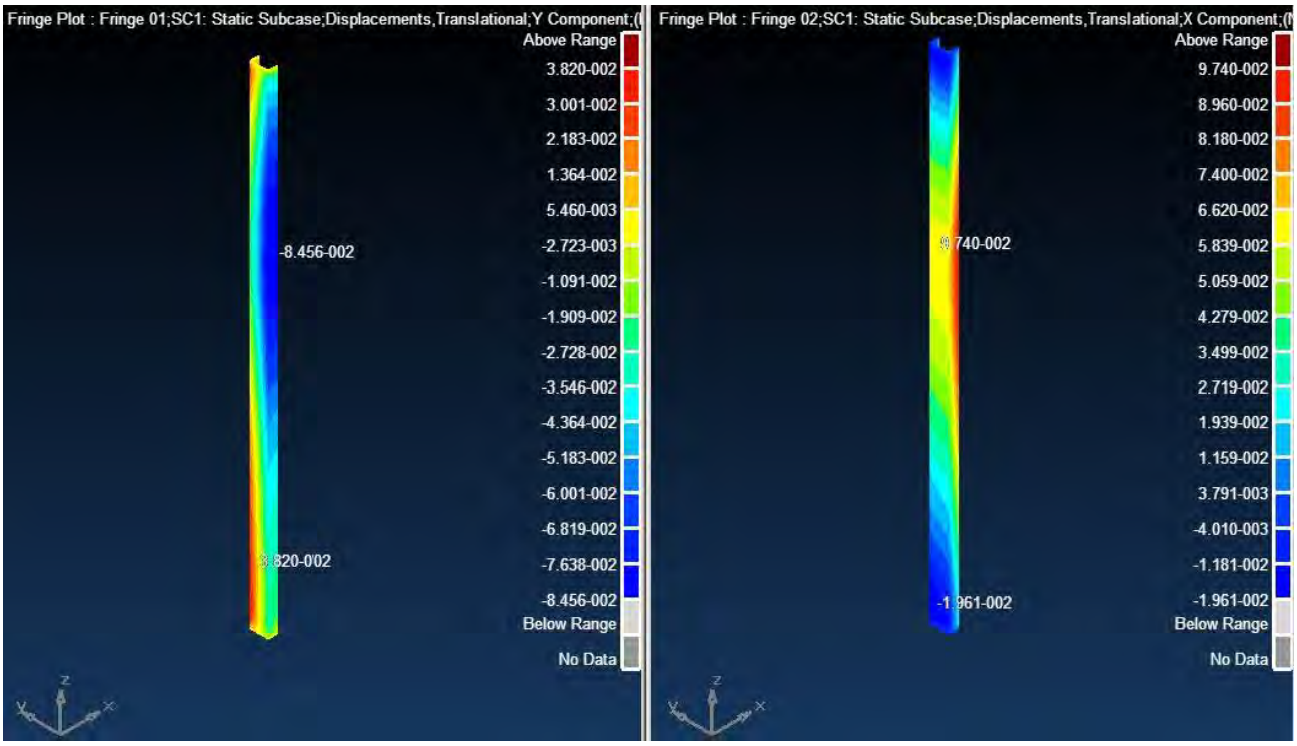

Figure L-14: Channel Section Lateral Displacements with SR=180

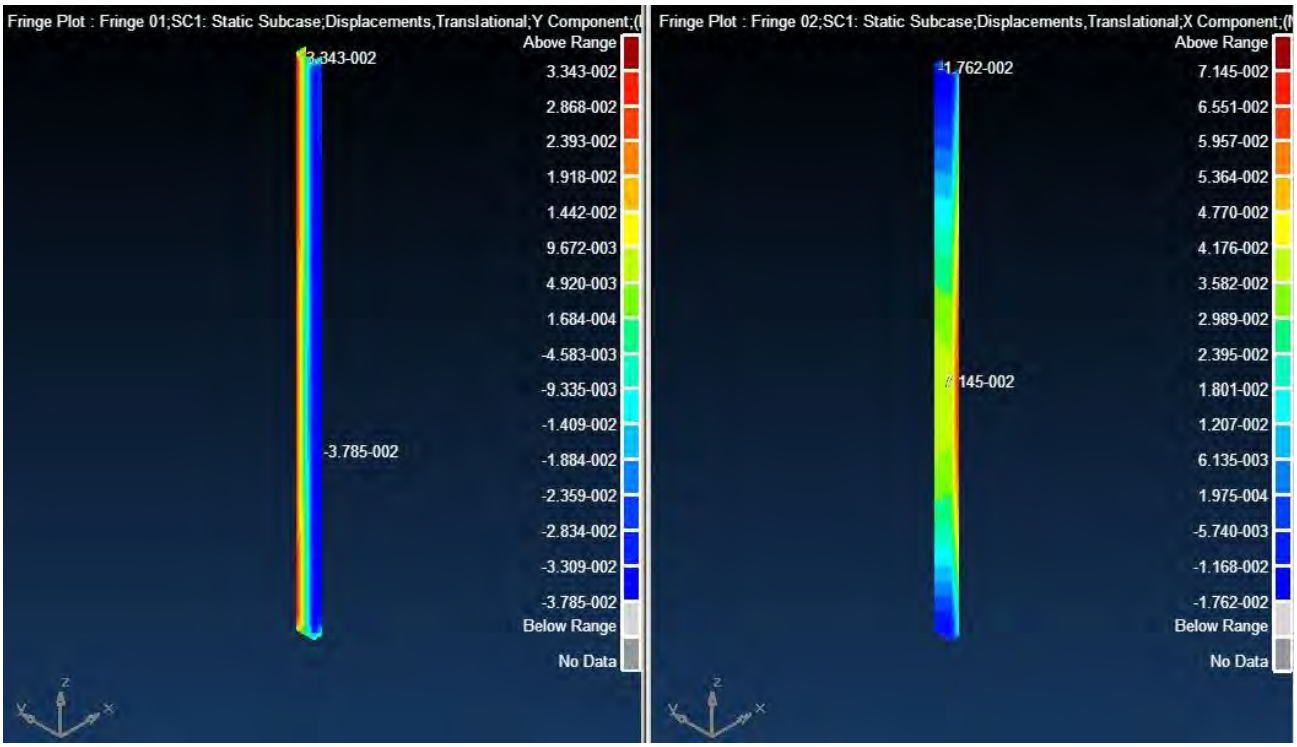

Figure L-15: Channel Section Lateral Displacements with SR=200

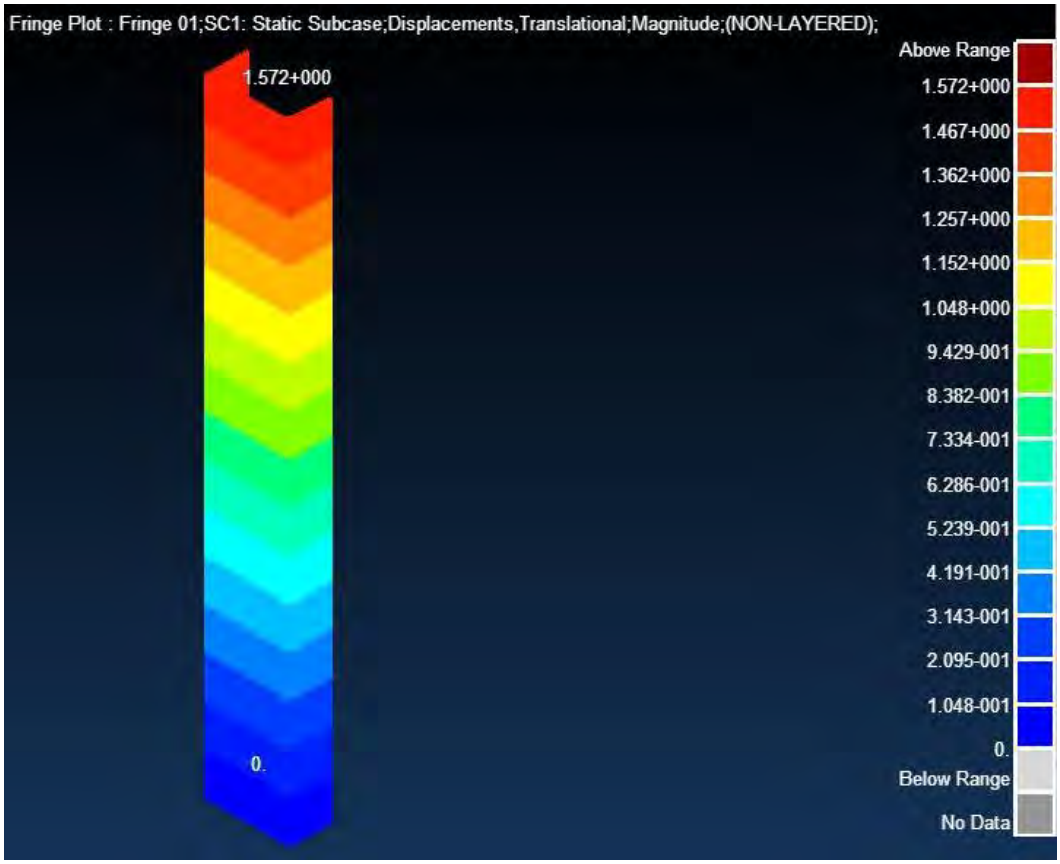

Figure L-16: Channel Section Total Displacement with SR=50

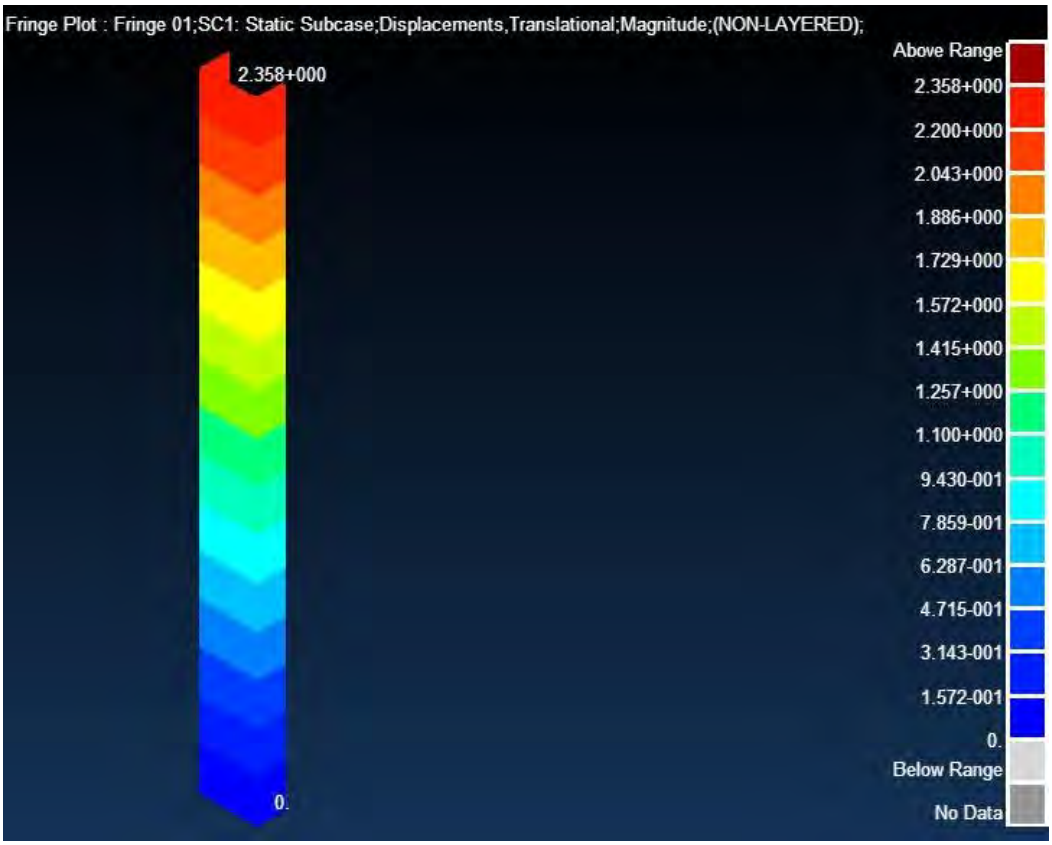

Figure L-17: Channel Section Total Displacement with SR=75

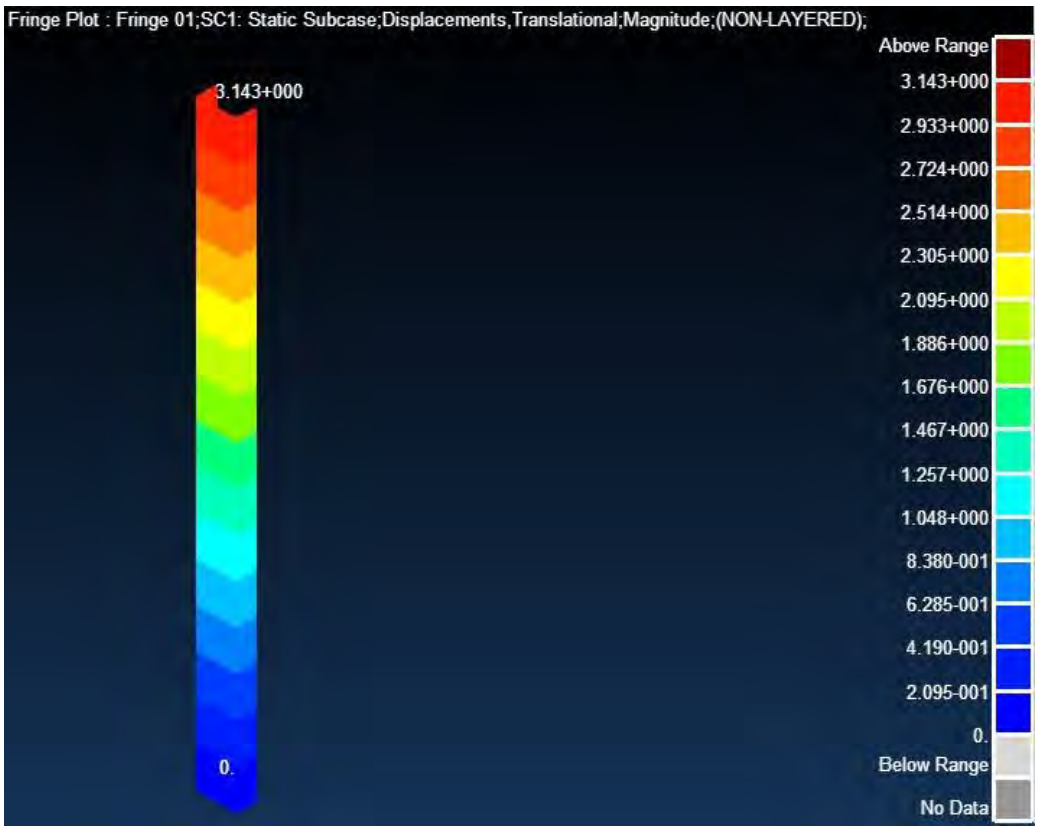

Figure L-18: Channel Section Total Displacement with SR=100

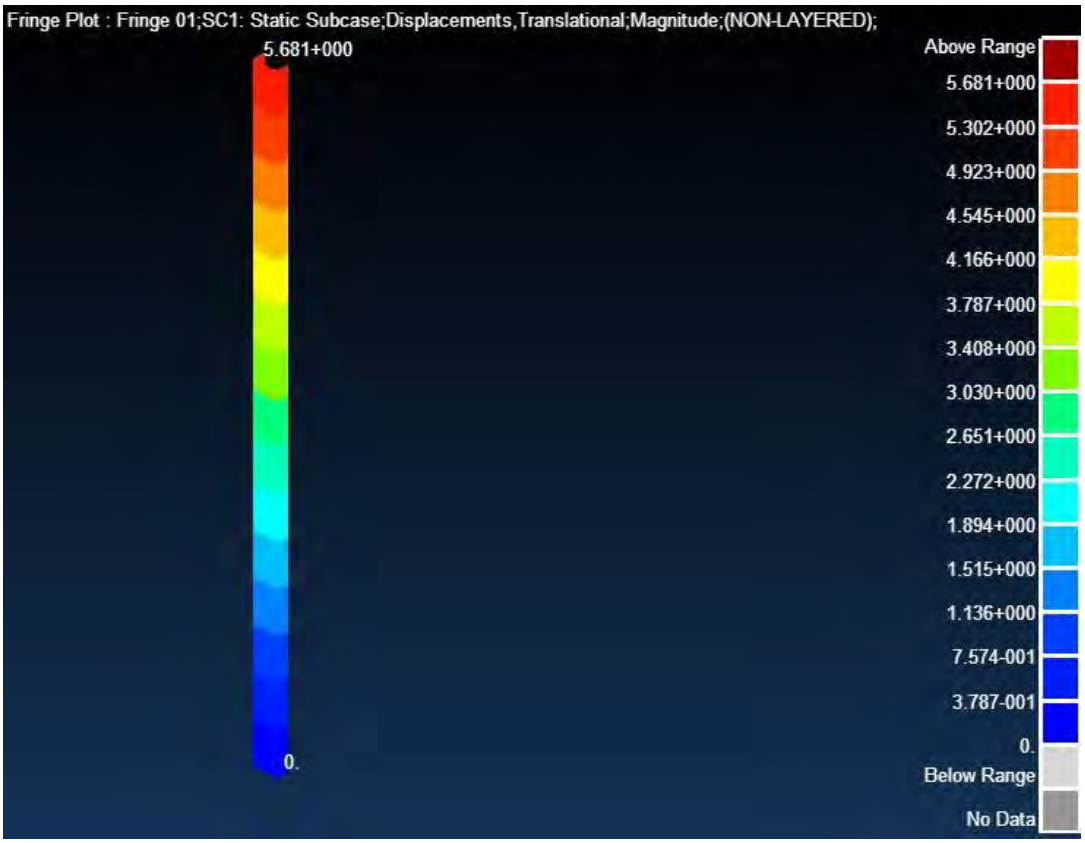

Figure L-19: Channel Section Total Displacement with SR=180

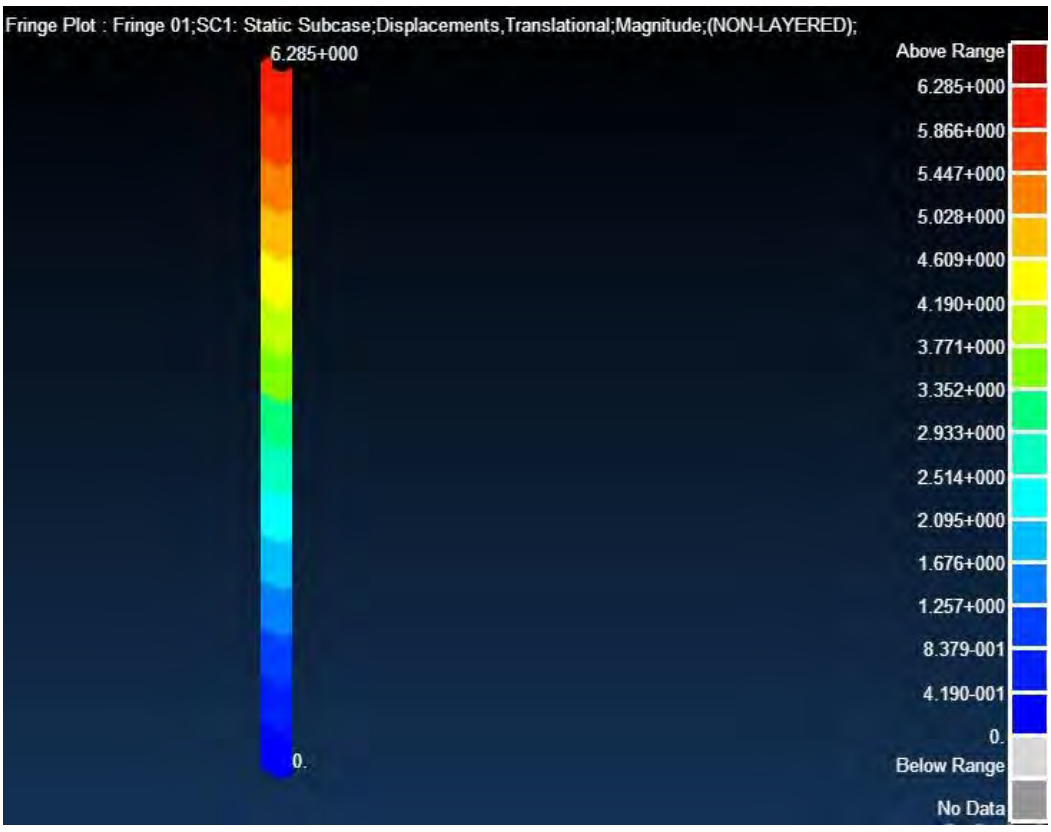

Figure L-20: Channel Section Total Displacement with SR=200